UNIVERSITY of CALIFORNIA
Santa Barbara

III-nitride Laser Diode for Visible Light Communication

A dissertation submitted in partial satisfaction of the
requirements for the degree of

Doctor of Philosophy

in

Materials

by

Changmin Lee

Committee in charge:

Professor Steven P. DenBaars, Chair
Professor Shuji Nakamura
Professor John E. Bowers
Professor Jonathan Klamkin
Professor Boon S. Ooi

December 2017

The dissertation of Changmin Lee is approved:

_____

Boon S. Ooi

_____

Jonathan Klamkin

_____

John E. Bowers

_____

Shuji Nakamura

_____

Steven P. DenBaars, Committee Chair

September 2017

III-nitride laser diode for visible light communication

To my parents,

for constantly encouraging me to survive in the battle of life.

Acknowledgements

My Ph.D years at UCSB were made not just by me but so many people. Before I join at UCSB, I first thank to Dr. Wayne Morrow, who was my mentor when I was an undergraduate researcher at the University of Texas at Dallas, for not only helping me take my first step on “Research” but also kindly and critically guiding my next step to apply UCSB. I would like to thank my best advisor, Professor Steven DenBaars, for finding out my unseen potential and allowing me to join in the world-class research lab. Also, he provided great research topic, VLC, to right person and then fully trusted what I worked on. I also appreciate his trouble-free answers for requesting helps or suggesting ideas. Thank for Professor Shuji Nakamura, for his lead of our group and boosting my research in the professional society. I especially thank to Professor John Bowers for his excellent high-speed photonics expertise which was critical to our project. He was 100 % winning troubleshooter for the problems in my study. Another special thank to my outside unofficial co-advisor, Professor Boon Ooi at King Abdullah University of Science and Technology (KAUST) for his unstinted support my visit and collaborative experiment. Then I thank Professor Jonathan Klamkin, who is another expertise of high-speed photonics, for his meaningful discussions and creative ideas by unexpected approach. I definitely appreciate Professor James Speck, who even though he was not on my committee worked closely with me about my new project on high-speed photodetector and his in-depth knowledge

was always meaningful to me. I would like to emphasize my highest appreciation to Professor Robert Farrell at University of Wisconsin at Madison for taking time for countless discussions, teaching the researcher's attitude, and definitely high-level knowledge. He almost co-advised whole my research and there might not be great achievements of this project without his effort. Dan Cohen is another great laser scientist who gave me many important inputs in my work.

Since my research topic was just new project and any high-speed things were not built in our lab, I needed many helps from different groups such as measurements and discussions. First of all, I specially thank to Chao Shen for his enthusiastic collaboration and always welcoming my visit at KAUST. We made a lot of progresses on this project and generated more than 10 papers and conference talks. I also appreciate to Chong Zhang for his expertise of high-speed measurements and especially many critical discussions related to the publishable data. Also, I learned a lot about basics of high-speed measurement at the beginning of the project. Then, I thank to my mentor in my initial years, Sang Ho Oh for his great teach as well as even letting me know how to do well in our group.

I would like to thank to all the staff in Nanofab, MOCVD lab, and CNSI labs for their great training and discussions. Also, my Ph.D went more smoothly with helps from administrative staff of both Materials Department and SSLEEC including Jocelyn, Stefani, Tawny, Yukina, Fukiko, Aldir, and Tara.

I should express my high appreciation to my research group members. Our group is quite different from typical other group, named for SSLEEC. This huge group consists of smart, passionate, thoughtful, and friendly students. The atmosphere that students voluntary discuss and share ideas each other was perfect to me. Among many great lab mates, I would like to especially thank to Daniel Becerra and Seunggeun Lee for consistent discussions, problem solving and sharing knowledge about laser growth, processing, and its characteristics.

For my internship at Soraa Laser Diode, Inc., I especially thank to the vice president, James Raring, for offering the work opportunity and great leadership to workers including me. Alex Stein was also great mentor at Soraa Laser Diode, Inc., for teaching skills and helping me understand the project.

Outside of my work places, my close and old friends who work on similar semiconductor area for Ph.D, Joon Sohn at Stanford, Sangeun Park at UT Austin, took countless time to talk about similar research issues, concerns, and general topics. These two best friends made my Ph.D life more enthusiastically, smoother, and happier. At UCSB, my local best friend, linguistic philosopher Jeonggyu Lee in Philosophy department inspired me to think critically and logically with a lot of alcohol-based relieves. I also thank to other Korean friends at UCSB including Hyunchul Park, Sungkyun Kim, Seojin Ko, Seon Kim, Joonho Back and others.

Finally, I want to thank my family for unperturbed support, belief, cheer and love. Nothing can describe how they are important in my life.

Curriculum Vitae
Changmin Lee
September 2017

Education

University of California, Santa Barbara Sep 2012 – Sep 2017

Doctor of Philosophy (Ph.D.) in Materials
Thesis: III-nitride Laser Diode for Visible Light Communication
Ph.D advisor: Prof. Steven P. DenBaars

The University of Texas at Dallas Aug 2010 – Jun 2012

Bachelor of Science (B.S.) in Electrical and Computer Engineering
Graduated with *Summa Cum Laude*
Undergrad Research Topic: Graphene Contact Interlayer as a Diffusion Barrier

Kyungpook National University Mar 2005 – Jun 2010

Bachelor of Science (B.S.) in Electrical and Computer Engineering
Selected for *Dual-degree scholarship program*

Professional Experience

Graduate Student Researcher Sep 2013 – present
Solid State Lighting and Energy Center (SSLEEC)
Materials Department, University of California, Santa Barbara
Developed Semipolar Laser Diode and System for Visible Light Communication.

Graduate Intern Jan 2014 – Jun 2014
Soraa Laser Diode, Inc.
Headquarters
Goleta, CA
Developed wafer scaling process for Laser Diode on Bulk GaN Substrate

Teaching Assistant Sep 2012 – Jun 2013
Department of ECE, University of California, Santa Barbara
Taught undergraduate core courses in fundamental electronic circuits, devices, and systems (ECE2A, 2B, and 2C)

Undergraduate Research Assistant Aug 2011 – May 2012
Laboratory for Surface and Nanostructure Modification

Department of Materials Science, The University of Texas at Dallas
Synthesized and characterized Graphene properties for a diffusion barrier as a contact interlayer

Aircraft Weapon Technician (Staff Sergeant) Mar 2006 – May 2008
122 Squadron Unit, Republic of Korea, Air Force (ROKAF)

Oragnization / Leadership / Activities

Reviewer for Journals Jun 2016 – Current
Optics Letters (OSA), Optics Express (OSA), and Photonic Technology Letters (IEEE)

IEEE Photonic Society UCSB Student Chapter Jul 2015 – Jul 2016
Role: Secretary

UCSB Korean Graduate Student Association Sep 2014 – Sep 2015
Role: President

Honors and Awards

Doctoral Student Travel Grant 2016
UCSB

13th DoE SSL R&D WORKSHOP Student Poster Contest Award 2016
US Department of Energy

Outstanding Graduate Student Researcher Achievement Award 2015
UCSB

IEEE Photonic Society's Summer Topical Meeting Series 2015
Best Poster Award
IEEE & NSF

Summa Cum Laude 2012
The University of Texas at Dallas

Phi Kappa Phi Honor Society Member 2011
UT-Dallas Chapter of Phi Kappa Phi

Dean's list: 3 semesters 2010 – 2012
The University of Texas at Dallas

The Korean Honor Scholarship 2011
Embassy of Republic of Korea in the USA

Erik Jonsson Scholarship 2011
The University of Texas at Dallas

National Science & Technology Scholarship 2009 – 2010
Ministry of Science and Technology, South Korea

Press Releases / Magazine Articles

"Near-ultraviolet laser diodes powering visible (white) light communication,"
Semiconductor Today, 2017
Link: http://www.semiconductor-today.com/news_items/2017/aug/usb_090817.shtml

"Turbocharging LiFi With Semi-Polar Lasers,"
Compound Semiconductor Magazine, 2017
Link: https://compoundsemiconductor.net/article/101642/Turbocharging_LiFi_With_Semi-polar_Lasers/feature

"US Researchers Show 4 Gbps Data Rate With GaN Laser Diode,"
Compound Semiconductor Magazine, 2015
Link: https://www.compoundsemiconductor.net/article/97277-us-researchers-show-4gbps-data-rate-with-gan-laser-diode.html

"4 Gbps data rate with GaN laser diode demonstrated,"
BIZLED Magazine, 2015
Link: http://bizled.co.in/4gbps-data-rate-with-gan-laser-diode-demonstrated

Publications

[1] **C. Lee**, C. Shen, C. Cozzan, Robert M. Farrell, S. Nakamura, R. Seshadri, B. S. Ooi, and S. P. DenBaars, "Gigabit-per-second white light-based visible light communication using near-ultraviolet laser diode and red-, green-, blue-emitting phosphors," *Opt. Express*, 25, 17480 (2017)

[2] **C. Lee**, C. Zhang, D. Becerra, S. Lee, R. M. Farrell, S. H. Oh, J. S. Speck, S. Nakamura, J. E. Bowers and S. P. DenBaars, "Dynamic characteristics of 410 nm semipolar $(20\bar{2}\bar{1})$ III-nitride laser diodes with modulation bandwidth over 5 GHz," *Appl. Phys. Lett.*, 109, 101104 (2016)

[3] W. K. Morrow*, **C. Lee***(co-1st author), S. P. DenBaars, Fan Ren and S. J. Pearton, "Role of Graphene Interlayers in Mitigating Degradation of Ni/Au Ohmic Contact Morphology on p-type GaN," *Vacuum*, 128, 34 (2016)

[4] **C. Lee**, C. Shen, H. Oubei, M. Cantore, B. Janjua, T. Ng, R. M. Farrell, M. M. El-Desouki, J. S. Speck, S. Nakamura, B. S. Ooi, and S. P. DenBaars, "2 Gbit/s data transmission from an unfiltered laser-based phosphor-converted white lighting communication system," *Opt. Express,* 23, 29779 (2015)

[5] **C. Lee**, C. Zhang, M. Cantore, R. M. Farrell, S. Oh, T. Margalith, J. S. Speck, S. Nakamura, J. E. Bowers, and S. P. DenBaars, "4 Gbps direct modulation of 450 nm GaN laser for high-speed visible light communication," *Opt. Express,* 23, 16232 (2015)

[6] C. Shen, T. Ng, **C. Lee**, S. Nakamura, J. S. Speck, S. P. DenBaars, A. Y. Alyamani, M. M. El-Desouki, and B. S. Ooi, "Dual-section InGaN quantum-well laser diode with integrated amplifier on semipolar GaN substrate," *Opt. Lett.,* (In review)

[7] C. Shen, **C. Lee**, E. Stegenburgs, J. H. Lerma, T. Ng, S. Nakamura, J. S. Speck, S. P. DenBaars, A. Y. Alyamani, M. M. El-Desouki, and B. S. Ooi, "Semipolar III-nitride quantum well waveguide photodetector integrated with laser diode for on-chip photonic system," *Appl. Phys. Express,* 10, 042201 (2017)

[8] C. Shen, **C. Lee**, T. Ng, S. Nakamura, J. S. Speck, S. P. DenBaars, A. Y. Alyamani, M. M. El-Desouki, and B. S. Ooi, "High-speed 405-nm superluminescent diode (SLD) with 807-MHz modulation bandwidth," *Opt. Express,* 24, 20281 (2016)

[9] B. P. Yonkee, E. C. Young, **C. Lee**, D. A. Cohen, J. T. Leonard, S. P. DenBaars, J. S. Speck, and S. Nakamura, "Demonstration of a III-nitride edge emitting laser diode utilizing a GaN tunnel junction contact," *Opt. Express,* 24, 7816 (2016)

Conference Presentations

[1] (Invited) **C. Lee**, et al. "High speed performance of III-nitride laser diode grown on semipolar plane for visible light communication," 2016 IEEE Photonic Conference (IPC), *29th Annual Conference of the IEEE Photonics Society*, Oct 2016, Waikoloa Village, HI, Oral presentation

[2] **C. Lee**, et al. "High-speed Performance of III-nitride 410 nm Ridge Laser Diode on $(20\bar{2}\bar{1})$ plane for Visible Light Communication," *2016 Compound Semiconductor Week (CSW) and the 43nd International Symposium on Compound Semiconductors (ISCS)*, Jun 2016, Toyama, Japan, Oral presentation

[3] **C. Lee**, et al. "High-speed Visible Light Communication utilizing Laser-based Solid-state Lighting," *13th US Department of Energy (DOE) SSL R&D WORKSHOP*, Feb 2016, Raleigh, NC, Poster presentation

[4] **C. Lee**, et al. "2.6 GHz High-Speed Visible Light Communication of 450 nm GaN Laser Diode by Direct modulation," *2015 IEEE Photonic Society Summer Topical Meeting Series (SUM)*, Jul 2015, Nassau, Bahamas, Oral presentation & poster presentation

[5] **C. Lee**, et al. "2.6 GHz High Speed Direct Modulation of 450 nm GaN Laser Diode for Visible Light Communication," *2015 Compound Semiconductor Week (CSW) and the 42nd International Symposium on Compound Semiconductors (ISCS)*, Jun 2015, Santa Barbara, CA, Oral presentation

[6] C. Shen, T. Ng, **C. Lee**, J. T. Leonard, S. Nakamura, J. S. Speck, S. P. DenBaars, A. Y. Alyamani, M. M. Eldesouki, and B. S. Ooi, "Semipolar InGaN-based superluminescent diode for solid-state lighting and visible light communication", *SPIE Photonics West*, Jan 2017, San Francisco, CA

[7] C. Shen, **C. Lee**, T. Ng, S. Nakamura, J. S. Speck, S. P. DenBaars, A. Y. Alyamani, M. M. Eldesouki, and B. S. Ooi, "Nitride-based Integrated Semiconductor Optical Amplifier-Laser Diode at 404 nm", *2016 IEEE International Electron Devices Meeting (IEDM)*, Dec 2016, San Francisco, CA

[8] C. Shen, **C. Lee**, T. Ng, J. S. Speck, S. Nakamura, S. P. DenBaars, A. Y. Alyamani, M. M. Eldesouki, and B. S. Ooi, "GHz Modulation Enabled Using Large Extinction Ratio Waveguide-Modulator Integrated with InGaN Laser Diode", *2016 IEEE Photonic Conference (IPC), 29th Annual Conference of the IEEE Photonics Society*, Oct 2016, Waikoloa Village, HI

[9] S. Nakamura, B. P. Yonkee, E. C. Young, J. T. Leonard, **C. Lee**, S. P. DenBaars, J. S. Speck, "Tunnel-Junction Blue LED, Edge Emitting Laser Diode and VCSEL", *33rd International Conference on the Physics of Semiconductors*, Jul 2016, Beijing, China

[10] B. P. Yonkee, E. C. Young, J. T. Leonard, **C. Lee**, S. P. DenBaars, J. S. Speck, S. Nakamura, "Hybrid MOCVD/MBE GaN Tunnel Junctions", *18th International Conference on Metal Organic Vapor Phase Epitaxy (ICMOVPE)*, Jul 2016, San Diego, CA

[11] B. P. Yonkee, E. C. Young, J. T. Leonard, **C. Lee**, S. H. Oh, S. P. DenBaars, J. S. Speck, S. Nakamura, "Hybrid MOCVD/MBE GaN Tunnel Junction LEDs with Greater than 70% Wall Plug Efficiency", *2016 Compound Semiconductor Week (CSW) and the 43rd International Symposium on Compound Semiconductors (ISCS)*, Jun 2016, Toyama, Japan

[12] B. P. Yonkee, E. C. Young, J. T. Leonard, **C. Lee**, S. H. Oh, J. S. Speck, S. Nakamura, "Hybrid MOCVD/MBE GaN Tunnel Junctions", *6th*

International Symposium on Growth of III-Nitrides (ISGN), Nov 2015, Hamamatsu, Japan

[13] B. P. Yonkee, E. C. Young, J. T. Leonard, **C. Lee**, S. H. Oh, S. P. DenBaars, J. S. Speck, S. Nakamura, "Hybrid MOCVD/MBE GaN Tunnel Junctions," *11th International Conference on Nitride Semiconductors (ICNS)*, Aug 2015, Beijing, China

Abstract

III-nitride Laser Diode for Visible Light Communication

by

Changmin Lee

Solid-state lighting based on III-nitride by light emitting diodes (LEDs) has been developed as a high efficient light source and has been successfully commercialized in the market. In addition to the function of lighting, visible light communication (VLC) has gained momentum to solve the data traffic of the radio frequency (RF) wireless communication. Many progresses in LED based VLC have been reported previously. However, since LEDs are limited by the carrier lifetime of its spontaneous emission and RC parasitics, the modulation bandwidth is typically on the order of MHz.

For white lighting communication, the bandwidth and data rate are significantly affected by a slow phosphor response due to its relaxation decay time on the order of 100 ns ~ 1 μs.

As an alternative to LED technology, the use of laser diodes (LDs) as a transmitter presents a viable approach to overcome the limitations of modulation bandwidth associated with transmitters and phosphors. Despite of these merits,

only a few studies have been reported for LD based VLC without a significant improvement in modulation bandwidth and data rate. In this dissertation, I discuss the materials, fabrication, and device characterization of III-nitride visible laser diodes on semipolar $(20\bar{2}\bar{1})$ orientation for high-speed performance. Furthermore, I demonstrated laser based white lighting communication system containing different phosphors in supporting the merits in high-speed data transmission resuling in world-record of high speed performance.

In the first part of this thesis, the initial VLC system by using commercial high-power laser diodes is discussed. It is important to study the capability of data transmission by utilizing the high-power designed laser diode because not only it suggests the guideline beyond the LED based VLC, but also high-power operation is necessary for LiFi application. Moreover, the bandwidth limiting effect by the phosphor commonly observed in LED based system is investigated for laser based system and an understanding of these effects is used to achieve high data rate of white lighting communication without filtering phosphor converted photons. In the second part of this thesis, the optimization of epitaxial structure, optical mode, and fabrication process of semipolar laser diodes are discussed. These include the relatively conventional structure with well-optimized topside ohmic n-type contact for high-speed microwave probing rather than backside n-type contact. Dynamic characteristics and a high-speed performance of LDs emitting at 410 nm are investigated resulting in a 3-dB bandwidth of 5 GHz and 5 Gbit/s direct

modulation with on-off keying (OOK), which were limited by the bandwidth of the photodetector used for the measurements. The differential gain of the LDs was determined to be $2.5 \pm 0.5 \times 10^{-16}$ cm^2 by comparing the slope efficiency for different cavity lengths. Analysis of the frequency response showed that the *K*-factor, the gain compression factor, and the intrinsic maximum bandwidth were 0.33 ns, 7.4×10^{-17} cm^3, and 27 GHz, respectively.

Finally, I will conclude with a demonstration of white lighting gigabit data transmission by utilizing red-, green-, and blue-emitting phosphors based on processed semipolar 410 nm LD. The advantage of near UV or violet LD in white lighting data communication involves lowest ambient light that can be significant noise level in other spectrum range.

Contents

1

Introduction

1.1 History of Visible Light Communication

The origin of visible light communication (VLC) traces back to signaling of smoke and fire many thousand of years ago. Reflecting sunlight onto a mirror is another way for long distance signaling. In 1880, the precursor to optical communication was invented by Alexander Graham Bell. The Photophone, utilized the sunlight to transmit a voice signal by vibrating reflecting mirror.[1] With the advent of quantum mechanics and semiconductors, the first light emitting diodes (LEDs) were demonstrated from several inventors. Notably, Nick Holonyak introduced the first visible laser diodes (LDs) emitting red as well as the first LEDs, both on gallium arsenide (GaAs).[2] His inventions with III-V semiconductor technology not only contributed to displays and lighting achievements, but also

ignited the field of optical communication. Typically, GaAs or indium phosphide (InP) material systems have been used for photonic devices such as LEDs, LDs, optical amplifiers, modulators, and photodetectors (PDs), since they have great epitaxial and optical merits. Specifically, AlGaAs/GaAs (typical emission wavelengths are 850 nm or 980 nm) and InGaAsP/InP (typical emission wavelengths are 1.3 μm for minima dispersion and 1.55 μm for minima loss in silica fiber) have been popularly developed for telecommunications. In fact, these studies contributed to all related fields including material science, solid-state physics, epitaxial techniques, device fabrication, and communication theories.

Many other researchers began to explore gallium nitride (GaN) and its alloys as alternative III-V materials to cover shorter wavelength in the visible range. Shuji Nakamura and other researchers (Akasaki and Amano) made a ground-breaking discovery that demonstrated high performing blue LEDs in 1993, which utilized GaN as an alternative III-V material.[3] Using the high efficiency and emission spectrum, GaN-based light emitters became one of the most popular applications for lighting, display, high-capacity optical data storage and projection displays. In addition to many existing applications, GaN-based visible light emitters, including LEDs and LDs, are also shown to have a great potential to be utilized in optical communication. The Nakagawa group in Japan demonstrated specific VLC prototypes and theoretical analysis using LEDs and photodetectors (PDs) in 2003.

Also, white LED-based indoor communication was proposed by T. Komine et al., from the Nakagawa group for the first time[4,5] and many studies have been performed in system development, equalization techniques, modulation schemes, and device improvements. The collaborative groups in United Kingdom and South Korea successfully demonstrated 100 Mbit/s of data rate by using a post-equalized commercial white LEDs.[6] More recently, a group in Scotland developed micro-sized LEDs for higher speed transmitter to minimize RC parasitic effect and maximize modulation bandwidth.[7–11] This dramatic improvement in the LEDs finally enabled for VLC to have the modulation bandwidth up to 1 GHz and data rates of Gbit/s. In parallel to the device development, modulation schemes, such as quadratic amplitude modulation (QAM) based orthogonal frequency division multiplexing, were also actively studied to efficiently increase data rate.[10] For indoor communication, new phosphor materials were studied to increase the modulation bandwidth of the white lighting.[12–15] The most recent approach was shown through utilizing the laser diode as a transmitter to achieve GHz bandwidth, which overcomes the theoretical limit of LEDs.[16–20]

1.2 Motivation

The growth of electronics, computing and mobile technologies enabled personal networking but is recently leading to an exponential data demand. According to many speculations, the spectral efficiency gains of mobile systems are slowing and expected to be saturated as shown in Fig 1.1.

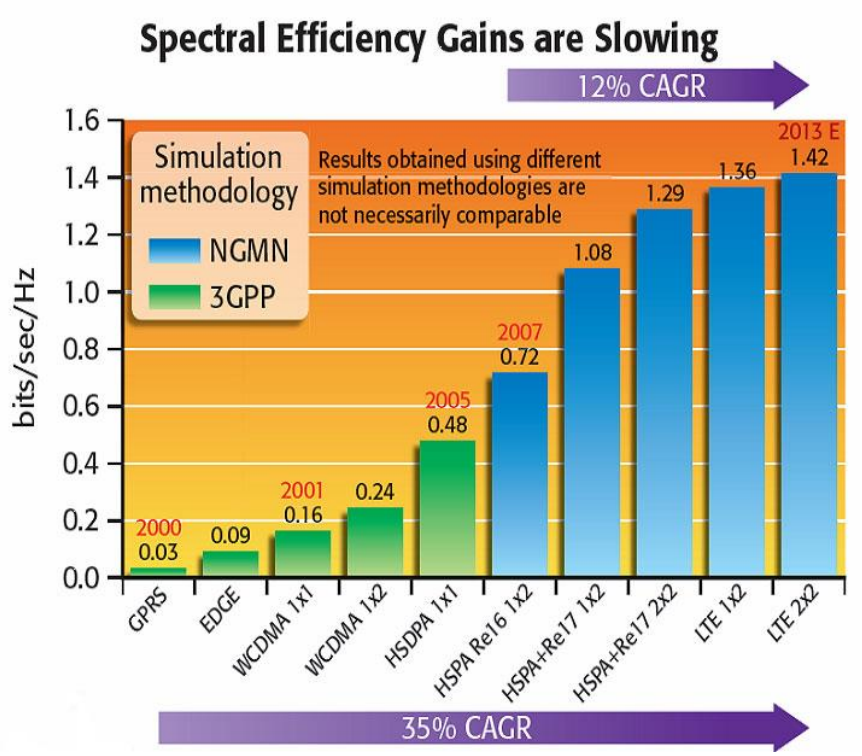

FIG. 1.1. Spectral efficiency gains versus new generations of communication technology over years.[21]

To support this explosive data demand, many efforts have been made to achieve high spectral efficiency and data rate in the radio frequency (RF) range of the electromagnetic spectrum (up to 300 MHz), which is conventionally used for wireless data transmission. Despite continued improvement in the fourth and fifth generation wireless networks (4G, 5G), it is predicted that the RF band will not be sufficient for the demand and eventually will become congested by limited spectral efficiency.[22] One of the available solutions is to share the other spectral bands rather than utilizing the RF band. One of the strong candidates is the visible spectrum ranging from 430 THz to 770 THz, which the spectral density is more than 1000 times wider than that of the RF spectral range as shown in Fig 1.2.

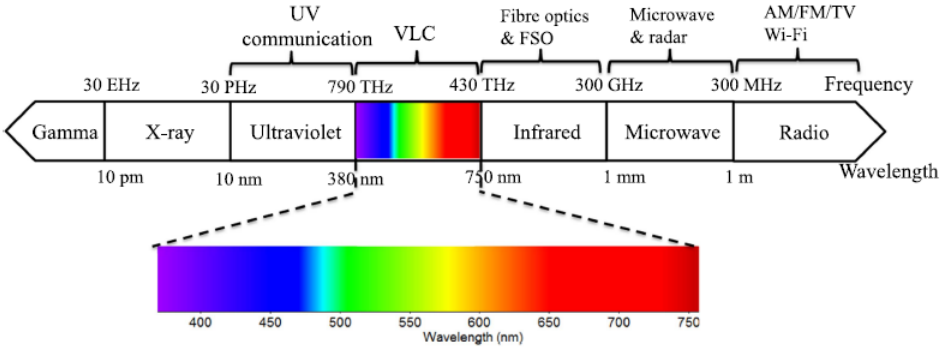

FIG. 1.2. The frequencies and wavelengths of the electromagnetic waves allocated for different communication technologies. (Wi-Fi: Wireless Fidelity, AM: Amplitude Modulation, FM: Frequency Modulation, and FSO: Free Space Optics)[23]

Even though a part of visible spectrum was already explored for fiber optic communication in near red color, utilizing the white color in free-space offers a

completely new technology with unexpected advantages. This white lighting communication is also known as “LiFi”, coined by Harald Haas in University of Edinburgh.[24] The technology is expected to be installed in light bulbs to satisfy both lighting and data transmission purposes. LiFi is a cost and energy efficient for the application for two purposes in one device. Since the optical spectrum does not penetrate any opaque obstacles, it is a highly secured communication technique for free space. Also, the same spectrum in the secured area can be reused without electromagnetic interferences in the other secured areas. In addition to LiFi applications, individual spectrum in visible range offers more advances in communications. Plastic optical fibers (POFs) have been popularly studied for alternative fiber optic communications due to the low attenuation in the blue to green spectrum.[25]

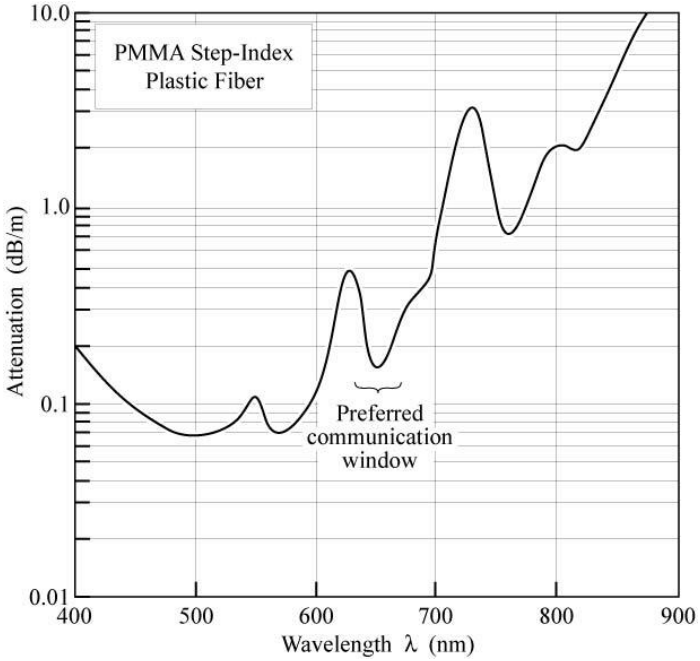

FIG. 1.3. The attenuation of a PMMA step-index plastic optical fiber. (Data sheet of Toray Industries Ltd., 2002)[25]

Blue LEDs or lasers have a high potential as a data transmitter in underwater communication with faster propagation than that of acoustic wave and lower seawater conductivity than RF.[26–28] The blue spectrum is also a candidate for transmitters in satellite-to-satellite communications due to its low beam divergence of the visible wavelength. More recently, there are increasing demands for visible laser based remote sensing (also called for Light Detection and Ranging: LIDAR) and free space data transmission in short range as autonomous technologies emerge.[29] Entertainment and toys are also another emerging market.[30] Thus, VLC

not only supports RF based wireless communication as a type of LiFi but also can be the excellent bridge fitting to other emerging technologies.

1.3 Challenges in Modulation Bandwidth

1.3.1 Optical Transmitters

Optical transmitters play a role in converting the electrical input signals to the optical output signals in optical communication system. LEDs have been one of the most popular transmitters for both fiber optic and free space communication. Since LEDs have several advantages over other transmitter technologies such as high efficiency, long-lasting reliability, compact size, small emissive area and cheap pricing, GaAs LEDs emitting IR light were first used in some local-area networks including short-range fiber optic communication. However, LEDs emit incoherent light containing a wide variety of light packets in different wavelengths, the signals have a significant loss and dispersion over the distance in the fiber. In addition to this temporal incoherence, LEDs are limited by the spatial incoherence resulting in a wide angle of the emission, low coupling efficiency to the fiber is another problem. For the free space transmitting applications, coupling efficiency and loss and dispersion in specific wavelengths are not considered to be the critical issues. However, low modulation bandwidth on the order of MHz from the nature

of spontaneous emission poses a critical factor hindering high speed operations. Many techniques have been investigated to improve these demerits.[31,32] Particularly, one study demonstrated that the modulation bandwidth was significantly improved from a few MHz up to several hundreds of MHz by developing resonant cavity light emitting diodes (RCLEDs) as a low power transmitter for fiber optics.[33]

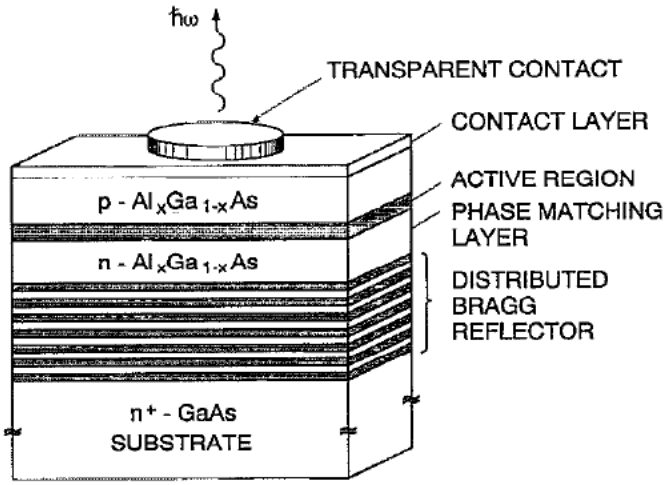

FIG. 1.4. Schematic of AlGaAs/GaAs RCLED with AlAs/AlGaAs mirrors[33]

For VLC applications, LEDs have been popularly used to satisfy the purpose of both indoor lighting and wireless communication. Early VLC researchers adopted commercial LEDs emitting white light as a transmitter in free space communication system.[6] However, comparatively large chip size (typically

0.1 ~ 1 mm^2) of commercial LEDs for lighting applications is associated with large RC parasitic which limits on the order of MHz.

One of the promising devices to improve bandwidth limit is micro-sized LED arrays. Micro-sized LEDs have a relatively small device size, (less than 100 μm^2) which can significantly reduce RC parasitic effects while maintaining a reasonable output power with its array for lighting purpose. *McKendry et al.* reported 245 MHz of the micro-sized LED pixel emitted at 450 nm, which can be translated into the data rate of 600 Mbit/s.[8] This result is comparable to that of the bandwidth of RCLEDs. However, micro-sized LEDs are more advantages than the RCLEDs in terms of the designing and processing microcavity. Following this work, more significant improvement was reported from same group of *McKendry* by demonstrating the segmented micro-sized LEDs exceeding 800 GHz.[11,34] Moreover, *Dinh et al.* achieved 1 GHz micro-sized LEDs by growing epitaxial structures on semi-polar GaN template.[35] Growing devices along semi-polar orientations could reduce the carrier recombination lifetime which is directly related to the theoretical bandwidth limit. A cyan micro-sized LED was also demonstrated with 1 GHz modulation bandwidth by optimizing epitaxial structure, which can be used for POF transmitter.[36] Despite of significant improvements, it is estimated that 1 GHz would be the theoretical limit of the LEDs with marginal room to improve. This limitation is supported by the theory that the recombination carrier

lifetime for spontaneous emission of LEDs can be as low as several nanoseconds which is converted to the modulation bandwidth (or 3 dB bandwidth, f_{3dB}) by the following equation:

$$f_{3\ dB} = \frac{\sqrt{3}}{2\pi\tau} \tag{1.1}$$

where τ is carrier lifetime. Thus, it is now expected that the development of high-speed LEDs is challenging to achieve a higher modulation bandwidth than 1 GHz. Even though many studies have been performed to improve the data rate by using complicated modulation schemes such as doubling and tripling quadrature amplitude modulation (QAM), a fundamental approach is preferred. Hence, replacing LEDs to LDs is potentially more beneficial to satisfy both high output power and modulation speed, which will be introduced in following chapters.

1.3.2 Color Converters

The primary application of LEDs is a light bulb emitting white light, which is called solid-state lighting. To generate white light, two or more wavelengths need to be mixed for an approximation of black body radiation. One way is to combine individual red, green, and blue LEDs. However, this method is commercially unfavorable due to high cost of the device and production. More preferred way is to use phosphor materials that absorb photons of single wavelength and emit

photons at another wavelength. One of the commonly used phosphor material is yellow emitting phosphor by which absorbing blue or ultraviolet (UV) photons, such as rare-earth-doped yttrium aluminum garnets (YAG:RE) due to its relatively high quantum efficiency. Another promising method is pumping red-, green-, and blue-emitting (RGB) phosphors by using UV or near UV light. This allows a significant improvement of the color rendering index (CRI), which indicates how the color quality is close to the sunlight. Figure 1.5 shows different ways to produce white light.

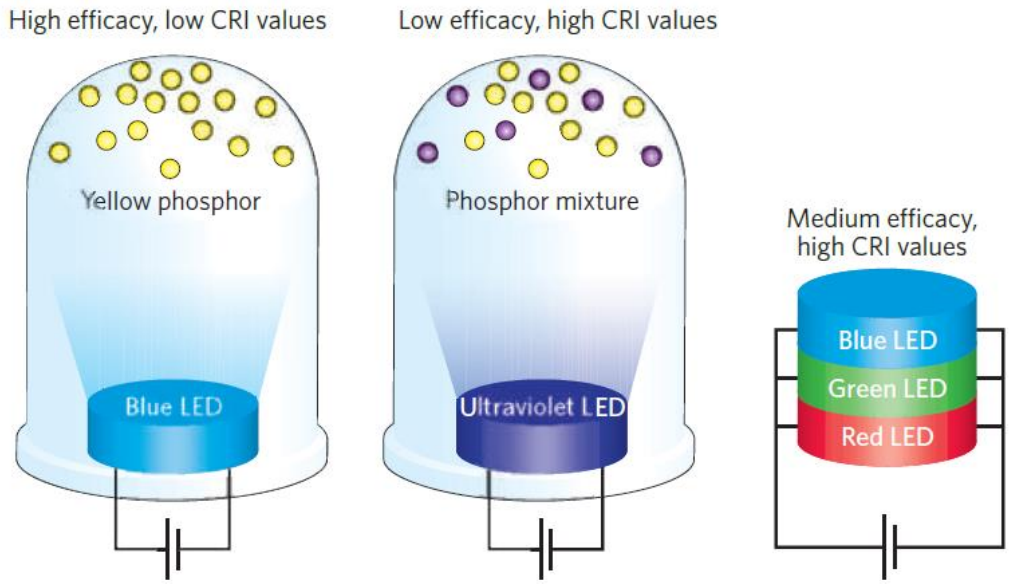

FIG. 1.5. Schematics of three dominant methods to produce white LEDs.[37]

However, phosphors are a critical limiting factor on the modulation bandwidth for communication applications. Previously, many studies were unsuccessful in demonstrating data transmission of white light commercial LED light bulbs, because the modulation bandwidth of the light bulb was significantly limited by the phosphor response rather than LED response as shown in Fig. 1.6.

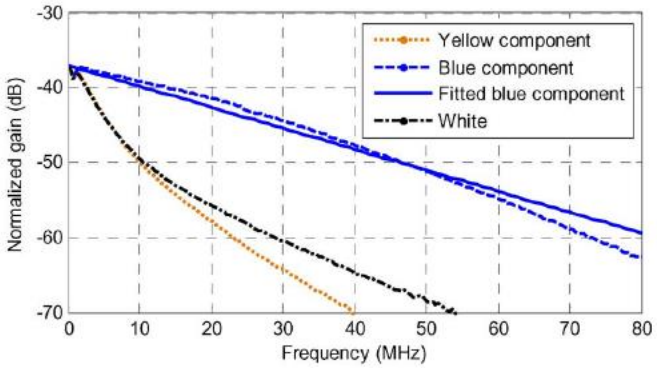

FIG. 1.6. Frequency response of commercial blue and white LEDs (LUXEON STAR)[6]

The limitation of white light LEDs is due to the long relaxation life time from the phosphor conversion process (on the order of μs). The relaxation life time is typically an order of magnitude slower than the LEDs (on the order of 10 ~ 100 ns). One of the solutions is to reject the yellow photons from phosphor conversion by adding an optical low pass filter, called blue filter, at the receiver at the cost of reduction in signal-to-noise ratio (SNR). Along with the development of higher speed LEDs, fast color converting materials were reported. Organic semiconductor materials were used as a color converter instead of phosphor materials with ~ 200

MHz of modulation bandwidth, which is 40 times higher than the commercially available phosphors.[12,13] More recently, Dursun et al. also demonstrated perovskite nanocrystals with the 491 MHz of phosphor bandwidth in laser-based VLC system.[14] Here, we will discuss more fundamental studies and potential advantages of laser based VLC using phosphors in later chapters.

1.4 Fundamental Dynamics of Laser Diodes

Dynamic characteristics for laser diodes are important not only to investigate modulation capability but also to study gain related physics. The small signal modulation technique is the method that adds a sinusoidal fluctuation in the injection current. The optical response of the lasers is directly coupled to the injected carriers by the stimulated emission. Thus, the small signal response can be derived from two rate equations in terms of injected carrier density and photon density in the cavity:[38]

$$\frac{dn}{dt} = \frac{\eta_i I}{qV} - \frac{n}{\tau} - v_g\left(g_{th} + \frac{dg}{dn}\Delta n\right)s \tag{1.2}$$

$$\frac{ds}{dt} = \Gamma v_g\left(g_{th} + \frac{dg}{dn}\Delta n\right)s - \frac{s}{\tau_p} \tag{1.3}$$

where n and s are the carrier and photon densities in the active region, respectively, η_i is the injection efficiency, I is the drive current, q is the electron charge, V is the

volume of the active layer, τ and τ_p are the carrier and photon (or cavity) lifetime, respectively, v_g is the group velocity, Γ is the optical confinement factor, and g_{th} is the threshold material gain. Under small signal conditions, a small fluctuation of gain is added onto the threshold gain by multiplying the differential gain, dg/dn, by the fluctuation in carrier density, Δn. The spontaneous emission that is coupled into the lasing mode is ignored far above the threshold for this modulation condition. The small signal modulation ($H(\omega)$) for both carriers and photons is proportional to a second-order transfer function:

$$H(\omega) = \frac{\omega_R^2}{\omega_R^2 + \omega^2 + j\omega\gamma} \tag{1.4}$$

where ω_R is the relaxation resonance frequency (or $f_R = \omega_R/2\pi$) and γ is the damping factor. Plotting the absolute value of $H(\omega)$ as a dB scale, $10\log|H(\omega)|^2$. This is important to analyze modulation characteristics as well as internal parameters such as –3 dB bandwidth, resonance frequency, bandwidth roll-off, damping factor, and gain compression factor. The modulation bandwidth is defined as typically –3 dB drops from DC level at 0 Hz of frequency. –3 dB is calculated to be a half of the power transferred from the transmitter to the receiver end.

$$f_R = \frac{1}{2\pi}\left[\frac{\Gamma v_g \frac{dg}{dn}}{qV}\eta_i(I - I_{th})\right]^{1/2} \tag{1.5}$$

Different from first order transfer function of the response of LEDs or PDs, the LDs have a second harmonic transfer function including a resonance point due to strong coupling of the carrier and the photon dynamics. Studying resonance characteristics offers a good estimation of theoretical maximum bandwidth as well as gain parameters. Particularly, differential gain, dg/dn, is an important parameter to estimate modulation capability as well as output power which is strongly related to the material properties and semipolar III-nitride materials expected to have high value, resulting in high modulation bandwidth. This will be discussed in detail in later chapter.

1.5 III-nitride Material System

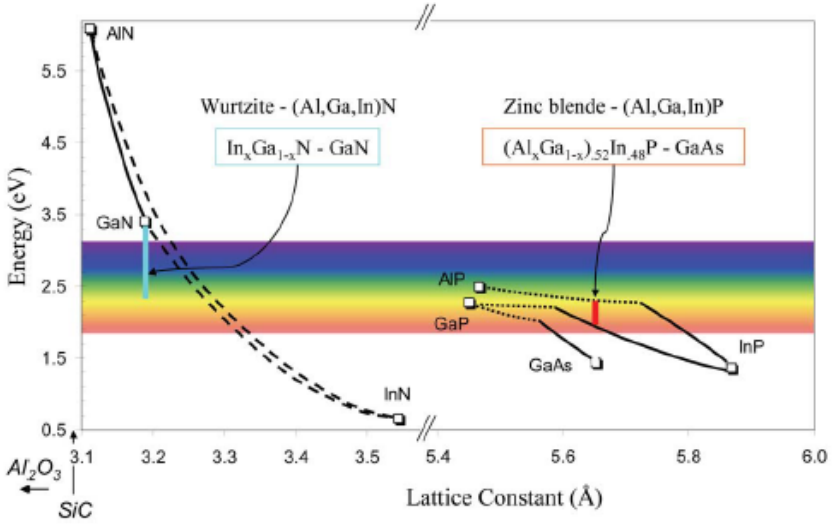

FIG. 1.7. Bandgap energy with respect to the lattice constant for wurtzite III-nitride and zinc blende III-phosphide material systems. The $(AlxGa_{1-x})_{.52}In_{.48}P$ is lattice-matched to GaAs and emission spectrum ranges from red to yellow. The $In_xGa_{1-x}N$ is heterogeneously grown on GaN and emission spectrum ranges from UV to yellow limited by strain and thermos-dynamical miscibility.[39]

III-nitride material system covers deep UV, near UV, violet, blue, and green emission from its direct bandgap energies ranging from 0.7 eV to 6.2 eV.[39] Figure 1.7. The advent of III-nitride materials quickly replaced II-VI material based inefficient LEDs and LDs, such as ZnSe, because of their high dislocation densities. Finally, III-nitride LEDs are widely used for efficient light bulbs, traffic signals, and display backlights. Also, III-nitride LDs were developed for optical data storage, pico projector, and laser headlights.[39] In addition to the light emission properties, high-frequency electronic device based on III-nitride have been

intensely investigated with the advantage of its high breakdown properties. Thus, III-nitride high electron mobility transistors (HEMTs) have been commercialized to meet the demand of power electronic devices as well as RF electronic devices.[40,41] Absorption of the light covering visible spectrum in III-nitride epitaxy facilitated the development of solar cells and UV photodetectors.[42–44] More recently, III-nitride LEDs and LDs have been spotlighted for LiFi devices as a great candidate in satisfying both lighting and communication roles. Despite of its wide usefulness, there are still many issues remaining to be solved in terms of physical property, material growth, and device fabrication.

1.5.1 Polarization Effect

Gallium Nitride (GaN) is the basis material to be alloyed by Indium (In) or Aluminum (Al) to form the energy bandgap of the visible spectrum. Most common and commercially available technology is to grow GaN and its alloy on sapphire substrate due to its low cost of wafer production. Typical GaN forms hexagonal Wurtzite crystal structure with cubic Zinc blend crystal structure that can also be formed in certain conditions. The polarization from asymmetry of Ga and N atoms exists along c-direction [0001] in Wurtzite crystal structure and induces internal electric field as shown in Fig. 1.8(a). This spontaneous polarization is combined

with piezoelectric polarization that depends on the strains of quantum wells (QWs) and the combined polarization generates strong internal electric field.[45] This internal electric field contributes to bend the energy bands in the QWs to the opposite direction of built-in electric field as shown in Fig. 1.8(b).

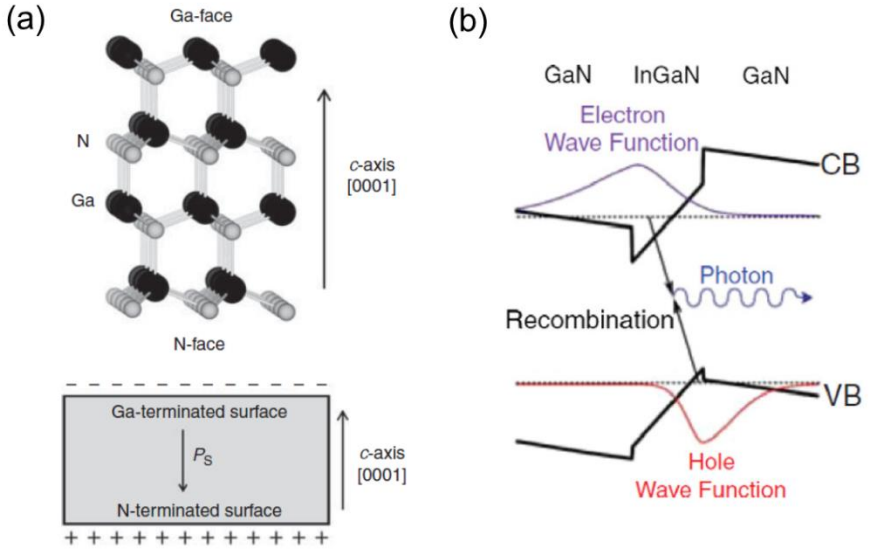

FIG. 1.8. (a) Crystal structure and spontaneous polarization of c-plane GaN. (b) Schematic of energy band near QWs in c-plane GaN.[46,47]

This unintentional band bending in QWs causes many issues related to the performance of LEDs and LDs, as also known as quantum confined Stark effect (QCSE).[48] As shown in Fig. 1.5(b), spatially separated wave-functions in the conduction and valence band reduces the overlap integral, leading to reduce the radiative internal efficiency. The effective band gap energy is lower than that of flat band, resulting in a red-shift of emission wavelength. Blue-shift also occurs due to

the combination of polarization screening and band filling as current density increases. In addition to wavelength shift, internal efficiency is dramatically reduced as the injection current density increases, due to the combination losses of carrier leakage and auger recombination, which is called efficiency droop. This can be explained by the ABC model and electron blocking layer (EBL) effect.[49] Different approaches have been proposed to reduce the polarization effect and QCSE by adding a thin AlGaN cap layer in thick QW,[50] using AlInGaN material,[51] or graded QW structures.[52] For recent a decade, research groups at UCSB have made significant efforts in droop improvement by using semipolar and nonpolar oriented substrates rather than c-plane.

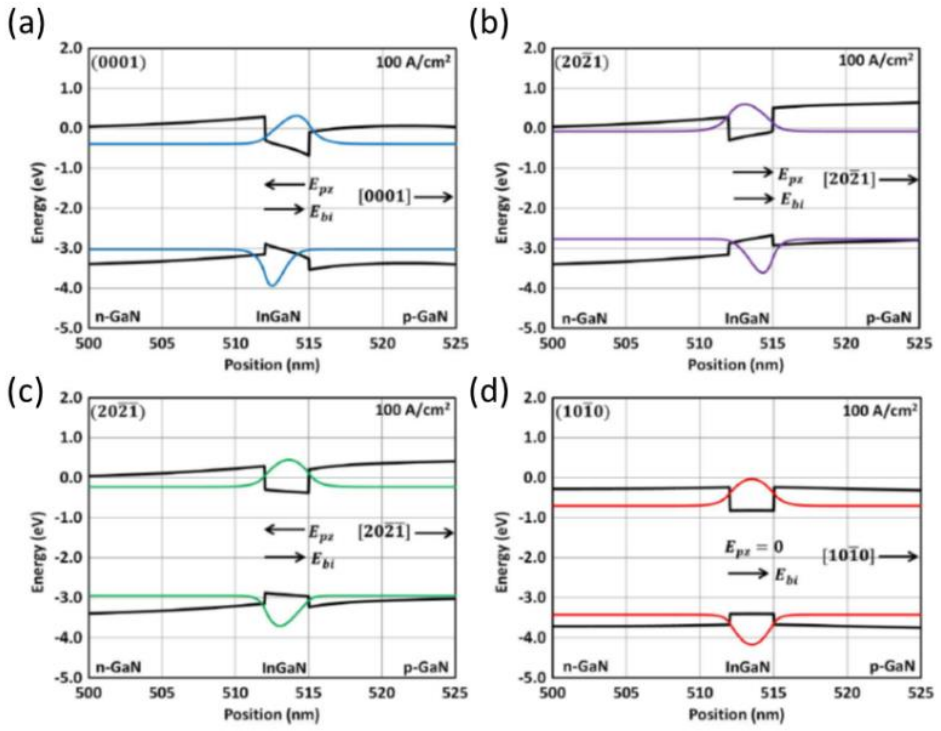

FIG. 1.9. Simulated energy band structures of polar c-plane (0001), semipolar ($\mathbf{20\bar{2}1}$), semipolar ($\mathbf{20\bar{2}1}$), and nonpolar ($\mathbf{10\bar{1}0}$) for 3 nm single QW including built-in and piezoelectric fields under 100 A/cm^3 bias.[53]

1.5.2 Semipolar/Nonpolar Laser Diode

Another approach to overcome the efficiency droop is using LDs rather than LEDs. In LDs, the carrier density in QWs is clamped after population inversion. Therefore, when lasing occurs, all additional injected carriers contribute in radiative recombination for stimulated emission and the droop associated with carrier density is also clamped. However, the peak external quantum efficiency (EQE) of *c*-plane

LDs is still as low as 20 % while EQE of LEDs already achieved near 80 %, as shown in Fig. 1.10.[54,55]

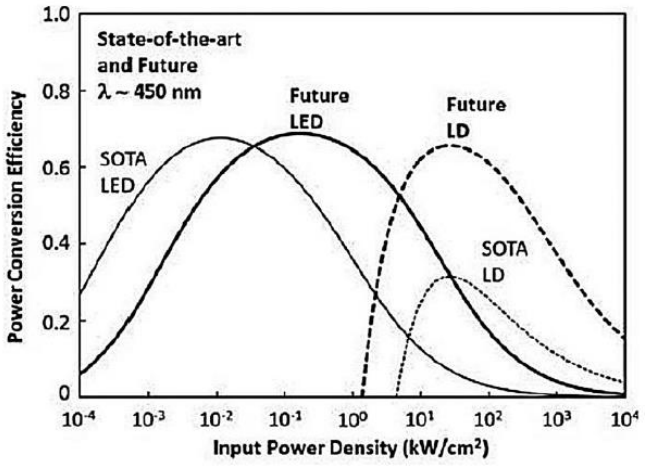

Figure 1.10 Comparison of state-of-the-art (SOTA), future blue LED, and LD.[55]

For LDs, a loss mechanism is based on the propagation of photons along the long cavity and optical gain which contribute to the efficiency but it can be achieved by overcoming the cavity loss. One of the reasons for low EQE is that the conventional III-nitride LDs have comparatively higher loss and lower gain than GaAs/AlGaAs LDs due to its subband structures of wurtzite GaN. Anisotropic biaxial strain of heterogeneous epitaxy usually reduces the valence band density of states (DOS) by splitting the subbands of valence band (HH1, HH2, or LH). By doing so, it is easier to overcome the loss and reach the population inversion, which in turn, generates optical gain, under injected carrier density and reduction in threshold current

density in typical GaAs/AlGaAs. However, III-nitride LDs do not have significant effects on both the separation of the topmost valence subbands and the reduction of threshold current density compared to other III-V QW LDs due to the isotropic in-plane strain on c-plane.[56,57]

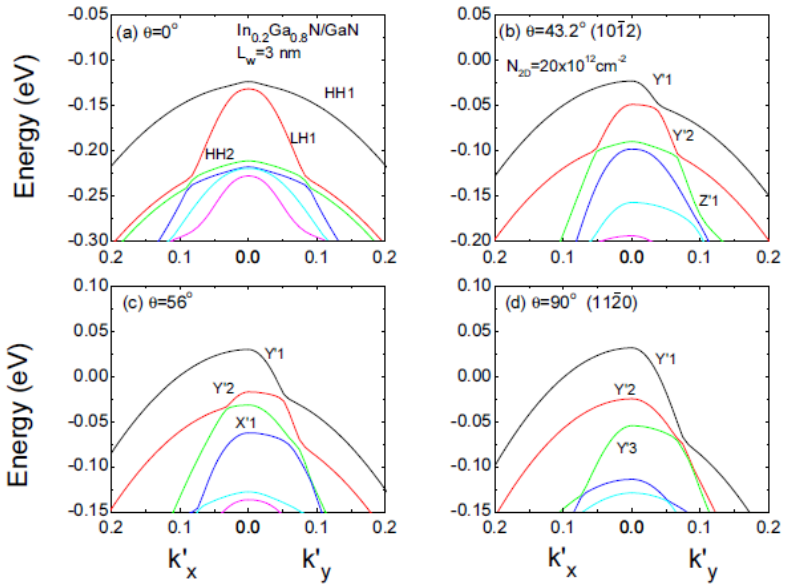

FIG. 1.11. Simulations of topmost valence subband structures for $In_{0.2}Ga_{0.8}N$/GaN QW structures (a width of QW, L_w =3 nm) with the angle along c-plane (0001) from θ = 0 ° to θ = 90 °. (Note: semipolar ($\mathbf{20\bar{2}1}$), θ = 105 °)[58]

Semipolar and nonpolar crystal plane have been predicted to break the balance of the in-plane strain, resulting in reduced DOS and threshold current density.[58] As shown in Fig. 9(a), an increased overlap integral of electron and hole wavefunctions also contributes to increase the radiative recombination rate leading to a low threshold current density and high optical gain.[59,60] Figure. 9(b) shows the

gain spectra for different crystal angles from 0 º (c-plane) to 90 º (a-plane). Nonpolar plane including a-plane $(1\bar{1}00)$ and m-plane $(10\bar{1}0)$ is expected to be most effective for reducing the threshold current density and increasing the material gain as well as improving QCSE. However, some of the well-known material issues including surface morphology,[61] basal plane stacking faults,[61] carrier localization associated with widen emission wavelength,[62] and low indium uptake on nonpolar planes[63] triggered a serious consideration of utilizing the semipolar $(20\bar{2}\bar{1})$ plane.

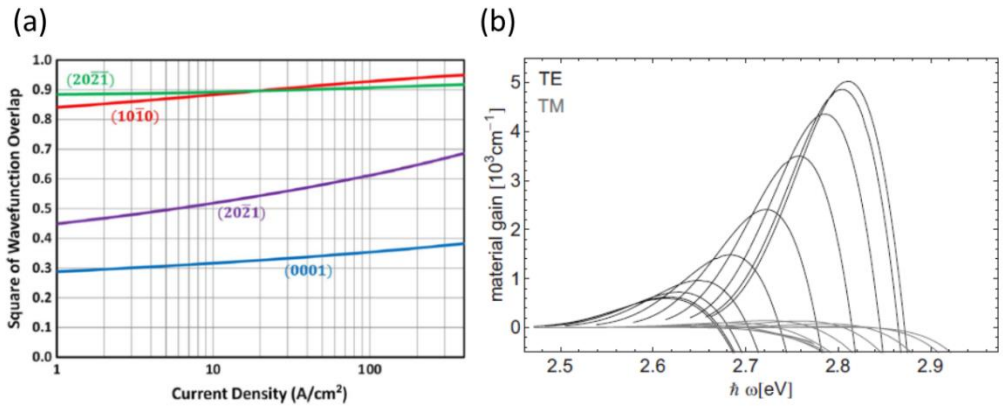

FIG. 1.12. (a) Simulated overlap integral of wavefunctions for $In_{0.23}Ga_{0.77}N$ SQW (L_w = 0.3 nm) for different crystal orientations. (b) Gain spectra of different crystal angles from c-plane, θ = 0 º to a- or m-plane, θ = 90 º, from left to right, with 10 º steps. (Note: semipolar $(\mathbf{20\bar{2}\bar{1}})$, θ = 105 º)[53,60]

The semipolar plane is a good compromise in overlap integral and its material gain shown in Fig. 1.12(a). Thus, semipolar LDs have been actively studied for high EQE and wall-plug efficiency (WPE) applications. In addition to these output

power properties, the semipolar and nonpolar LDs have a high differential gain which can increase the modulation bandwidth for high-speed application as seen in the equation x in previous chapter 1.4. Hence, semipolar and nonpolar crystal plane are also suitable substrates to develop high-speed LDs with material and physical proofs.

1.5.3 High-speed III-nitride Laser Diodes

High-speed LDs of AlGaAs/GaAs and InGaAsP/InP system have actively been developed for more than 50 years since the first LDs was reported in 1962.[64] In these material system, vertical cavity surface emitting lasers (VCSELs) and distributed feedback lasers (DFB) have already achieved more than 50 Gbit/s of data rate and 30 GHz of modulation bandwidth.[65,66] Beyond focusing on high-speed performance, now high-speed LDs can operate on silicon substrate for CMOS compatible process.[67,68]

For III-nitride LDs, most of studies focused on high power and efficient performance for display and lighting applications. Also, more complicated material and device issues than other III-V systems hindered to expectations. Prior to the many studies that focused on high speed characteristics, several researchers performed small signal modulation to analyze gain parameters. A research group

in Osram Inc. reported the transfer function data including 1.5 GHz of – 3 dB bandwidth for blue LDs grown on c-plane in 2010.[69] Similar studies on gain analysis have reported 2.4 GHz and 3.1 GHz of – 3 dB bandwidth for red-emitting quantum dot (QD) and nanowire (NW) LDs, respectively, even though the epitaxial structures and devices are governed by different physical phenomenon from QW LDs.[70,71] With the advent of VLC and LiFi market, researchers began to demonstrate data rate as well as modulation bandwidth by setting up data transmission system. Initial works demonstrated using only blue LD with on-off keying (OOK) modulation. 1.4 GHz of – 3 dB bandwidth and 2.5 Gbit/s were reported from the 422 nm emitting LDs grown on c-plane by a research group from TopGaN Inc. and University of Glasgow in 2013.[18] Then, UCSB has demonstrated 2.6 GHz of – 3 dB bandwidth and 4 Gbit/s of OOK data rate by using high power designed blue LD.[16] Even though many researches have improved data rates by developing novel modulation scheme and system, the development of high speed LDs has not been reported. This was because majority of device researches had been focusing on optimization of LEDs as a transmitter, and only limited research groups had proper facility capability of developing high performing LDs. Hence, there is a great need for developing high speed III-nitride LDs and studying the dynamic characteristics of III-nitride LDs for high speed performance.

1.6 Synopsis of the dissertation

This dissertation reports the visible light communication system and device development of high speed semipolar (20-2-1) plane InGaN/GaN edge emitting LDs. As my work is the first high-speed studies for III-nitride LDs and their system at UCSB, this dissertation introduces the initial technical approaches followed by conclusions including significant achievements. Furthermore, the studies on optical communication system for visible LDs are described in a support for the high-speed measurement, emphasizing the development and physical analysis of high-speed LDs. My work includes not only the world records for visible LD optical communication speed, but also in-depth analysis of the physical mechanisms.

Chapter 2 introduces the initial results of free space optical measurement by using commercially available high power blue LDs. The characteristics of output power and modulation of high power designed LD were reported. The system was meticulously investigated including bandwidth limiting factors predictions. Limitations of the early work suggested the motivation for the development of higher speed LDs than commercial LDs. Despite of limitations, the potentials of this optical system enabled to be expanded for white lighting data transmission as a LiFi demonstration.

CHAPTER 1. INTRODUCTION

Chapter 3 describes a study on the development of high speed III-nitride violet LD grown on semipolar $(20\bar{2}\bar{1})$ plane. The epitaxial structure grown by metalorganic chemical vapor deposition (MOCVD) was explored in terms of QWs, waveguides (WGs), and contact layers. The two-dimensional optical mode simulations were also studied for optical confinement and internal loss. DC performance including CW *L-I-V* and spectral characteristics were necessary to be studied prior to the modulation studies. Small and large signal modulation were performed resuing in the modulation bandwidth of 5 GHz and data rate of 6 Gbit/s as highest values among III-nitride QW LDs. Furthermore, internal loss and optical modal gain were studied, and differential gain was calculated to be significantly higher value comparable with other III-V materials, which is reported at the first time for semipolar III-nitride. Finally, important dynamic parameters were extracted from *L-I-V* and modulation characteristics including damping factor, *K*-factor, and intrinsic maximum bandwidth. This is the first report for these dynamic parameters in III-nitride, which is expected to play a significant role in LiFi and VLC applications in near future.

In Chapter 4, I have demonstrated data transmission of white light generated by a direct modulation with previously discussed violet LD using red-, green-, and blue-emitting phosphors. High color rendering index (CRI) of 79 and low correlated color temperature (CCT) of 4050 K were achieved. 1.25 Gbit/s free-

space data transmission rate was achieved by NRZ-OOK modulation. More significantly, the measured spectral data under ambient sunlight shown near-ultraviolet laser as a transmitter has the potential advantage of lower spectral overlap under sunlight in regards to signal-to-noise ratio (SNR) of data transmission link.

References

[1] A.G. Bell, J. Franklin Inst. **110**, 237 (1880).

[2] N. Holonyak, IEEE J. Quantum Electron. **23**, 684 (1987).

[3] S. Nakamura, T. Mukai, and M. Senoh, Appl. Phys. Lett. **64**, 1687 (1994).

[4] T. Komine and M. Nakagawa, IEEE Trans. Consum. Electron. **50**, 100 (2004).

[5] T. Komine and M. Nakagawa, IEEE Trans. Consum. Electron. **49**, 71 (2003).

[6] H. Le Minh, D. O'Brien, G. Faulkner, L. Zeng, K. Lee, D. Jung, Y. Oh, and E.T. Won, IEEE Photonics Technol. Lett. **21**, 1063 (2009).

[7] J. McKendry, B.R. Rae, Zheng Gong, K.R. Muir, B. Guilhabert, D. Massoubre, E. Gu, D. Renshaw, M.D. Dawson, and R.K. Henderson, IEEE Photonics Technol. Lett. **21**, 811 (2009).

[8] J.J.D. McKendry, R.P. Green, A.E. Kelly, Z. Gong, B. Guilhabert, D. Massoubre, E. Gu, and M.D. Dawson, IEEE Photonics Technol. Lett. **22**, 1346 (2010).

[9] J.J.D. McKendry, D. Massoubre, S. Zhang, B.R. Rae, R.P. Green, E. Gu, R.K. Henderson, A.E. Kelly, and M.D. Dawson, J. Light. Technol. **30**, 61 (2012).

[10] D. Tsonev, H. Chun, S. Rajbhandari, J.J.D. McKendry, S. Videv, E. Gu, M. Haji, S. Watson, A.E. Kelly, G. Faulkner, M.D. Dawson, H. Haas, and D. O'Brien, IEEE Photonics Technol. Lett. **26**, 637 (2014).

[11] R.X.G. Ferreira, E. Xie, J.J.D. McKendry, S. Rajbhandari, H. Chun, G. Faulkner, S. Watson, A.E. Kelly, E. Gu, R. V. Penty, I.H. White, D.C. O'Brien, and M.D. Dawson, IEEE Photonics Technol. Lett. **28**, 2023 (2016).

[12] C. Hyunchae, P. Manousiadis, S. Rajbhandari, D.A. Vithanage, G. Faulkner, D. Tsonev, J.J.D. McKendry, S. Videv, E. Xie, E. Gu, M.D. Dawson, H. Haas, G.A. Turnbull, I.D.W. Samuel, D.C. O'Brien, Hyunchae Chun, P. Manousiadis, S. Rajbhandari, D.A. Vithanage, G. Faulkner, D. Tsonev, J.J.D. McKendry, S. Videv, Enyuan Xie, Erdan Gu, M.D. Dawson, H. Haas, G.A. Turnbull, I.D.W. Samuel, and D.C. O'Brien, IEEE Photonics Technol. Lett. **26**, 2035 (2014).

[13] M.T. Sajjad, P.P. Manousiadis, H. Chun, D.A. Vithanage, S. Rajbhandari, A.L. Kanibolotsky, G. Faulkner, D. O'Brien, P.J. Skabara, I.D.W. Samuel, and G.A. Turnbull, ACS Photonics **2**, 194 (2015).

[14] I. Dursun, C. Shen, M.R. Parida, J. Pan, S.P. Sarmah, D. Priante, N. Alyami, J. Liu, M.I. Saidaminov, M.S. Alias, A.L. Abdelhady, T.K. Ng, O.F. Mohammed, B.S. Ooi, and O.M. Bakr, ACS Photonics **3**, 1150 (2016).

[15] M.F. Leitao, J.M.M. Santos, B. Guilhabert, S. Watson, A.E. Kelly, M.S. Islim, H. Haas, M.D. Dawson, and N. Laurand, IEEE J. Sel. Top. Quantum Electron. **23**, 1 (2017).

[16] C. Lee, C. Zhang, M. Cantore, R.M. Farrell, S.H. Oh, T. Margalith, J.S. Speck, S. Nakamura, J.E. Bowers, and S.P. DenBaars, Opt. Express **23**, 16232 (2015).

[17] J.R.D. Retamal, H.M. Oubei, B. Janjua, Y.-C. Chi, H.-Y. Wang, C.-T. Tsai, T.K. Ng, D.-H. Hsieh, H.-C. Kuo, M.-S. Alouini, J.-H. He, G.-R. Lin, and B.S. Ooi, Opt. Express **23**, 33656 (2015).

[18] S. Watson, M. Tan, S.P. Najda, P. Perlin, M. Leszczynski, G. Targowski, S. Grzanka, and A.E. Kelly, Opt. Lett. **38**, 3792 (2013).

[19] B. Janjua, H.M. Oubei, J.R.D. Retamal, T.K. Ng, C.-T. Tsai, H.-Y. Wang, Y.-C. Chi, H.-C. Kuo, G.-R. Lin, J.-H. He, and B.S. Ooi, Opt. Express **23**, 18746 (2015).

[20] D. Tsonev, S. Videv, and H. Haas, Opt. Express **23**, 1627 (2015).

[21] Harald Haas, (n.d.).

[22] C.-X. Wang, F. Haider, X. Gao, X.-H. You, Y. Yang, D. Yuan, H. Aggoune, H. Haas, S. Fletcher, and E. Hepsaydir, IEEE Commun. Mag. **52**, 122 (2014).

[23] S. Rajbhandari, J.J.D. McKendry, J. Herrnsdorf, H. Chun, G. Faulkner, H. Haas, I.M. Watson, D. O'Brien, and M.D. Dawson, Semicond. Sci. Technol. **32**, 23001 (2017).

[24] Harald Haas, *Harald Haas: Wireless Data from Every Light Bulb | TED Talk | TED.com* (TED, 2011).

[25] E.F. Schubert, *Light-Emitting Diodes* (2006).

[26] H.M. Oubei, C. Li, K.-H. Park, T.K. Ng, M.-S. Alouini, and B.S. Ooi, Opt. Express **23**, 20743 (2015).

[27] H.M. Oubei, J.R. Duran, B. Janjua, H.-Y. Wang, C.-T. Tsai, Y.-C. Chi, T.K. Ng, H.-C. Kuo, J.-H. He, M.-S. Alouini, G.-R. Lin, and B.S. Ooi, Opt. Express **23**, 23302 (2015).

[28] C. Shen, Y. Guo, H.M. Oubei, T.K. Ng, G. Liu, K.-H. Park, K.-T. Ho, M.-S. Alouini, and B.S. Ooi, Opt. Express **24**, 25502 (2016).

[29] P. Luo, Z. Ghassemlooy, H. Le Minh, E. Bentley, A. Burton, and X. Tang, in *2014 9th Int. Symp. Commun. Syst. Networks Digit. Sign* (IEEE, 2014), pp. 1011–1016.

[30] G. Corbellini, K. Aksit, S. Schmid, S. Mangold, and T. Gross, IEEE Commun.

Mag. **52**, 72 (2014).

[31] C.A. Burrus and R.W. Dawson, Appl. Phys. Lett. **17**, 97 (1970).

[32] E.F. Schubert, Y. - H. Wang, A.Y. Cho, L. - W. Tu, and G.J. Zydzik, Appl. Phys. Lett. **60**, 921 (1992).

[33] M. Guina, S. Orsila, M. Dumitrescu, M. Saarinen, P. Sipila, V. Vilokkinen, B. Roycroft, P. Uusimaa, M. Toivonen, and M. Pessa, IEEE Photonics Technol. Lett. **12**, 786 (2000).

[34] M.S. Islim, R.X. Ferreira, X. He, E. Xie, S. Videv, S. Viola, S. Watson, N. Bamiedakis, R. V. Penty, I.H. White, A.E. Kelly, E. Gu, H. Haas, and M.D. Dawson, Photonics Res. **5**, A35 (2017).

[35] D. V. Dinh, Z. Quan, B. Roycroft, P.J. Parbrook, and B. Corbett, Opt. Lett. **41**, 5752 (2016).

[36] J. Vinogradov, R. Kruglov, R. Engelbrecht, O. Ziemann, J.-K. Sheu, K.-L. Chi, J.-M. Wun, and J.-W. Shi, IEEE Photonics J. **9**, 1 (2017).

[37] S. Pimputkar, J.S. Speck, S.P. DenBaars, and S. Nakamura, Nat. Photonics **3**, 180 (2009).

[38] L.A. Coldren, S.W. Corzine, and M.L. Masanovic, *Diode Lasers and Photonic Integrated Circuits*, 2nd ed. (John Wiley & Sons, Inc., Hoboken, NJ, USA, 2012).

[39] M.R. Krames, O.B. Shchekin, R. Mueller-Mach, G.O. Mueller, L. Zhou, G. Harbers, and M.G. Craford, J. Disp. Technol. **3**, 160 (2007).

[40] U.K. Mishra, P. Parikh, and Yi-Feng Wu, Proc. IEEE **90**, 1022 (2002).

[41] U.K. Mishra, Shen Likun, T.E. Kazior, and Yi-Feng Wu, Proc. IEEE **96**, 287 (2008).

[42] C.J. Neufeld, N.G. Toledo, S.C. Cruz, M. Iza, S.P. DenBaars, and U.K. Mishra, Appl. Phys. Lett. **93**, 143502 (2008).

[43] R.M. Farrell, C.J. Neufeld, S.C. Cruz, J.R. Lang, M. Iza, S. Keller, S. Nakamura, S.P. DenBaars, U.K. Mishra, and J.S. Speck, Appl. Phys. Lett. **98**, 201107 (2011).

[44] E. Monroy, F. Omn s, and F. Calle, Semicond. Sci. Technol. **18**, R33 (2003).

[45] F. Bernardini, V. Fiorentini, and D. Vanderbilt, Phys. Rev. B **56**, R10024 (1997).

[46] J.S. Speck and S.F. Chichibu, MRS Bull. **34**, 304 (2009).

[47] S.P. DenBaars, D. Feezell, K. Kelchner, S. Pimputkar, C.-C. Pan, C.-C. Yen, S. Tanaka, Y. Zhao, N. Pfaff, R. Farrell, M. Iza, S. Keller, U. Mishra, J.S. Speck, and S. Nakamura, Acta Mater. **61**, 945 (2013).

[48] M. Leroux, N. Grandjean, M. Laügt, J. Massies, B. Gil, P. Lefebvre, and P. Bigenwald, Phys. Rev. B **58**, R13371 (1998).

[49] J. Piprek, Phys. Status Solidi **207**, 2217 (2010).

[50] S.-H. Park, J. Park, and E. Yoon, Appl. Phys. Lett. **90**, 23508 (2007).

[51] S.-H. Park and D. Ahn, J. Appl. Phys. **112**, 43107 (2012).

[52] H. Zhao, G. Liu, J. Zhang, J.D. Poplawsky, V. Dierolf, and N. Tansu, Opt. Express **19**, A991 (2011).

[53] D.F. Feezell, J.S. Speck, S.P. DenBaars, and S. Nakamura, J. Disp. Technol. **9**, 190 (2013).

[54] J.Y. Tsao, M.H. Crawford, M.E. Coltrin, A.J. Fischer, D.D. Koleske, G.S. Subramania, G.T. Wang, J.J. Wierer, and R.F. Karlicek, Adv. Opt. Mater. **2**, 809 (2014).

[55] C. Weisbuch, M. Piccardo, L. Martinelli, J. Iveland, J. Peretti, and J.S. Speck, Phys. Status Solidi **212**, 899 (2015).

[56] M. Suzuki and T. Uenoyama, Jpn. J. Appl. Phys. **35**, 1420 (1996).

[57] S.-H. Park, Jpn. J. Appl. Phys. **42**, L170 (2003).

[58] S.-H. Park and D. Ahn, in *Proc. SPIE 8625, Gall. Nitride Mater. Devices VIII*, edited by J.-I. Chyi, Y. Nanishi, H. Morkoç, J. Piprek, E. Yoon, and H. Fujioka (International Society for Optics and Photonics, 2013), p. 862511.

[59] D. Sizov, R. Bhat, J. Napierala, C. Gallinat, K. Song, D. Allen, and C. Zah, Phys. Status Solidi **207**, 1309 (2010).

[60] W.G. Scheibenzuber, U.T. Schwarz, R.G. Veprek, B. Witzigmann, and A. Hangleiter, Phys. Rev. B - Condens. Matter Mater. Phys. **80**, 115320 (2009).

[61] R.M. Farrell, E.C. Young, F. Wu, S.P. DenBaars, and J.S. Speck, Semicond. Sci. Technol. **27**, 24001 (2012).

[62] V. Liuolia, A. Pinos, S. Marcinkevičius, Y.D. Lin, H. Ohta, S.P. DenBaars, and S. Nakamura, Appl. Phys. Lett. **97**, 151106 (2010).

[63] J.E. Northrup, Appl. Phys. Lett. **95**, 133107 (2009).

[64] R.N. Hall, G.E. Fenner, J.D. Kingsley, T.J. Soltys, and R.O. Carlson, Phys. Rev. Lett. **9**, 366 (1962).

[65] D. Kuchta, A. V. Rylyakov, C.L. Schow, J. Proesel, C. Baks, P. Westbergh, J.S. Gustavsson, and A. Larsson, in *Opt. Fiber Commun. Conf.* (OSA, Washington, D.C., 2014), p. Th3C.2.

[66] W. Kobayashi, T. Ito, T. Yamanaka, T. Fujisawa, Y. Shibata, T. Kurosaki, M. Kohtoku, T. Tadokoro, and H. Sanjoh, IEEE J. Sel. Top. Quantum Electron. **19**, 1500908 (2013).

[67] D. Liang and J.E. Bowers, Nat. Photonics **4**, 511 (2010).

[68] C. Zhang, S. Srinivasan, Y. Tang, M.J.R. Heck, M.L. Davenport, and J.E. Bowers, Opt. Express **22**, 10202 (2014).

[69] J. Müller, M. Scheubeck, M. Sabathil, G. Brüderl, D. Dini, S. Tautz, T. Lermer, A. Breidenassel, and S. Lutgen, Appl. Phys. Lett. **96**, 131105 (2010).

[70] T. Frost, A. Banerjee, and P. Bhattacharya, Appl. Phys. Lett. **103**, 211111 (2013).

[71] S. Jahangir, T. Frost, A. Hazari, L. Yan, E. Stark, T. LaMountain, J.M. Millunchick, B.S. Ooi, and P. Bhattacharya, Appl. Phys. Lett. **106**, 71108

(2015).

2

Laser-based VLC System

2.1 Introduction

Great progress has been reported for high-speed data transmission using LEDs as a visible light transmitter from many different groups.[1–4] However, high-speed modulation of phosphor-based LED white light has been significantly hindered by the long relaxation time of the phosphor (On the order of 100s ns ~ several μs),[5] long spontaneous carrier lifetimes (On the order of ns),[6] and large RC parasitics,[7] limiting the transmission capacity of the VLC. Furthermore, LEDs suffer a loss in external quantum efficiency (EQE) as operating current increases, commonly known as "efficiency droop".[8] In contrast to LEDs, laser diodes (LDs) do not exhibit efficiency droop and have faster relaxation times above lasing threshold. The output power and external quantum efficiency (EQE) of LDs

increase monotonically with input current without significant efficiency droop.[9] Recent study by Cantore *et al*. demonstrated 442 nm laser based white lighting using YAG:Ce phosphor with a luminous efficacy of 86.7 lm/W.[10] As such, it should be possible to create a high-speed laser-based VLC that still leverages a white lighting system. Laser-based VLC will suffer less from the phosphor response than LED systems due to its higher power operation at high current density and larger inherent bandwidth than LEDs.

In this chapter, the first novel high-speed VLC measurement limited by the bandwidth of 450 nm LD with a UV-extended high-speed PD. The system specifically includes a UV-extended high-speed Si PD for GHz level bandwidth measurement in blue range, which has not been reported. Also, data transmission from unfiltered white light generated by direct modulation of a 450 nm LD exciting YAG:Ce phosphors. The effect of phosphors on the modulation characteristic is investigated, and it is observed that the modulation bandwidth was not limited by the phosphor.

2.2 Early Work

2.2.1 Commercial Blue Laser and System

As an early work, setting up the free space optical system and calibrating the optical components were first required due to the absence of RF setup for violet-blue spectra at UCSB. It has another importance for testing high-power designed, packaged, and stable operating LDs for high-power illuminating LiFi demonstration. For our early system, commercially available 450 nm laser diode was used as a transmitter by extracting from a Casio XJ-M140 projector. The laser diode, had a cavity length of 1150 μm, ridge width of 15 μm, and a 10 μm current aperture, as shown in Fig. 2.1(a). Scanning electron microscopy (SEM) image of packaged LD in TO can is shown in Fig. 2.1(b).

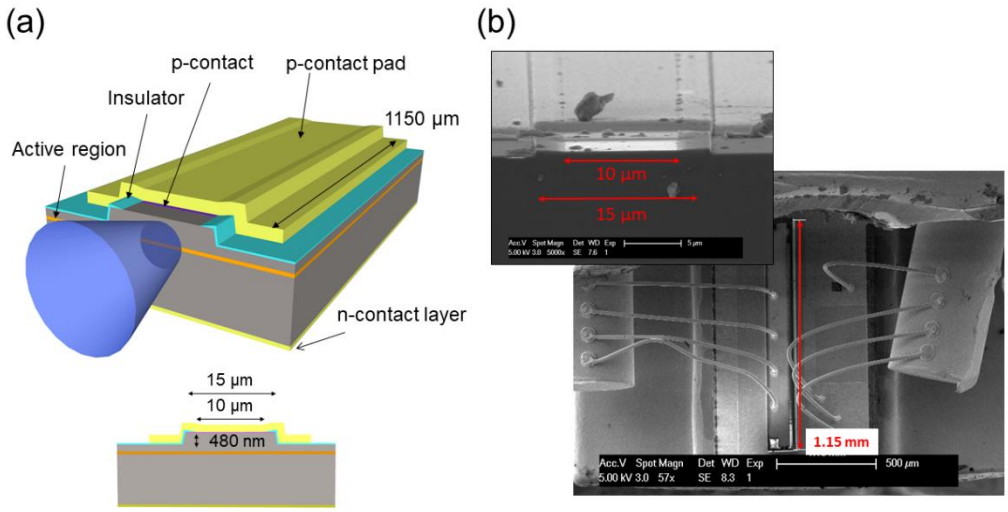

FIG. 2.1. (a) Illustration of the edge emitting laser design. (b) Scanning electron microscopy (SEM) image of LD in the TO package. Reprinted with permission from OSA Publishing[11]

Continuous wave (CW) operation of this wide ridge laser is necessary for direct modulation. The light-current-voltage (*L-I-V*) characteristics and spectrum were measured to determine the large signal properties of the laser diode by Keithley . For the frequency response measurement shown in Fig. 2.2, a sinusoidal signal with small RF power (0 dBm ~ 10 dBm) generated by an RF signal generator (R&S SMF100A) was directly modulated on top of a DC bias baseline using a bias-tee (Mini-Circuit ZFBT - 6GW). The signal of the CW laser diode was transmitted to a high-speed silicon photodiode with a 0.13 ~ 0.14 A/W responsivity at 450 nm (ALPHALAS UPD-50-UP). The light output from laser diode traversed about 15 cm of free space and then was collected into the photo detector via a 0.25 NA lens.

The received signal was measured by a digital component analyzer (DCA, Agilent 86100C) at different drive currents. To determine the high data rate characteristics of the blue laser diode, a pseudo-random bit sequence (PRBS) from a pattern generator (Anritsu MP1763C) was added at each DC operating bias and eye diagrams were measured by the DCA as depicted in Fig. 2.2.

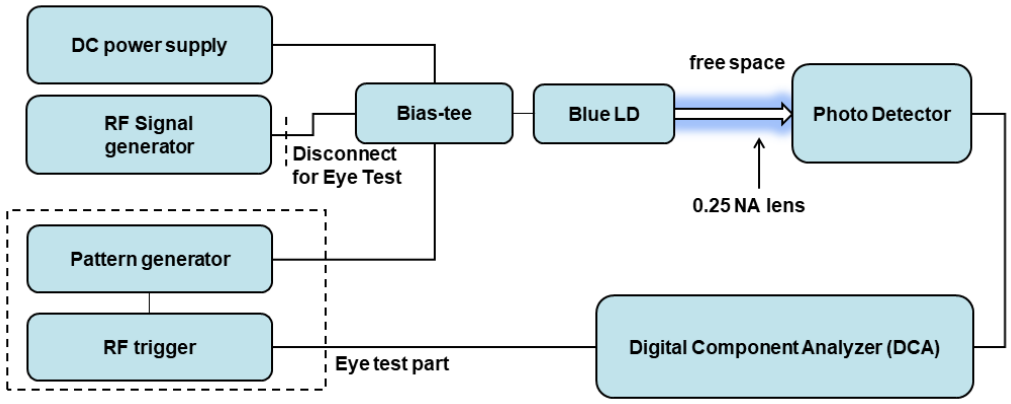

FIG. 2.2. Block diagram of free space optical measurement for a small signal modulation and an eye diagram of data transmission. Reprinted with permission from OSA Publishing[11]

Table 2.1 shows the bandwidth limit of each component in the measurement system. It was expected that the laser diode would limit the bandwidth of the measurement system, below the 6 GHz limit of the bias-tee. The laser diode was mounted in a TO5 package surrounded by a large aluminum heat sink. Thus, experiments were performed at room temperature without a temperature controller.

Table 2.1. Bandwidth limits of VLC components

Component	Bandwidth limit (GHz)
RF generator	40
Pattern generator	12.5
Bias-tee	6
Photodetector	7
Digital component analyzer	80

2.2.2 DC Characteristic

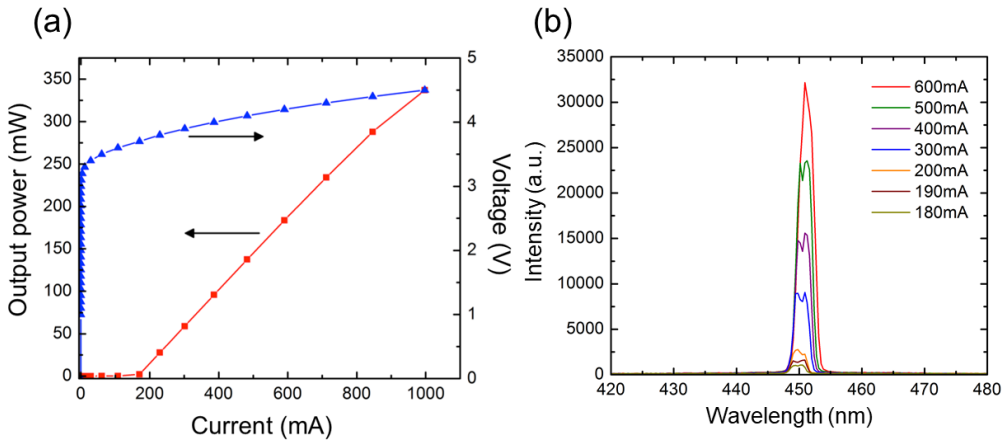

FIG. 2.3. (a) Characteristics of Light-current-voltage (L-I-V) and (b) optical spectra of different current of the 450 nm emitting LD. Reprinted with permission from OSA Publishing[11]

L-I-V characteristic curves for the laser are shown in Fig. 2.3(a). Since the PD was set up 15 cm away from the laser diode, actual output power of the laser is higher than the measured data when placed in front of the PD. The threshold current

of 170 mA and the threshold current density of and 1.48 kA/cm^2 assuming current injection through 10 μm width of the cavity (0.81 kA/cm2 for 15 μm width if assuming 100 % current spreading in p-GaN) were measured at room temperature through the free space optical link of 15 cm, with a threshold voltage of 4 V. Higher light output of back-to-back measurement will be discussed later in this chapter. Fig. 2.3(b) shows, the optical spectrum measured at each drive current. The wavelength only shifted 1~2 nm around 450 nm for drive currents ranging from 180 mA to 600 mA, the same drive currents points used in the frequency response test.

2.2.2 Modulation Characteristic

Sinusoidal RF signals were applied to the biased laser diode by a RF signal generator and measured by the DCA to study the high-speed characteristics of the frequency response of the 450 nm ridge laser. The magnitude of the frequency response was calculated by dividing the output amplitude obtained at the PD by the reference noise level at the PD in the frequency domain. The measured data was fitted by a 6th order polynomial curve to the data points as shown in Fig. 2.4.

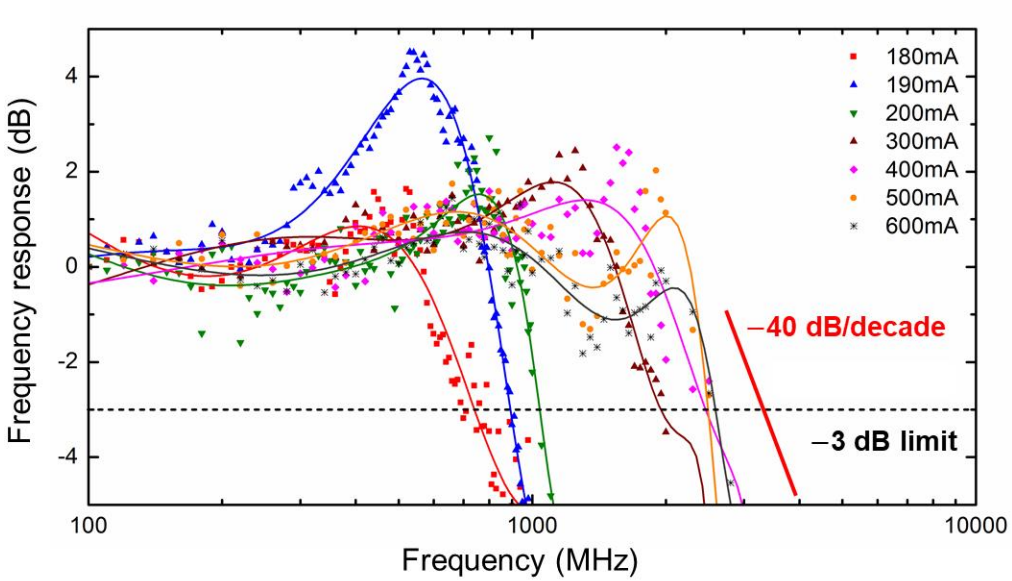

FIG. 2.4. Normalized frequency response of LD under different drive currents. The – 3 dB bandwidth is indicated by black dotted line and the slope of roll-off is indicated by red solid line. Reprinted with permission from OSA Publishing[11]

Each data point was collected at 20 MHz increments below 1 GHz and 50MHz increments above 1 GHz with 1 min pauses between each measurement for cooling down the laser. Each curve corresponds to the individual drive current from 180mA, which is right above threshold, up to 600 mA, which is where the bandwidth stops increasing. The measured maximum – 3 dB bandwidth is 2.6 GHz at a drive current of 500 mA. The 2.6 GHz limit is attributed to the modulation bandwidth of the laser diode since the other components of the VLC system have more bandwidth than the 6 GHz bandwidth of the bias tee. This – 3 dB bandwidth

is determined by the relaxation resonance frequency (f_R) roll-off past the peak resonance.

From the two-parameter modulation transfer function (small signal photon density/small ac current) of the laser given by Eq. (2.1), damping characteristics are described by the relaxation resonance frequency, ω_r, and the damping factor, γ. At small bias current, the frequency response is in an under-damped regime and has a high and narrow peak near ω_r. As the drive current increases, the bandwidth finally reaches the maximum at the critical damping regime around 400 mA ~ 600 mA. At higher drive currents, the bandwidth starts to be limited by damping, rolling off gradually from a broad and low peak. This corresponds to 2.6 GHz near 600 mA, similar to the maximum value at 500 mA.

$$\left|H(\omega)\right| = \frac{\omega_r^{\,2}}{\sqrt{(\omega_r^{\,2} - \omega^2)^2 + \gamma^2\omega^2}} \tag{2.1}$$

$$f_R = \frac{1}{2\pi}\left[\frac{\Gamma v_g a}{qV}\eta_i (I - I_{th})\right]^{1/2} \tag{2.2}$$

From the equation for relaxation resonance frequency Eq. (2.2), the square root of the driving current above the threshold is linearly proportional to the relaxation oscillation frequency (f_R) because the current term is approximately proportional to the photon density, where Γ is the confinement factor, v_g is the group velocity, a is

the differential gain with respect to the current density, V is the active region volume, η_i is the injection efficiency, and I_{th} is the threshold current. This is shown in Fig. 2.5(a). The slope value, 0.11 GHz/mA$^{1/2}$, represents the capability of the laser relative to the frequency characteristics. It is hard to to analyze the slope efficiency of the resonance frequency due to limited information of internal values for commercially available LD. The measured – 3 dB bandwidth is eventually limited near 2.6 GHz around 500 mA ~ 600 mA, as shown in Fig. 2.5(b).

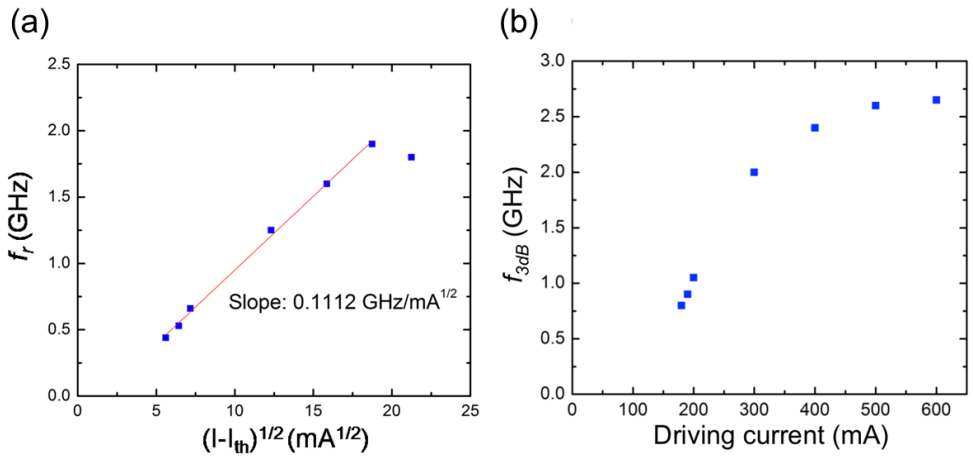

FIG. 2.5 (a) The dependence of resonance frequency to the drive current above threshold and (b) – 3 dB bandwidth of each drive current. Reprinted with permission from OSA Publishing[11]

Typical TO package of high-power III-nitride and other III-V LDs consists of bonding pad and wire bonds can even though microwave package for telecommunication has different design as shown in Fig. 2.6(a). The equivalent circuit model is described as Fig. 2.6(b) including series resistance, R, capacitance,

C, and inductance from wire bonds, L_{wire}. The series resistance of 1.22 Ω was measured at 500 mA and it includes bond wire, contact resistance, and resistive p-GaN but is typically dominated by p-contact and p-GaN resistance in III-nitride devices. The capacitance is typically dominated by the charge traps in the junction. Even though dynamic capacitance above the threshold is difficult to measure due to the shunted junction under forward bias, it is still in a good agreement by measuring the capacitance at zero bias to assuming the RC parasitic effect.[12,13] Measured capacitance was 25.5 pF at 100 MHz under zero bias as shown in Fig. 2.6(c). It is also acceptable that the measured capacitance at 100 MHz will not have significant change up to 10 GHz. The bandwidth by RC parasitic was calculated to be 5.12 GHz by $1/2\pi RC$, which is higher than measured 2.6 GHz of – 3 dB bandwidth from small signal modulation of the LD. From Fig. 4, the slope of the roll-off is approximately fitted to be – 40 dB/decade, which is derived by the second order transfer function of diode lasers. More steep slope will be expected if the roll-off by RC parasitic effect (typically – 20 dB/decade of the first order transfer function) is added. Thus, the bandwidth limiting factor can be expected to be heating of active region, gain compression, or spectral hole burning of LD itself. It is also noted that the inductance of wire bonds does not significantly affect below 2.6 GHz even though it might affect in RC parasitics at the high frequency.[12]

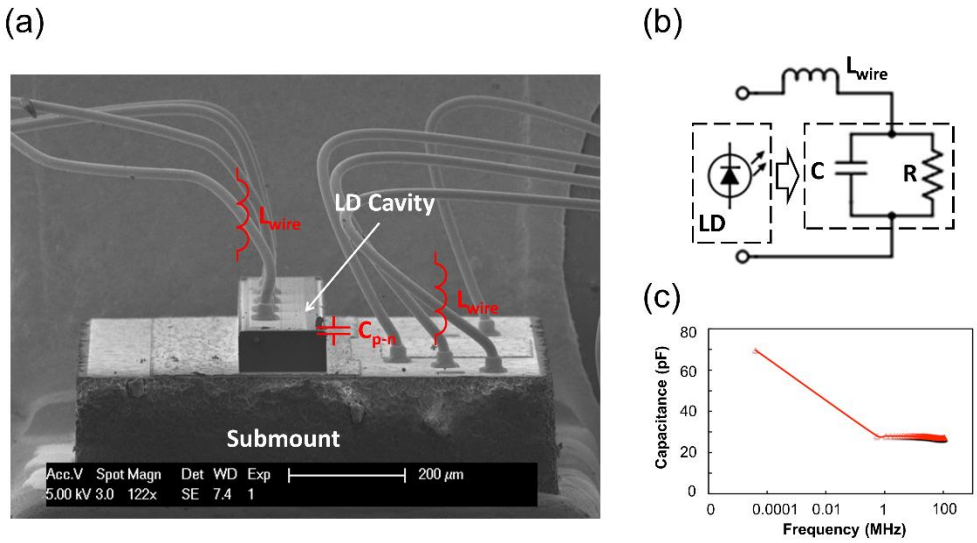

FIG. 2.6. (a) SEM image of the packaged LD with wire-bond and bonded heatsink. (b) Equivalent circuit of packaged LD structure including the effect of wire-bonds and bonding pads.

The measurement of the data transmission rate was performed with 2^7-1 psudo-random bit sequence (PRBS) for non-return-to-zero (NRZ) on-off keying (OOK) modulation testing. For the highest data rate performance, the patterns were biased at a DC drive current of 500 mA having the maximum modulation frequency of 2.6 GHz. As shown in Fig. 2.7, peak-to-peak 2 V of output data signal is applied and the maximum data rate for the open eye diagram was 4 Gbit/s. The measured extinction ratios were 0.950 dB and 0.735 dB for 2 Gbit/s and 4 Gbit/s, respectively. The Q-factors were calculated to be 12.06 dB and 10.78 dB for 2 Gbit/s and 4 Gbit/s, respectively, using Eq. (2.3), where $I_{1,2}$ is the photo-current at the state 0 and 1, $\sigma_{1,2}$ is the noise variance at 0 and 1, Q is the quality factor, and BER is the

bit error rate. Also, BER were 3.06× 10^{-5} bits and 2.70× 10^{-4} bits for 2 Gbit/s and 4 Gbit/s, respectively, as calculated using Eq. (2.4). This BER is mainly outcome of the high loss in free space path as well as the low PD responsivity.

$$Q = \frac{I_1 - I_0}{\sigma_1 + \sigma_0} \tag{2.3}$$

$$BER \approx erfc\left[\frac{Q}{\sqrt{2}}\right] \tag{2.4}$$

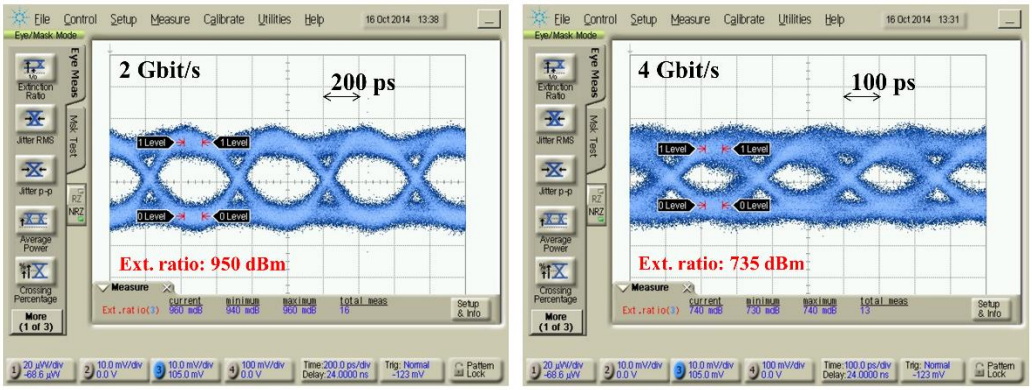

FIG. 2.7. Eye diagrams of the NRZ OOK modulation for 2 Gbit/s (left) and 4 Gbit/s (right). Reprinted with permission from OSA Publishing[11]

2.3 Filter-free Laser-based White Lighting VLC

Beyond transmitting data through blue laser, generating white lighting by using blue laser and phosphor is promising demonstration for LiFi technology as well as droop-free solid-state lighting.[10,14] LD-based white lighting communication system is great candidate overcoming the limitations of slow response of LEDs and phosphors.

2.3.1 Experimental Setup

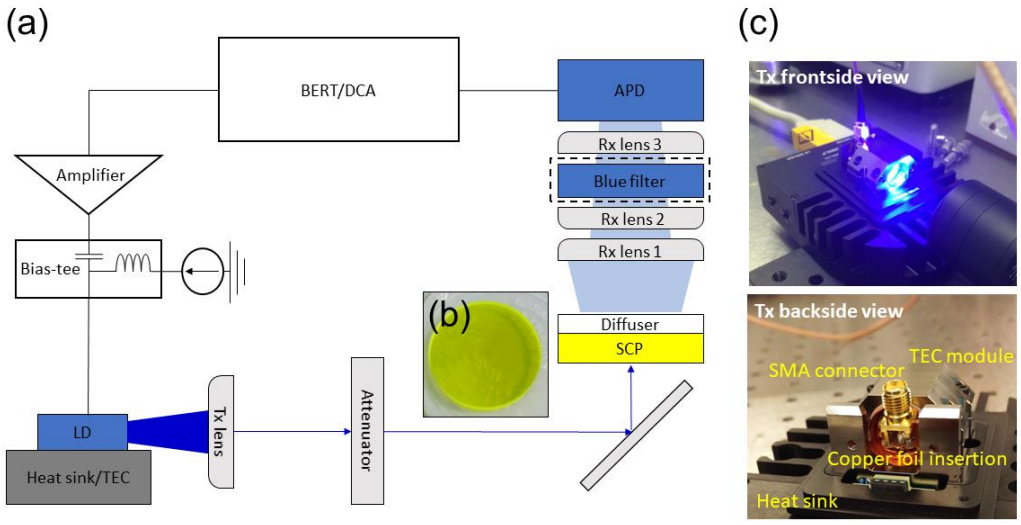

FIG. 2.8. (a) Schematic diagram of free space communication setup for white lighting by using a LD and a phosphor. (b) The photograph of YAG:Ce single crystal phosphor (SCP) plate, and of frontside and backside of LD mounted on thermos-electric cooler (TEC) and heat sink module in transmitter part (Tx). Reprinted with permission from OSA Publishing[15]

Figure 2.8 shows the experimental setup of laser-based white light VLC data transmission and illumination system using phosphor conversion. The same 450 nm LD of previous chapter was used. As shown in Fig. 2.8(c), the packaged LD was mounted on a thermoelectric cooler (TEC) module with temperature controller included. The interface between the circular LD module and TEC was filled with copper foil to avoid an air gap in the thermal path. The SubMiniature version A (SMA) connector was directly soldered to the leads from the LD module to minimize impedance mismatch. The input signal from the bit error rate tester (BERT, Agilent N4903B J-BERT) was pre-amplified using a 12.5 Gbit/s driver amplifier (Picosecond 5865) and then jointed with a DC bias using a bias-tee before being feed into the LD. The light output was collimated through the transmitter (Tx) lens (Thorlabs LA1145-A) followed by a variable attenuator for controlling the intensity level. The blue laser light was then used to excite a cylindrical single crystal cerium-doped Yttrium aluminum garnet (YAG:Ce) phosphor plate. The light was then passed through a commercially available 80 μm thick polyethylene terephthalate (PET) plastic diffuser film to generate uniform white emission. The single crystal YAG:Ce phosphor was thinned to 700 μm to make the combined laser-phosphor emission spectrum white. The modulated white light travelled 5 cm from phosphor conversion where it was received by a 1 GHz Si avalanche photodetector (APD, Menlo Systems APD 210) with three receiver (Rx) lenses in

series (Thorlabs LA 1145-A, LA1401, and LA1145). The eye diagram and BER of received signals were measured by a digital communications analyzer (DCA, Agilent 86100) and BERT. The VLC system bandwidth was limited by APD having a cut-off bandwidth of 1 GHz. However, this issue can be mitigated via using a faster photodetector (PD) as demonstrated in the previous chapter.

2.3.1 Characteristics of YAG:Ce Phosphor

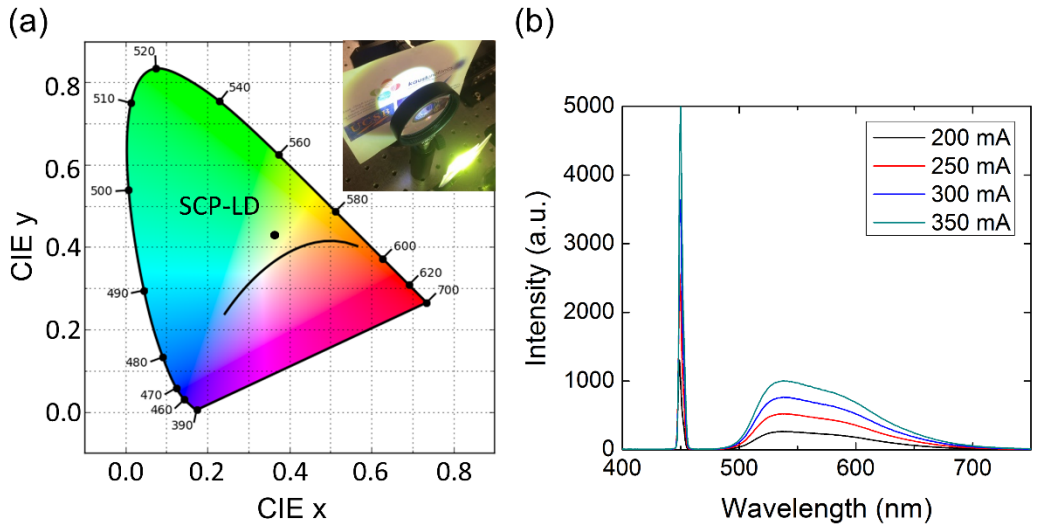

FIG 2.9. (a) CIE chromaticity coordiates and (b) optical spectra of YAG:Ce phosphor converted 450 nm LD based white emission. Reprinted with permission from OSA Publishing[15]

The properties of white light emission were investigated as shown in Fig. 2.9. The measurements were performed using a GL Spectis 5.0 Touch spectrometer with an integrating sphere. As shown in Fig. 2.9(a), the white emission from the

LD combined with the single crystal phosphor (SCP) had Commission Internationale de l'Eclairage(CIE) 1931 x,y chromaticity coordinates (0.3628, 0.4310) with a color rendering index (CRI) of 58 and a CCT of 4740 K at 300 mA of drive current. CRI and CCT show little variation with drive current between 200 mA and 400 mA with CRI change of ± 0.1 and CCT change of ± 10K. The ratio of unconverted to converted photons observed in the SCP-LD combined emission is determined by the amount of laser emission absorbed by the single crystal phosphor. At normal incidence this ratio is minimized with the shortest optical path through the phosphor of 700 μm, but can be increased by increasing the incidence angle. The CIE coordinates can be moved near the Planckian locus with further optimization of phosphor thickness and mounting angle. The choice of single crystal phosphor rather than conventional powder based phosphor is due to thermal degradation of typical phosphor-in-matrix composites which occurs at high laser power intensity. The spectra of the laser-based white lighting system with different drive currents are presented in Fig. 2.9(b).

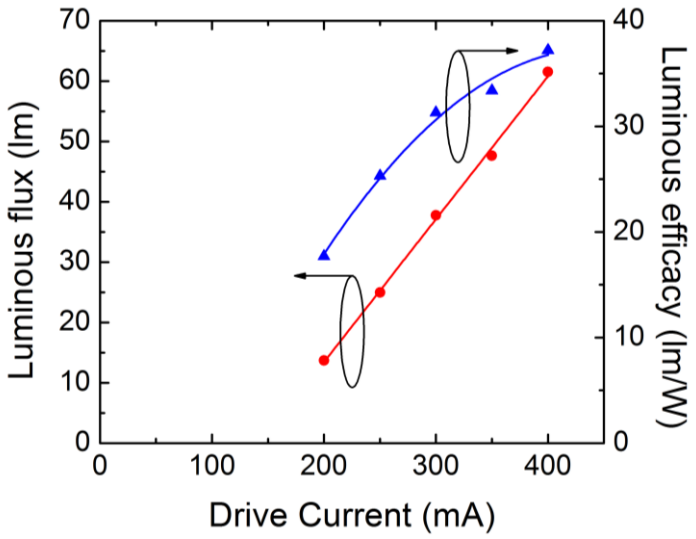

FIG. 2.10. Measured luminous flux and luminous efficacy of LD based white lighting system. Reprinted with permission from OSA Publishing[15]

The luminous flux and efficacy of the white emission by LD and SCP was also measured, as plotted in Fig. 2.10. The luminous flux increases linearly above the threshold current up to 61.5 lm at 400 mA, following the trend of the laser output power. The luminous flux linearly increases up to the drive current of 400 mA, which corresponds to 2.32 kA/cm^2, without undergoing significant heating of LD. The increase of luminous efficacy begins to saturate at 400 mA due to the thermal effects, showing a peak value of 37.2 lm/W. This saturation was originated from non-linear dissipated power due to the exponentially increasing characteristic of the voltage. This LD-based white lighting system is expected to have low

efficacy droop compared to the LED-based white lighting system as seen in similar work but more optimized for lighting performance by Cantore *et al*.[10]

The relaxation decay time of the phosphor materials is critical factor and the short relaxation decay time is necessary to avoid the saturation of emissive conversion. The relaxation time of single crystal YAG:Ce was investigated by time-resolved photoluminescence lifetime (TRPL) measurement as shown in Fig. 2.11. By using $y = A\exp(-x/\tau) + y_0$ as a fitting equation, ~73 ns of relaxation time (τ) was obtained for the single crystal phosphor. The 3 dB bandwidth can be calculated by the power transfer function as:[16]

$$H^2{}_{PL}(\omega) = \frac{1}{1 + j\omega\tau} \tag{2.5}$$

$$f_{3dB} = \frac{\sqrt{3}}{2\pi\tau} \tag{2.6}$$

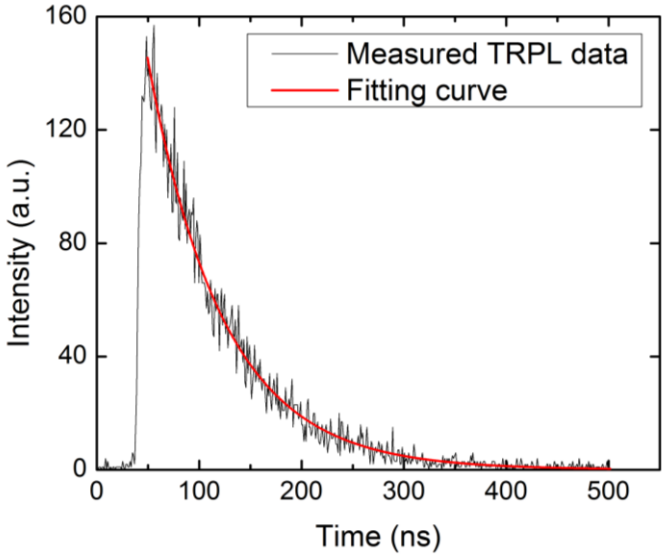

FIG. 2.11. Time resolved photoluminescence lifetime of single crystal YAG:Ce phosphor with fitting curve of an exponential model. Reprinted with permission from OSA Publishing[15]

The half of absolute power transfer function ($|H^2_{PL}(\omega)|$) corresponding to the value at – 3 dB frequency of single crystal YAG:Ce phosphor is ~3.8 MHz, which is the expected order of frequency. The relaxation decay time of typical phosphors is 100 ns ~ 1 μs and it is considered as the slowest limiting factor compared to radiative recombination time (on the order of several hundered picosecond to nanosecond) and RC time constant (varies with device structure). Even though measured relaxation time of single crystal YAG:Ce is comparatively short, it is still slower than typical bandwidth of blue LEDs.

2.3.3 Effective Modulation Bandwidths

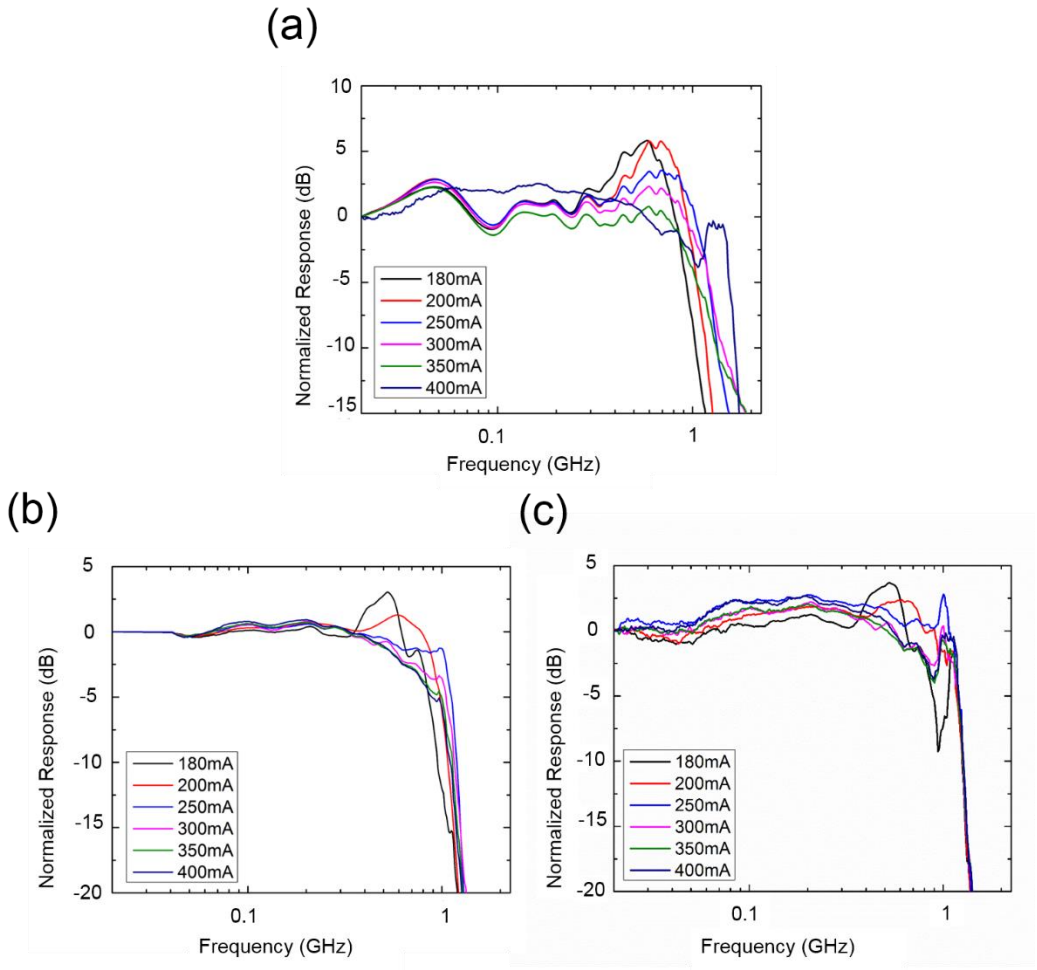

FIG. 2.12. Measured small signal responses of (a) blue LD emission only, (b) phosphor-converted white emission, and (c) phosphor-converted white emission with optical blue filter installed at the APD to filter out the phosphor-converted yellow components. Reprinted with permission from OSA Publishing[15]

The small signal response measurement was performed under different drive currents using a network analyzer (Agilent E8361C PNA, 10 MHz to 67 GHz)

in three scenarios: (a) only blue laser emission, (b) phosphor converted white emission, and (c) white emission with blue-filter installed in front of the APD to filter out the phosphor converted yellow components, as shown in Fig. 2.12. The blue-filter is a dielectric coated bandpass optical filer with a central wavelength of 450 nm and a full-width-half-maximum (FWHM) of 10 nm. The measured transmittance for blue light (~ 450 nm) is 36% and the phosphor converted yellow light was completely blocked off by the filter (transmittance < 0.001%). The obtained highest –3 dB bandwidths for the three scenarios were 1.2 GHz, 1.1 GHz, and 1.2 GHz, respectively. All three modulation bandwidths are approximately 1 GHz, which was limited by the APD. The increase in normalized response above 1 GHz in 400 mA of the drive current in Figs. 2.12(a) and 2.12(c) is most likely related to APD noise. It is noted that the phosphor converted white emission exhibited a flat frequency response in the low frequency range (< 500 MHz), as shown in Fig. 2.12(b), when compared to the modulation response of blue-LD in Fig. 2.12(a). We attribute this observation to a pre-equalization-like effect when employing the phosphor in LD-based white-light communication system. As a result, the blue-filter becomes an unnecessary component in the system, since the pre-equalization-like effect of phosphor has already served to compensate the unflatten response of the LD in low frequency range. This is also supported by an increasing unflatten response in the case of having the blue-filter installed, as shown

in Fig. 2.12(c). The effect of blue-filter and its impact on data transmission rate and BER will be further evaluated and discussed later. Since the photons are scattered in the phosphor conversion process, a reduction of received power will cause a lower SNR, resulting in slight reduction of bandwidth. In addition, since the yellow component has a 3.8 MHz bandwidth, which is almost three orders of magnitude lower than that of the blue component, it has a negligible effect on the normalized response. Even though the system bandwidth is limited to 1 GHz, it is important to note that the modulation bandwidth of the phosphor-converted white light is not limited by the bandwidth of the phosphor components, which is on the order of several MHz.

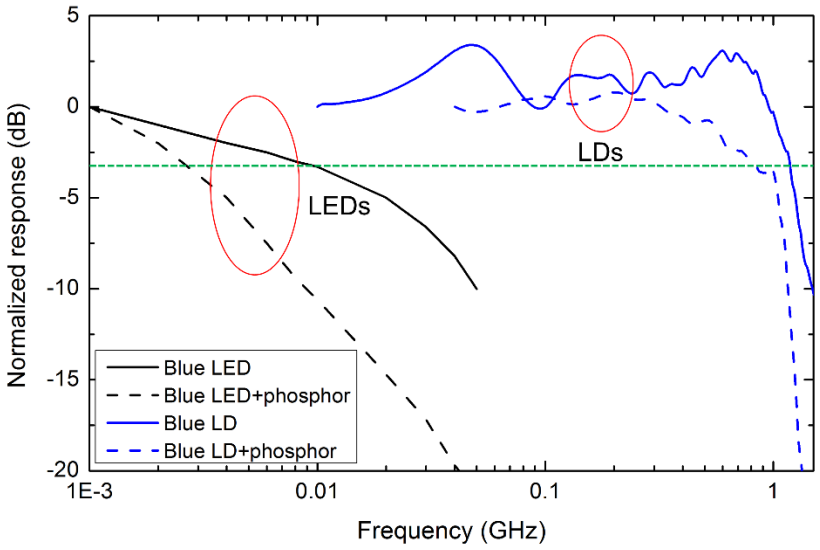

FIG. 2.13. Comparison of the modulation bandwidth of commercial blue LEDs and blue LDs with and without phosphor conversion. Reprinted with permission from OSA Publishing[15]

Figure 2.13. shows the modulation bandwidths of commercial blue LEDs (Luxeon STAR) and blue-LDs (extracted from Casio XJ-M140 projector) with and without phosphor-conversion. The operating current of the LED was 200 mA and the operating current of the LD was 300 mA. The reported bandwidth of the LED with and without phosphor conversion with a blue-filter in front of the PD was only 2.5 MHz and 14 MHz, respectively.[7] The bandwidth of LEDs with phosphor conversion is limited by the phosphor lifetime (on the order of 100 ns). In contrast, the bandwidth of LDs with phosphor conversion is not limited by the phosphor lifetime. The bandwidth of LDs depends on photon lifetime (on the order of 1 ps ~

10 ps), while the bandwidth of LEDs depends on radiative recombination lifetime (on the order of 100 ns ~ 1 ns), so the modulation bandwidth of LDs can be at least 100 times higher than LEDs. For a LED with phosphor conversion, the decay time of the radiative recombination is of the similar order as the decay of phosphor and the emission has similar intensity, so the total frequency response is highly affected by the frequency response of the phosphor. For a blue LD with phosphor conversion, since the photon lifetime of LD is at least two orders of magnitude lower than decay time of the phosphor, the modulation at high frequency is dominated by the photon lifetime of the LD. In this case, the slow phosphor-converted yellow component is received as a noise level in the total emission, hence the fast-modulating blue component superimposes on the background noise level induced by slow yellow component. Thus, laser-based phosphor-converted white VLC system does not require an optical blue-filter or a post-equalization circuit, which are typical ways to recover the bandwidth compromised by the phosphor in LED-based phosphor-converted white VLC systems, in order to recover the system bandwidth.[7,17]

2.3.4 Effective Data Rate and BERs

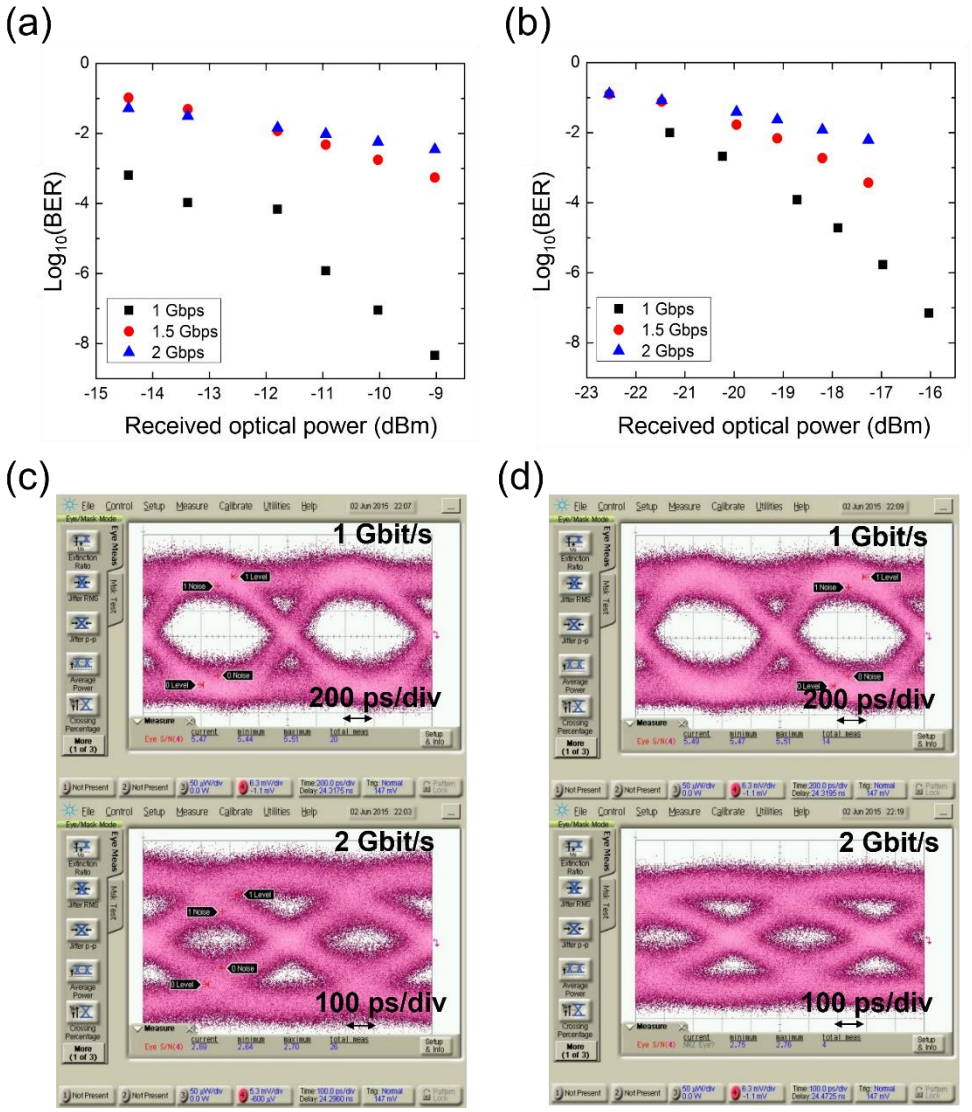

FIG. 2.14. Measured BERs at different data rates with (a) white emission and (b) blue-filtered emission from white emission. Eye diagrams of (c) white emission and (d) blue-filtered emission at 1 Gbit/s and 2 Gbit/s. Reprinted with permission from OSA Publishing[15]

The data transmission measurement was performed at a drive current of 300 mA by a 2^{10}-1 pseudo-random binary sequence (PRBS) for BER and an eye test. As shown in Fig. 2.14(a) and Fig. 2.14(b), unfiltered white emission passed FEC criteria with a BER of 3.50×10^{-3} at 2 Gbit/s while the signals after blue-filter had a BER of 6.20×10^{-3} at 2 Gbit/s. Open eyes were obtained at 1 Gbit/s and 2 Gbit/s without significant difference between the scenarios of filtered and unfiltered receiver, as shown in Fig. 2.14(c) and 2.14(d), with measured SNR of 5.5 and 2.7, respectively. Unlike LED-based white light communication, the measured data transmission shows that a blue-filter is not necessary to improve the data transmission rate for laser-based white light communication.

References

[1] J.-W. Shi, K.-L. Chi, J.-M. Wun, J. Bowers, Y.-H. Shih, and J.-K. Sheu, IEEE Electron Device Lett. 1 (2016).

[2] R.X.G. Ferreira, E. Xie, J.J.D. McKendry, S. Rajbhandari, H. Chun, G. Faulkner, S. Watson, A.E. Kelly, E. Gu, R. V. Penty, I.H. White, D.C. O'Brien, and M.D. Dawson, IEEE Photonics Technol. Lett. **28**, 2023 (2016).

[3] D. V. Dinh, Z. Quan, B. Roycroft, P.J. Parbrook, and B. Corbett, Opt. Lett. **41**, 5752 (2016).

[4] M.S. Islim, R.X. Ferreira, X. He, E. Xie, S. Videv, S. Viola, S. Watson, N. Bamiedakis, R. V. Penty, I.H. White, A.E. Kelly, E. Gu, H. Haas, and M.D. Dawson, Photonics Res. **5**, A35 (2017).

[5] D.C. O'Brien, L. Zeng, H. Le-Minh, G. Faulkner, J.W. Walewski, and S. Randel, in *2008 IEEE 19th Int. Symp. Pers. Indoor Mob. Radio Commun.* (IEEE, 2008), pp. 1–5.

[6] A. Rashidi, M. Nami, M. Monavarian, A. Aragon, K. DaVico, F. Ayoub, S. Mishkat-Ul-Masabih, A. Rishinaramangalam, and D. Feezell, J. Appl. Phys. **122**, 35706 (2017).

[7] H. Le Minh, D. O'Brien, G. Faulkner, L. Zeng, K. Lee, D. Jung, Y. Oh, and E.T. Won, IEEE Photonics Technol. Lett. **21**, 1063 (2009).

[8] A. David and M.J. Grundmann, Appl. Phys. Lett. **96**, 103504 (2010).

[9] C. Weisbuch, M. Piccardo, L. Martinelli, J. Iveland, J. Peretti, and J.S. Speck, Phys. Status Solidi **212**, 899 (2015).

[10] M. Cantore, N. Pfaff, R.M. Farrell, J.S. Speck, S. Nakamura, and S.P. DenBaars, Opt. Express **24**, A215 (2016).

[11] C. Lee, C. Zhang, M. Cantore, R.M. Farrell, S.H. Oh, T. Margalith, J.S. Speck, S. Nakamura, J.E. Bowers, and S.P. DenBaars, Opt. Express **23**, 16232 (2015).

[12] J. Bowers, B. Hemenway, A. Gnauck, and D. Wilt, IEEE J. Quantum Electron. **22**, 833 (1986).

[13] J.E. Bowers, Solid. State. Electron. **30**, 1 (1987).

[14] K.A. Denault, M. Cantore, S. Nakamura, S.P. DenBaars, and R. Seshadri, AIP Adv. **3**, 72107 (2013).

[15] C. Lee, C. Shen, H.M. Oubei, M. Cantore, B. Janjua, T.K. Ng, R.M. Farrell, M.M. El-Desouki, J.S. Speck, S. Nakamura, B.S. Ooi, and S.P. DenBaars, Opt.

Express **23**, 29779 (2015).

[16] E.F. Schubert, *Light-Emitting Diodes* (2006).

[17] H. Li, X. Chen, B. Huang, D. Tang, and H. Chen, IEEE Photonics Technol. Lett. **26**, 119 (2014).

3

High-speed III-nitride Semipolar Laser Diode

3.1 Introduction

III-nitride laser diodes (LDs) were first demonstrated in 1996 and have been developed for high-power applications such as optical storage, medical, and solid-state lighting.[1] The most preferred crystal orientation is polar (0001) c-plane because this orientation can be directly grown on cheap Al_2O_3 sapphire substrate with lattice match. However, the performance of LDs grown on conventional *c*-plane GaN has been hindered due to polarization-induced electric fields, leading to a reduction of wave-function overlap.[2,3] Also, balanced biaxial strain of *c*-plane crystal structure generates relatively high density of states (DOS) causing high threshold current density in LDs. Recent progress on semipolar and nonpolar

planes has shown significant improvement in high-power performance of light emitting diodes (LEDs) and LDs by reducing the polarization-induced electric field.[4–12] In addition, semipolar and nonpolar LDs are expected to have higher optical gain than *c*-plane LDs due to a higher wave-function overlap and a reduction in the density of states.[13–15]

Since semipolar and nonpolar LDs are expected to have higher differential gain than *c*-plane LDs, they also have the potential for improvements in modulation bandwidth. Although blue LEDs and LDs are typically used as the excitation source for solid-state lighting systems, violet LEDs and LDs have potential candidates in high quality white lighting with RGB phosphors. In addition, violet LDs may have advantages in terms of LiFi system performance due to potential challenges with creating high-speed photodetectors that absorb light in the blue region of the spectrum.[16–18] In this chapter, we overview the design of epitaxial structure and edge emitting LDs on semipolar $(20\overline{2}1)$ free-standing substrate grown by MOCVD. Characteristics of light output, emission spectrum, and modulation are first discussed. Theoretical approaches verify the internal parameters in carrier injection efficiency, losses, and optical gain. Dynamic parameters related to high-speed performance are reported at the first time for GaN LDs. Temperature dependent studies related to transfer function by small signal modulation are also discussed.

3.2 Design and Optimization

3.2.1 Epitaxial Structure Design

Previously, UCSB demonstrated violet, blue and green (400 nm ~ 550 nm) laser diodes on different crystal orientations. As mentioned in previous chapter, nonpolar and semipolar GaN have the inherent advantages in material gain and threshold current. And semipolar crystal orientation is good compromise from known issues on nonpolar crystal orientation such as surface morphology, basal plane stacking faults, carrier localization broadening emission wavelength, and indium uptake.

FIG. 3.1. Schematic of the epitaxial structure of the LD on a ($\mathbf{20\bar{2}1}$) substrate. Reproduced with the permission of AIP Publishing[19]

Violet LDs were grown by atmospheric pressure (AP) metalorganic chemical vapor deposition (MOCVD) manufactured from TAIYO NIPPON SANSO. The bulk GaN semipolar $(20\bar{2}1)$ substrates in all of our experiments were prepared by Mitsubishi Chemical Corporation and Suzhou Nanowin Science and Technology Corporation. As shown in Fig. 3.1, the epitaxial structure consisted of a 1 μm Si-doped *n*-GaN cladding layer, a 500 nm n^+-GaN topside contact layer ([Si] = 5.2×10^{19} cm^{-3}), a 350 nm *n*-GaN buffer layer ([Si] = 6.2×10^{18} cm^{-3}) to

minimize the absorption loss, and a 60 nm composition graded *n*-$In_{0.025}Ga_{0.975}N$ waveguiding layer. The active region consisted of a 4 period undoped $In_{0.1}Ga_{0.9}N$/GaN (3.5 nm / 7 nm) multiple quantum well (MQW) structure, followed by a 16 nm *p*-$Al_{0.18}Ga_{0.82}N$ electron blocking layer (EBL) linearly graded in composition and doping down to GaN at the topside. Then a 60 nm composition graded *p*-$In_{0.025}Ga_{0.975}N$ waveguiding layer and 600 nm thick Mg-doped *p*-GaN cladding layer were grown followed by a 10 nm highly Mg-doped p^+-GaN contact layer. The detail optimization was discussed in previous reports, Yonkee *et al*.[20] The doping level of the n^+-GaN contact layer was optimized to obtain a low resistance topside *n*-type contact, which is essential for reducing the resistance of the device as well as enabling radio frequency (RF) measurements with ground-signal (GS) or ground-signal-ground (GSG) probe configurations.

3.2.2 Mode Profile and Confinement Factor

The transverse mode profile was shown in Fig. 3.2(a). Refractive indices of 2.51, 2.54, 2.63, 2.45 were used for the GaN, $In_{0.025}Ga_{0.975}N$, $In_{0.1}Ga_{0.9}N$/GaN, $Al_{0.18}Ga_{0.82}N$ layers, respectively. The optical mode was well-confined by the active region of undoped $In_{0.1}Ga_{0.9}N$/GaN (3.5 nm / 7 nm) and $In_{0.025}Ga_{0.975}N$ separate confinement heterostructures (SCH). 16 nm *p*-$Al_{0.18}Ga_{0.82}N$ electron

blocking layer (EBL) affects a little optical loss showing the kink-like discontinuity due to its high Al composition generating low refractive index. This can be improved by reducing doping concentration of Mg or removing unintentional oxygen in EBL.[21]

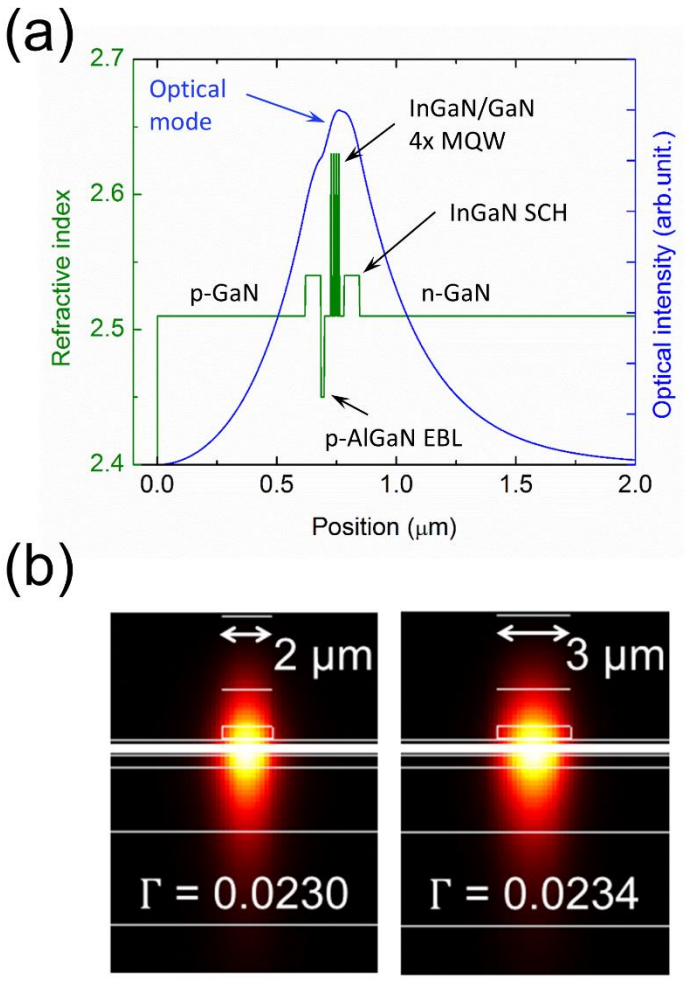

FIG. 3.2 (a) Simulated 1-D transverse mode profile for the LD structure. (b) Calculated optical mode for waveguide widths of 2 μm and 3 μm. Reproduced with the permission of AIP Publishing[19]

Also, simulated illustrations of lateral mode for two different cavity width, 2 μm and 3 μm, are shown in Fig. 3.2(b). The fundamental mode was calculated to be

single mode for both cavity widths. Calculated optical confinement factors, Γ, for 2 μm and 3 μm cavity widths are 0.0230 and 0.0234, respectively. The optical confinement factors are important to calculate gain related parameters as well as frequency related parameters.

3.2.3 Process Flow

The whole fabrication process was developed in nanofabrication facility at UCSB. Historically, UCSB has been developed the ridge LD process in different aspects and reported great improvements by optimizing self-aligning passivation layers, polished and Chemically Assisted Ion Beam Etched (CAIBE) facets.[8,9,11] Since bulk GaN is inherently n-type conductive substrate, backside *n*-contact has been preferred to reduce the processing steps. However, for high-speed design and its measurement, the wide pitch distance of backside *n*-contact to the *p*-contact on laser cavity is at least several hundreds of micron (> 500 μm) while typical pitch sizes of microwave probes over 10 GHz bandwidth are less than 100 μm. Alternative way can be wire bonding the contacts on the probing board but the measurement includes the parasitic effect of the inductance from bonding wires. Thus, topside contact design with short pitch size between *n*- and *p*-contact is important especially for high-speed ridge LD.

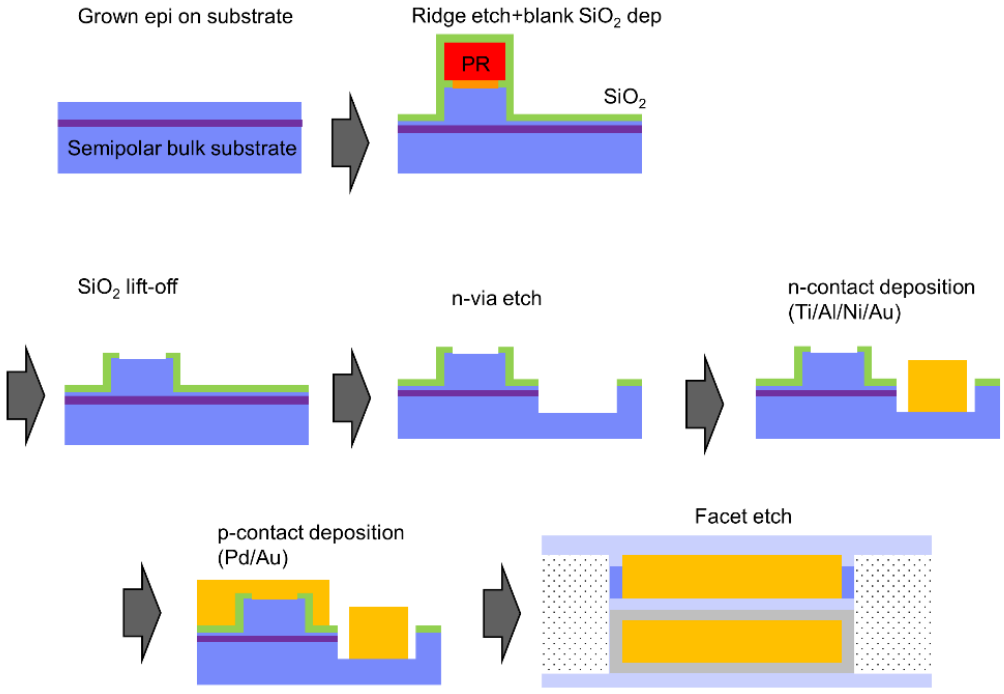

FIG. 3.3. Schematic fabrication process of topside contact ridge LD.

Figure 3.3. shows the overview of topside contact LD process. After the MOCVD growth and *p*-GaN activation, the sample was first cleaned by aqua regia (1:3 = HNO_3:HCl). Each steps were patterned by stepper lithography. Since the ridges are narrow down to 1.5 μm wide, a self-aligned process was used to form effective sidewall passivation. Ridges were formed by reactive ion etching (RIE) using Cl_2/BCl_3. As a self-aligned process, instead of stripping off the photoresist (PR), 200 nm of SiO_2 was deposited as a passivation layer onto the field area and ridge sidewalls via sputtering and was lifted off of the laser ridges.[8] After wet

etching a portion of the SiO_2 layer by HF, the *n*-via was etched via RIE using Cl_2/BCl_3 down to the center of a 500-nm n^+-GaN layer to form the topside *n*-type contact. Ti/Al/Ni/Au (15/100/100/100 nm) *n*-contacts were deposited by electron beam evaporator, followed by rapid thermal annealing (RTA) with N_2 ambient at 450 ºC to lower the contact resistance. Pd/Au (30/100 nm) *p*-contacts were deposited on top of the ridges, followed by common pad metals of Ti/Au (15/1000 nm) for both *p*- and *n*-pads. Mirror facets were formed by RIE using Cl_2/BCl_3 and were left uncoated. Fully processed structure is shown in Fig. 3.4.

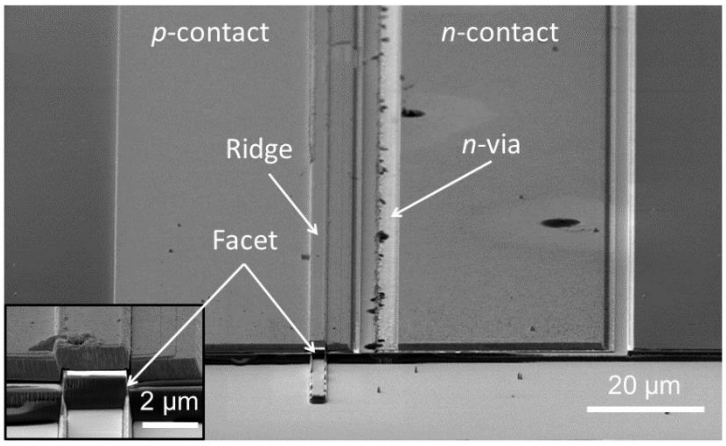

FIG. 3.4. SEM image of 2 μm wide and 1200 μm long LD cavity with topside contacts and etched facet (inset). Reproduced with the permission of AIP Publishing[19]

3.3 DC Performance

3.3.1 Topside *n*-contact

Several aspects are discussed for optimization of topside *n*-contact in this chapter. Previously reported m-plane LD was fabricated with topside n-contact without n^+-GaN layer.[7] However, different from *c*-plane GaN, it is hard to achieve ohmic contact without highly doped layer in the epitaxial structure. As shown in Fig. 3.5(a), n^+-GaN contact layer was grown as a sandwich structure between *n*-GaN template and buffer layer. The depth of *n*-via was carefully optimized based on the etching rate (BCl_3/Cl_2: 20/5 sccm, 15 W for precleaning and Cl_2 10 sccm, 200 W for etching). Contacts on *n*-GaN buffer layers ([Si] = 6.2×10^{18} cm^{-3}), which is same condition of *n*-GaN template, generates non-ohomic contact characteristics in current-voltage (*I-V*) curve as shown in Fig.3.5(b). However, contacts on n^+-GaN layer shown ohmic contact characteristics ([Si] = 5.2×10^{19} cm^{-3}). The etch depth was controlled to be down on the center of 500 nm n+-GaN layer, which corresponds to approximately 1500 nm from the top of the *p*-GaN on the ridge.

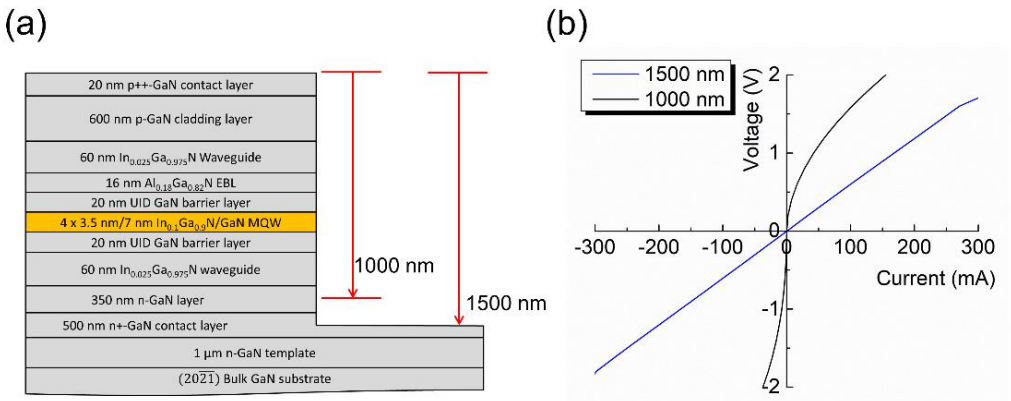

FIG. 3.5 (a) Epitaxial structure with different etch depth to *n*- or n^+- GaN layer (b) *I-V* curve for first circle of CTLM pattern on the LD structure.

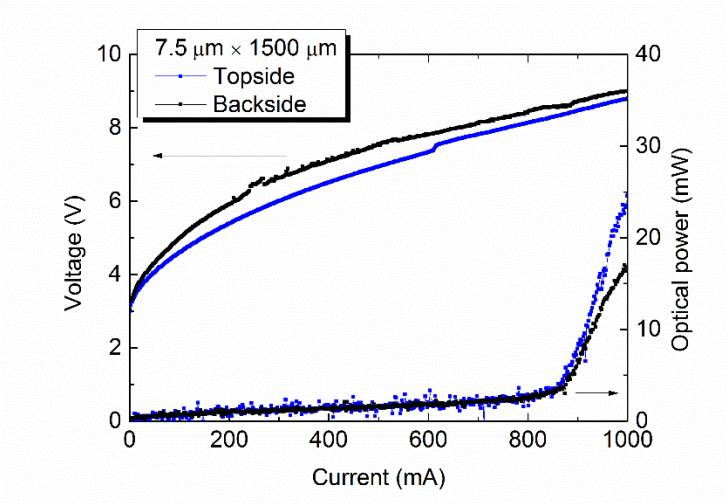

FIG. 3.6. The light-current-voltage (*L-I-V*) characteristics of 7.5 µm wide and 1500 µm long LDs having n-contact on topside and backside.

The light-current-voltage (*L-I-V*) characteristics were measured in both topside and backside *n*-contact on same LD under pulsed-electrical input with 500 ns pulse width and 10 kHz of frequency as shown in Fig. 3.6. The representative performance of 7.5 μm × 1500 μm shown slightly better in both *L-I* and *I-V*. The threshold voltages of backside and topside contacts are 8.1 V and 8 V, respectively. The series resistance at threshold current was 3 Ω for both contacts. Threshold current was also similar at 870 mA but the slope efficiency was better in topside contact design. This is presumably due to the difference in lateral current spreading or lateral mode profile changes.

The capacitance of two different designs was measured to investigate the parasitic effect potentially originated from topside n-contact design. Measured capacitances in 3 μm wide with the cavity length ranging from 900 μm to 1800 μm are shown in Fig. 3.7(a) and (b). The capacitance from 26 pF to 52 pF depends on the size of the cavity. The difference of measured capacitances between backside and topside *n*-contact is negligible with 0.1 pF as shown in Fig. 3.7(c). Hence, the topside *n*-contact design has no trade-off in output power and RC parasitics for high-speed applications.

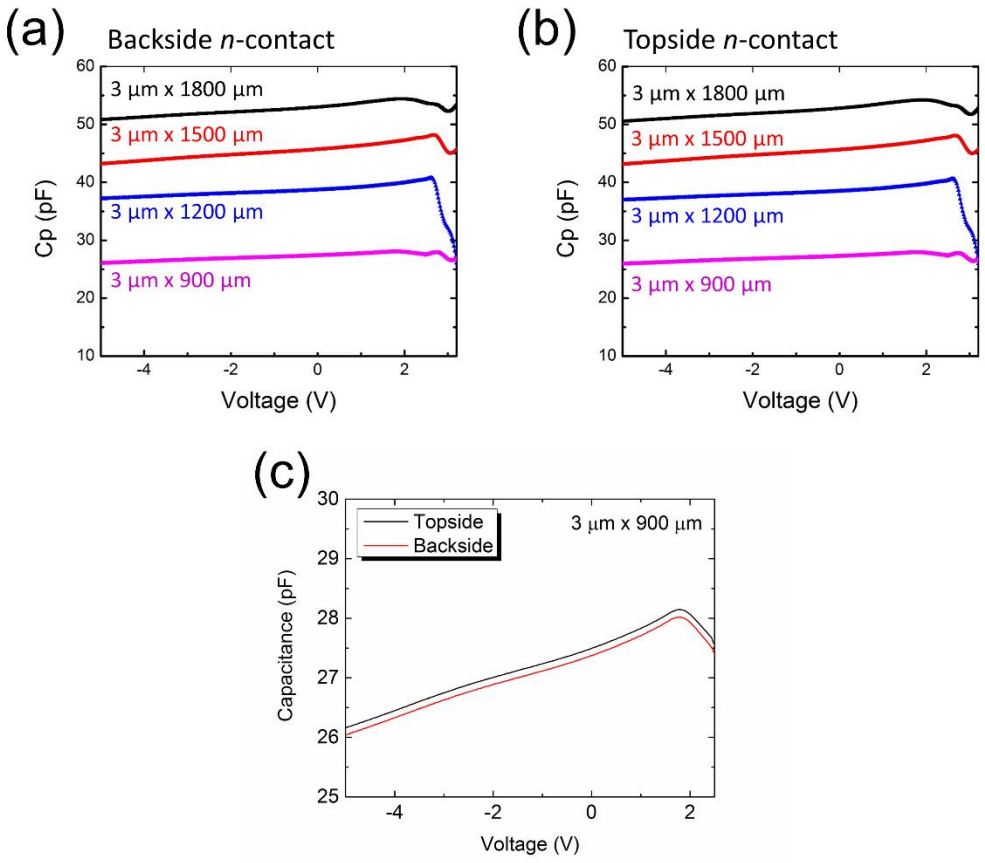

FIG. 3.7. Parasitic capacitances for (a) backside and (b) topside n-contact in different cavity size. (c) A comparison of capacitance for the topside and backside design of 3 µm × 900 µm cavity.

3.3.2 *L-I-V* Characteristics

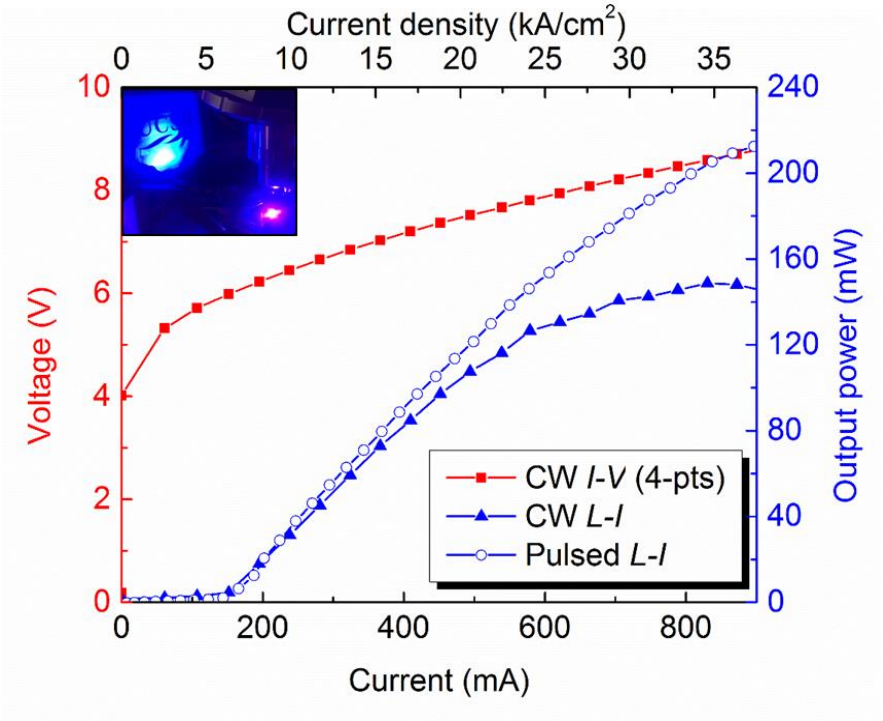

FIG. 3.8. CW and pulsed *L-I-V* characteristic for a 2 μm × 1200 μm LD measured with 4-point probes configuration.

The light-current-voltage (*L-I-V*) characteristics of the different cavities (2 μm and 3 μm wide with 600 μm ~ 1800 μm long) were measured to investigate the performance of the output power under both pulsed (0.5 % duty cycle with 500 ns pulse width and 10 kHz of frequency) and CW operation at 15 ºC. The result of 2 μm wide and 1200 μm long were representatively shown in Fig. 3.8. The threshold

current (I_{th}) and threshold current density (J_{th}) for CW (pulsed) were 150 mA (140 mA) and 6.25 kA/cm^2 (5.83 kA/cm^2), respectively, with a corresponding threshold voltage (V_{th}) of 5.1 V under CW using a four-probe measurement. The slope efficiency and differential efficiency were 0.70 W/A (0.86 W/A) and 23 % (28 %), respectively, for both facets without high-reflection coating. The results for different cavity sizes will be discussed to extract internal parameters in later chapter.

3.3.3 Spectral Characteristics

The spectral characteristics were measured by optical spectral analyzer (OSA, YOKOGAWA AQ6373B) under pulsed input with 0.5 % duty cycle. The wavelength resolution of OSA is 10 ~ 20 pm for ranging from 400 nm to 470 nm. The calculated mode spacing of 410 nm lasing LDs with 600 μm to 1800 μm are shown in Table 3.1.

Table 3.1. Calculated and measured mode spacing of different cavity lengths.

Cavity lengths (μm)	600	900	1200	1500	1800
Calculated $d\lambda$ (pm)	43.56	29.04	21.78	17.43	14.52
Measured $d\lambda$ (pm)	46	31	25	-	-

Mode spacing, $d\lambda$, for 409 nm lasing ridge lasers can be calculated by using $d\lambda = \lambda^2/2n_gL$, where λ is the emission wavelength, ng is the group index of gain media, and L is the cavity length. Passive region is ignored in our device design. Since the

calculated mode spacing of 1500 μm and 1800 μm are not in a range of the resolution of OSA, the cavities from 600 μm to 1200 μm were measured for mode spacing. The measured mode spacings are in a good agreement with the theoretical calculations. The spectra of 2 μm × 1200 μm are shown in in Fig. 3.9. The dominant lasing peak started near 409.3 nm and the multiple modes exist at $1.0I_{th}$, which is near threshold, as shown in Fig. 3.9(b). Also, it can be seen that the mode spacing is approximately 25 pm. At $1.5I_{th}$, the lasing peak red shift to 409.95 nm and shows single transverse mode lasing characteristics with 10 pm full width half maximum (FWHM), which is expected due to the resolution limit of OSA. As shown in Fig. 3.9(a), gain spectra shifts to the longer wavelength as current increases and finally multiple modes appear after $1.8I_{th}$. This is typical behavior in other III-V semiconductor lasers probably due to the combination of many body effect or thermal effect.

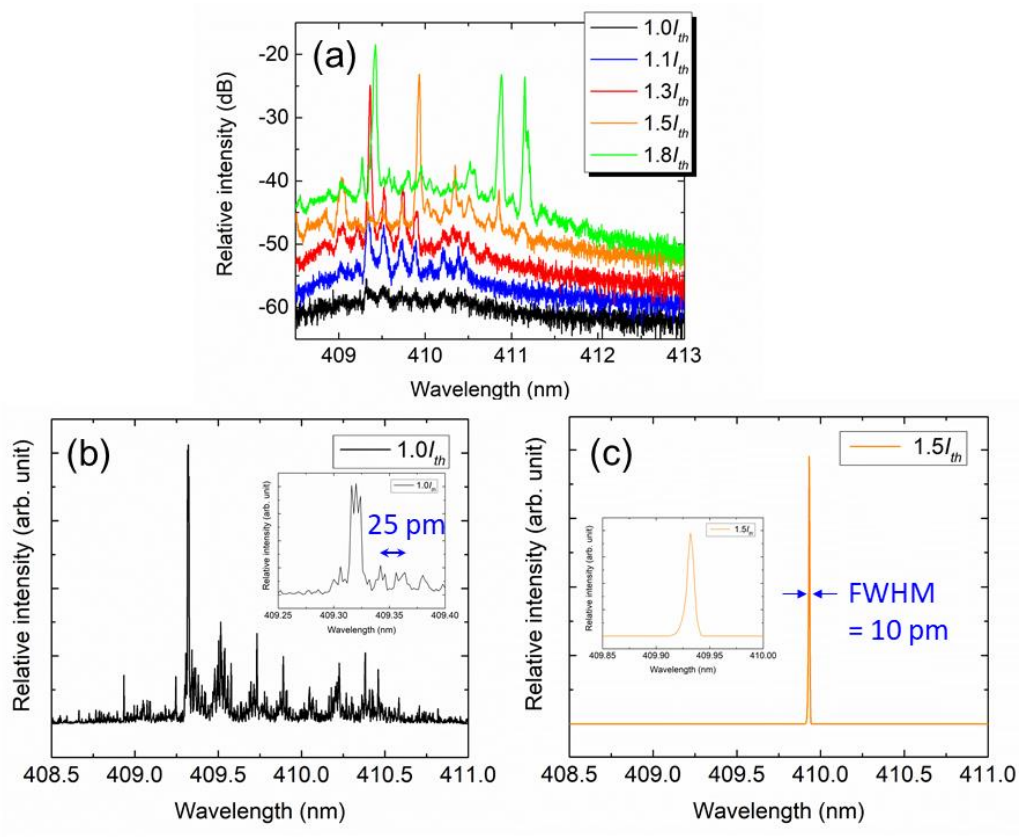

FIG. 3.9 (a) Spectra of 2 μm x 1200 μm cavity in different injection current. Specific spectrum of (a) 1.0 × I_{th} and (b) 1.5 × I_{th}.

3.4 Modulation Characteristics

3.4.1 Experimental Setup

The small signal modulation characteristics were measured to investigate high-speed performance as well as to study dynamic parameters. The experimental setup is important to avoid system effect and achieve intrinsic characteristics of LDs. The experimental system is shown in Fig. 3.10.

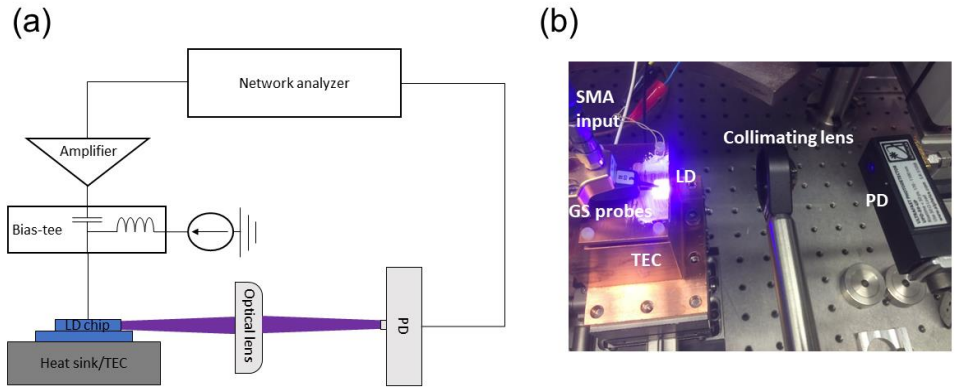

FIG. 3.10. (a) Schematic diagram of experimental system for small signal modulation. (b) The photograph of experimental system with free space link.

The LDs on the bulk GaN substrate were mounted on a thermoelectric cooler (TEC) controlled heatsink with thermo-paste for better heat transfer. 40 GHz microwave GS probes (Cascade Microtech ACP40-GS-50) were used to apply small signals at high frequencies. The SMA cable was directly connected to GS probes. Since the

LDs were designed to be etched facets without polishing the substrate, the remaining substrate (~ 1 mm) in front of facets hindered the coupling directly to the active area of the photodetector (PD). Hence, the free space link was setup to collimate diverged light with proper working distance and optical lens. 7 GHz UV extended Si *p-i-n* PD (ALPHALAS UPD-50-UP) covering short wavelength was used for high frequency measurement. The input signal from the 67 GHz network analyzer (PNA, Agilent E8361C) was pre-amplified using a 38 GHz amplifier (SHF 906E).

3.4.2 Small Signal Modulation

The sinusoidal small signal modulation was performed for different size of cavities. The frequency response of the 2 μm wide by 1200 μm long LD is shown in Fig. 3.11(a) as a representative result among many cavities.

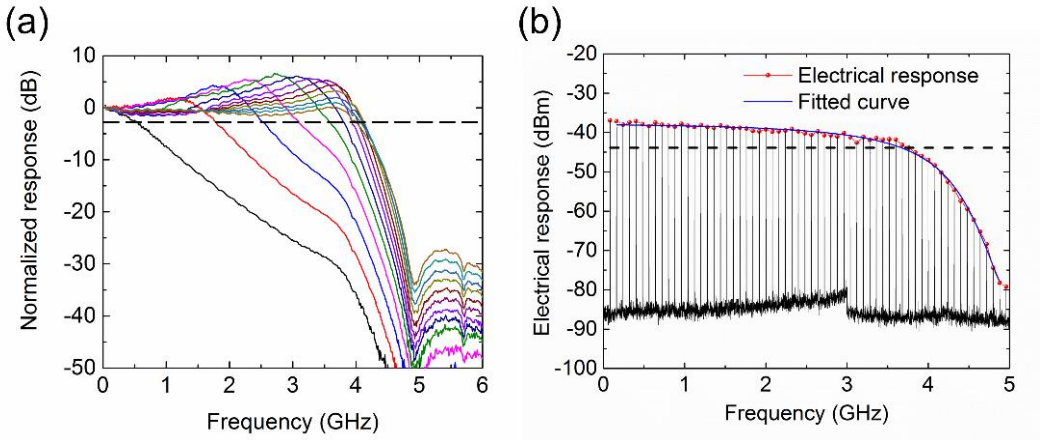

FIG. 3.11. (a) Normalized frequency response of 2 μm × 1200 μm LD without correcting PD response. (b) Electrical frequency response of Si *p*-*i*-*n* PD measured by the spectrum analyzer. Reproduced with the permission of AIP Publishing[19]

The modulation bandwidth of 4.1 GHz was obtained due to the significant roll-off regardless of resonance frequencies. It was expected that the roll-off was not originated from the intrinsic response of the LDs but presumably from other bandwidth limiting factor in the system. This is because the measured slope of the roll-off is more than 100 dB/decade, while intrinsic roll-off is typically 40 dB/decade or up to 60 dB/decade associated with RC parasitic effect. The electrical response of the PD was measured with a 410 nm pulse train by frequency doubling a mode-locked Ti-Sapphire laser emitting at 820 nm.[22] The measured bandwidth of the PD was 3.76 GHz as shown in Fig. 3.11(b). Thus, it is obvious that the steep roll-off of Fig. 3.11(a) is due to the bandwidth limit of PD.

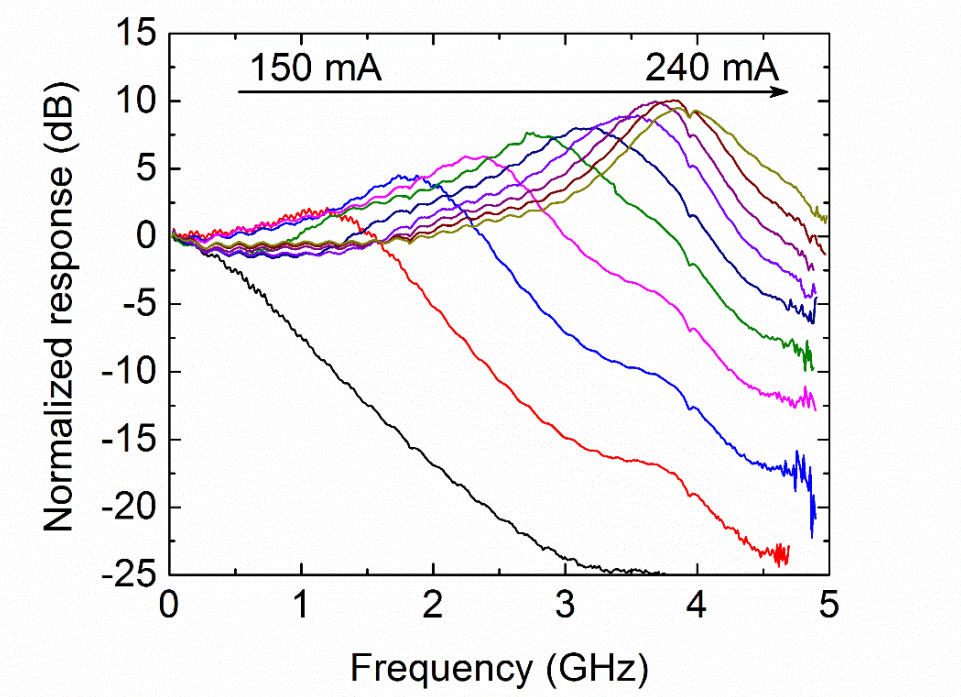

FIG. 3.12. Corrected frequency response of 2 μm wide by 1200 μm long LD after subtracting PD response. Reproduced with the permission of AIP Publishing[19]

As shown in Fig. 3.12, the frequency response of the 2 μm wide by 1200 μm long LD was recovered by subtracting the fitted PD response, although the resonance peaks were still saturated near 4 GHz. The highest measured 3-dB bandwidth of the LD was 5 GHz at 220 mA of drive current. This is because the data before subtracting the PD response hit the noise floor near 4.8 GHz and the bandwidth at 240 mA should be higher than 5 GHz. It is also expected to obtain higher 3-dB bandwidths with a higher speed PD that covers the UV-violet spectrum. To the best of the authors' knowledge, this is the highest reported modulation

bandwidth in blue-violet spectral range and any III-nitride QW LDs on current records.

3.4.3 Large Signal Modulation

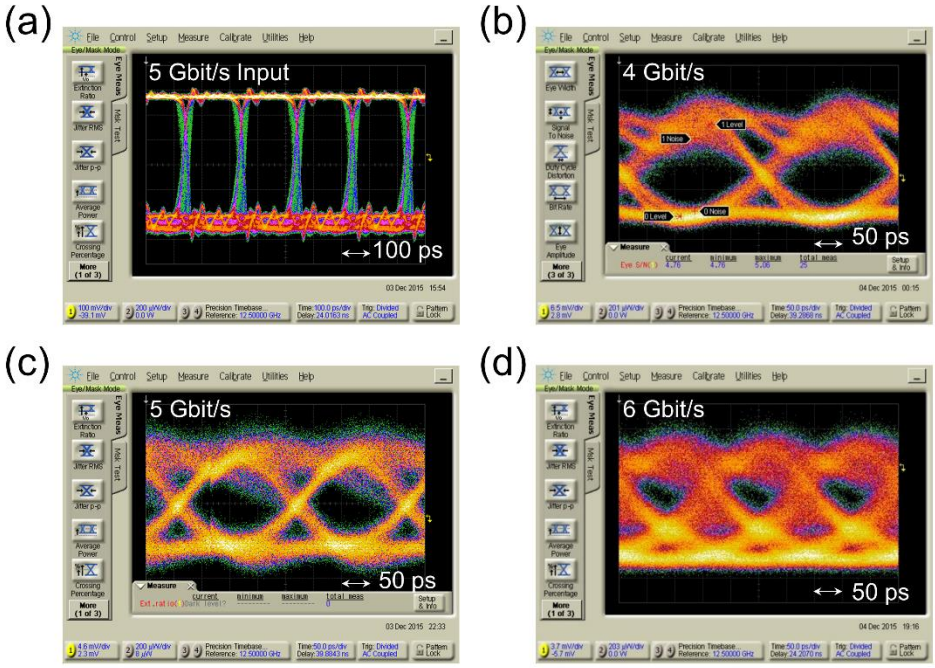

Figure 3.13. Eye diagram of (a) input digital modulation signal at the data rate of 5 Gbit/s, and received output digital signal at (b) 4 Gbit/s, (c) 5 Gbit/s, and (d) 6 Gbit/s for 2 μm × 1200 μm LD cavity. Reproduced with the permission of AIP Publishing[19]

Large signal modulation was performed to evaluate the capability for data transmission. The LD was driven by using a $2^{31} - 1$ non return-to-zero (NRZ) on-off keying (OOK) pseudorandom bit sequence (PRBS) with a peak-peak 1.5 V

drive input signal by the pattern generator (Anritsu MP17838). The transmitted digital signals were measured by the digital component analyzer (Agilent DCA-J 86100C) and and external clock (ROHDE & SCHWARZ SMP 04) to the pattern generator. As shown in Fig. 3.13, different data rate was applied from 4 Gbit/s to 6 Gbit/s. The open eye diagram was obtained at 280 mA of drive current up to 4 Gbit/s with a 4.76 of signal-to-noise (SNR) ratio, as shown in Fig. 3.13(b). The highest data rate with a clearly open eye diagram was 5 Gbit/s (Fig. 3.13(c)), while 6 Gbit/s was limited by the bandwidth of PD (Fig. 3.13(d)).

3.5 Internal Parameters

The study for internal parameters including carrier dynamics and gains parameters is beneficial to estimate the performance of LDs and potential improvements. Even though there are many reports on theoretical calculations, only few experimental studies have been reported in both conventional *c*-plane and semipolar III-nitride LDs. Especially, there have been no reports in differential gain, gain compression factor for semipolar and nonpolar LDs. Also, dynamic parameters including K-factor and maximum bandwidths were never reported for any III-nitride QW LDs. In this section, the cavity length dependent characteristics were studied to determine gain parameters. Then, resonance characteristics of the

frequency response were used to estimate high-speed parameters as well as differential gain and gain compression factor.

To estimate injection efficiency and internal loss, *L-I* characteristics of different length of cavities were studied. The angle of etched facets by RIE was first considered for mirror reflectance as shown in Fig. 3.14(a). The average value of facet angles shown 6 º with only 1 º fluctuation in different size of cavities and the corresponding reflectivity was reduced to 0.054 from 0.18 of the case of vertical facets.[23] The mirror loss depending on the length of the cavity is described as $\alpha_m = 1/L \ln(1/R)$, where L is the cavity length, and R is the reflectivity derived from the product of front and rear reflection coefficient. Figure 3.14(b) shown the determination of injection efficiency, η_i, and internal loss, $\langle \alpha_i \rangle$, by analyzing differential efficiency in different length of cavities. Differential efficiencies obtained from *L-I* curve of different length of cavities were fitted for the equation:

$$\frac{1}{\eta_d} = \frac{\langle \alpha_i \rangle}{\eta_i \ln(1/R)} L + \frac{1}{\eta_i}, \tag{3.1}$$

where η_d is differential efficiency, which is described as $\eta_d = \eta_i \, \alpha_m/(\alpha_m + \langle \alpha_i \rangle)$.

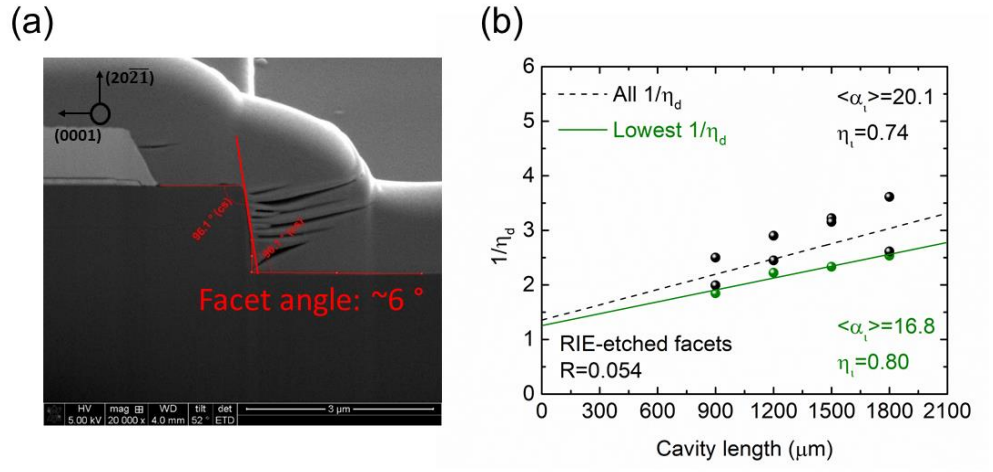

FIG. 3.14 (a) Cross-sectional SEM image of RIE-etched facet measured by FIB-SEM. (b) Differential efficiency versus cavity length to determine injection efficiency and internal loss.

Calculated injection efficiency of 80 % was obtained by fitting lowest value of differential efficiency on different cavity length of LDs. Internal loss was also calculated to be 16.8 cm^{-1} for R = 0.054 of non-vertical case with 6 ° facet angle. The injection efficiency is in a good agreement with previously reported similar epitaxial structure on $(20\bar{2}\bar{1})$ semipolar plane.[11] Higher internal loss is presumably caused from the combination of mode overlaps in highly doped *n*-contact layer and high absorption of shorter wavelengths in cladding layers with lower confinement factor compared to the Becerra *et al.*[11] Finally, total modal gain can be calculated to be for different cavities by $\Gamma g_{th} = \langle \alpha_i \rangle + \alpha_m$. The obtained values ranged from 65.5 cm^{-1} for 600 μm to 33.1 cm^{-1} for 1800 μm.

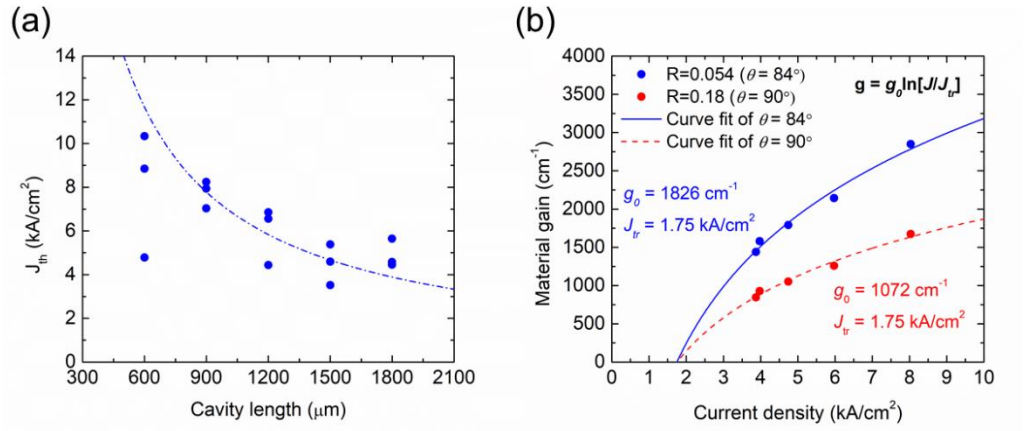

Figure 3.15 (a) Scatter data with fitted curve of threshold current density versus cavity length for 3 μm wide LDs. (b) Material gain versus current density of LDs for 6 º (84 º from substrate) angled and vertical facet.

Figure 3.15(a) shows the experimental relationship between the threshold current density and the cavity length of LDs. The threshold current densities inverse proportional to the cavity lengths due to the mirror loss even though the 600 μm cavities are a bit scattered more. By dividing the modal gain by confinement factor, the material gain dependent on current density was achieved and fitted by the simple two-parameter logarithmic model assuming the gain saturation at high current density as shown in Fig. 3.15(b). Calculated transparency current density and gain coefficient of etched facets (vertical facets) was 1.75 kA/cm^2 (1.75 kA/cm^2) and 1826 cm^{-1} (1072 cm^{-1}). It could be fitted better with three-parameter fit

assuming the low gain saturation effect even though three-parameter fit to our data offered more plausible estimation.[8]

3.6 Dynamic Parameters

The small signal modulation characteristics can be derived from the carrier and photon density rate equations:[24]

$$\frac{dn}{dt} = \frac{\eta_i I}{qV} - \frac{n}{\tau} - \upsilon_g \left(g_{th} + \frac{dg}{dn}\Delta n \right) s \tag{3.2}$$

$$\frac{ds}{dt} = \Gamma \upsilon_g \left(g_{th} + \frac{dg}{dn}\Delta n \right) s - \frac{s}{\tau_p} \tag{3.3}$$

where n and s are the carrier and photon densities in the active region, respectively, η_i is the injection efficiency, I is the drive current, q is the electron charge, V is the volume of the active layer, τ and τ_p are the carrier and photon (or cavity) lifetime, respectively, υ_g is the group velocity, Γ is the optical confinement factor, and g_{th} is the threshold material gain. Under small signal conditions, a small fluctuation of gain is added onto the threshold gain by multiplying the differential gain, dg/dn, by the fluctuation in carrier density, Δn. The spontaneous emission that is coupled into the lasing mode is ignored far above the threshold for this modulation condition. The small signal modulation for both carriers and photons is proportional to a second-order transfer function[24]

$$H(\omega) = \frac{\omega_R^2}{\omega_R^2 + \omega^2 + j\omega\gamma} \tag{3.4}$$

where ω_R is the relaxation resonance frequency (or $f_R = \omega_R/2\pi$) and γ is the damping factor.

To investigate the intrinsic modulation capability of the LDs, the differential gain, $\partial g/\partial n$, can be derived by the following the equation for f_R:

$$f_R = \frac{1}{2\pi}\left[\frac{\Gamma v_g \frac{dg}{dn}}{qV}\eta_i(I - I_{th})\right]^{1/2} \tag{3.5}$$

The relaxation resonance frequency can be expressed by the product of pumping current density and several material parameters. The only unknown is differential gain, dg/dn because Γ and η_i was obtained by the simulation and experimental analysis, respectively.

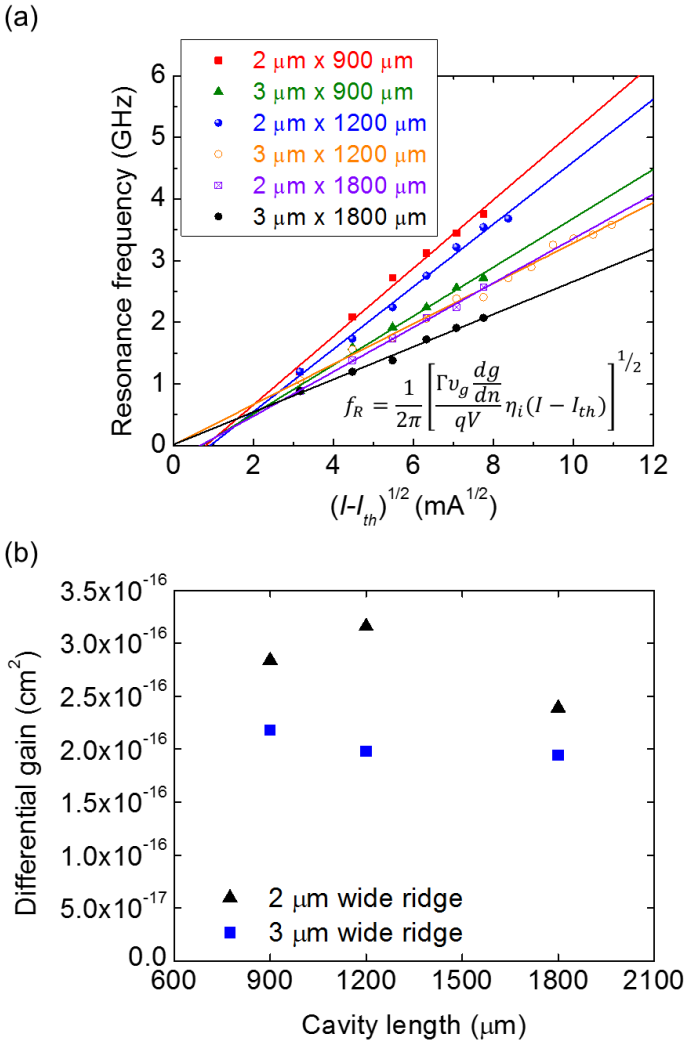

FIG. 3.16. a) Dependence of relaxation resonance frequency on $(I\text{-}I_{th})^{½}$, where I is the drive current and I_{th} is threshold current. b) Dependence of differential gain on cavity size. Reproduced with the permission of AIP Publishing[19]

Figure 3.16(a) shows the dependence of relaxation resonance frequency on the drive current for different cavity sizes. The slopes of the curves were highly

dependent on each cavity size, resulting in similar differential gains as expected. The slopes ranged from 0.5543 GHz/mA$^{1/2}$ for the largest cavity to 0.2646 GHz/mA$^{1/2}$ for the smallest cavity. The differential gains ranged from 1.94×10^{-16} cm^2 for the largest cavity to 2.84×10^{-16} cm^2 for the smallest cavity, as shown in Fig. 3.16(b). These values are in a good agreement with the reported differential gains of other III-nitride QW LDs and even comparable with those of quantum dot (QD) and nanowire (NW) LDs.[25–29] Compared to conventional polar *c*-plane LDs, the differential gain of semipolar $(20\bar{2}\bar{1})$ LDs are expected to be higher due to the higher electron-hole wave-function overlap in the lower density of states.[13,30,31] At low power operation, where gain compression is not significant, high differential gain leads to a higher f_R, resulting in a higher modulation bandwidth.[32]

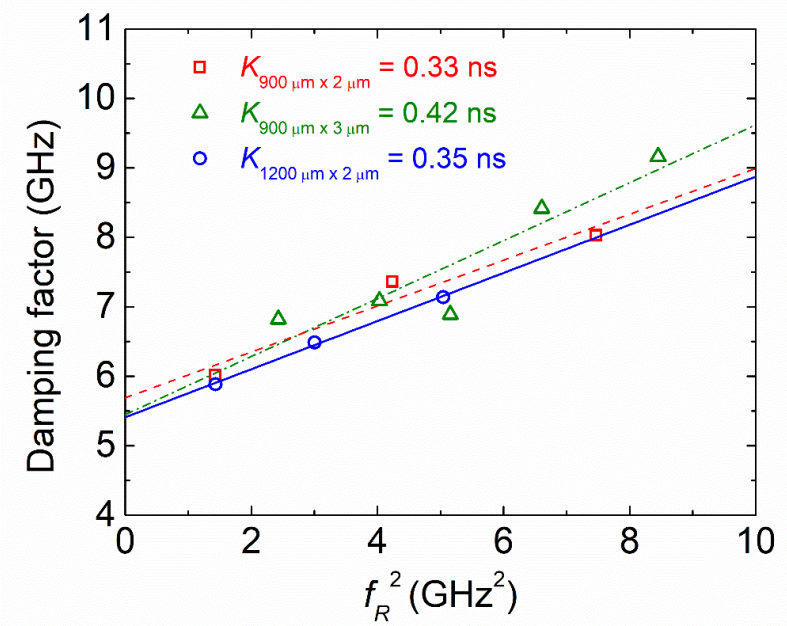

Figure 3.17 Dependence of the damping factor on the square of the resonance frequency (f_R^2) for the three smallest devices with lowest *K*-factors. Reproduced with the permission of AIP Publishing[19]

For high power operation, where gain compression is significant, the modulation bandwidth depends more on the damping factor (or *K*-factor) than f_R.[24] As shown in Fig. 3.17, the *K*-factors were obtained by fitting the measured damping factor and f_R with the following relationship:

$$\gamma = K f_R^2 + \gamma_0 \tag{3.6}$$

where is γ_0 is the damping factor offset. Since parasitic roll-off of larger cavities occurs at lower frequencies, the smallest three cavities were analyzed at low

injection levels and found to be in a good agreement. The lowest *K*-factor and corresponding damping factor offset were 0.33 ns and 5.69 GHz for the 2 μm wide by 900 μm long LD, respectively. The gain compression factor was calculated to be 7.4×10^{-17} cm^3 by $K = 4\pi^2\tau_p\left(1 + \varepsilon\Gamma g_{th}/(dg/dn)\right)$, where ε is gain compression factor.[31] Intrinsic maximum bandwidth can be also obtained by *K*-factor, which is the bandwidth limit due to the photon lifetime of the cavity. The maximum bandwidth occurs when 3-dB bandwidth is at the resonance frequency. Hence, calculated intrinsic maximum bandwidth was 27 GHz by $f_{3dB}^{max} = \sqrt{2}(2\pi/K)$, where $(\gamma/\omega_R)^2 = -3$ dB, in Eq. (3.4).

3.7 Temperature Dependent Characteristics

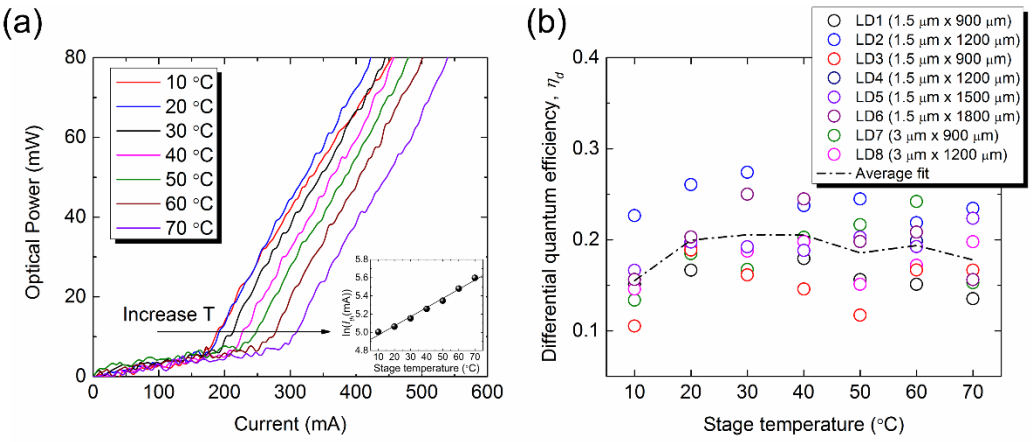

FIG. 3.18 (a) Temperature dependent *L-I* characteristics for 1.5 μm × 1200 μm cavity. (The inset shows the dependency of threshold current on stage temperature.) (b) Scattered differential quantum efficiency versus stage temperature for different size of the LD cavities.

Temperature dependent measurements for light-current (*L-I*) characteristics were performed to investigate carrier transport and its effect in modulation capability. To avoid self-heating of LDs, the pulse input with pulse width of 500 ns and a repetition rate of 1 kHz, corresponding to a duty cycle of 0.5 %, was driven to the different sized LD cavities as depicted in Fig. 3.18(a). The threshold current increased monotonically with the stage temperature except the case of 10 ºC. The differential quantum efficiencies, η_d of different cavities at different stage temperature were shown in Fig. 3.18(b). The trend fit of scattered η_d is stable from 20 ºC to 40 ºC and starts to decrease above 40 ºC. The lowest η_d

appears at 10 ºC, which can be seen that the red curve (10 ºC) crosses black curve (30 ºC) in Fig. 3.18(a). The low η_d at 10 ºC can be caused by low carrier transport in the MQWs at low temperature. Thus, non-uniform carrier distribution with a separation of electron-hole in MQWs leads low η_d. By the rule of Fermi-Dirac distribution of carriers in the QW, the carrier leakage over the well height competes with the carrier transport in the range of 20 ºC to 40 ºC. At high temperature above 40 ºC, carrier leakage becomes more dominant than the carrier transport, resulting in low η_d.

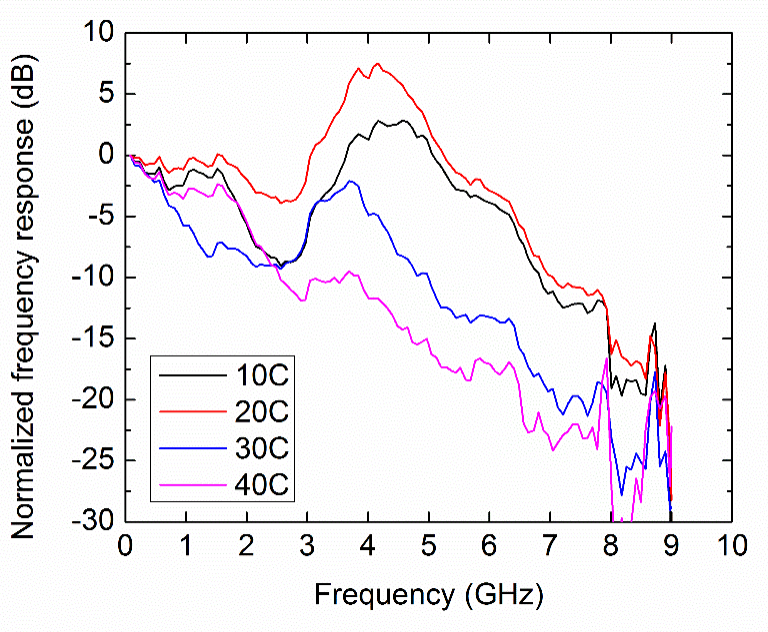

FIG. 3.19 Temperature dependent frequency response of 1.5 μm × 1200 μm cavity.

Strong dependence on temperature was observed in small signal modulation as shown in Fig. 3.18. As expected, the response at higher temperature dramatically degraded than lower temperature due to more significant carrier leakage and nonlinear gain compression from increased carrier temperature.[33] Even though the resonance frequencies at 10 ºC and 20 ºC appears near 4.2 GHz, the intensity of the signal response is higher at 20 ºC than 10 ºC. This is presumably due to the low differential efficiency and suppressed gain from poor carrier transport.

References

[1] S. Nakamura, M. Senoh, S. Nagahama, N. Iwasa, T. Yamada, T. Matsushita, H. Kiyoku, and Y. Sugimoto, Jpn. J. Appl. Phys. **35**, L74 (1996).

[2] S. Chichibu, T. Azuhata, T. Sota, and S. Nakamura, MRS Proc. **449**, 14 (1996).

[3] H. Masui, J. Sonoda, N. Pfaff, I. Koslow, S. Nakamura, and S.P. DenBaars, J. Phys. D. Appl. Phys. **41**, 165105 (2008).

[4] S.P. DenBaars, D. Feezell, K. Kelchner, S. Pimputkar, C.-C. Pan, C.-C. Yen, S. Tanaka, Y. Zhao, N. Pfaff, R. Farrell, M. Iza, S. Keller, U. Mishra, J.S. Speck, and S. Nakamura, Acta Mater. **61**, 945 (2013).

[5] D.F. Feezell, J.S. Speck, S.P. DenBaars, and S. Nakamura, J. Disp. Technol. **9**, 190 (2013).

[6] D.F. Feezell, M.C. Schmidt, S.P. Denbaars, and S. Nakamura, MRS Bull. **34**, 318 (2009).

[7] R.M. Farrell, D.F. Feezell, M.C. Schmidt, D.A. Haeger, K.M. Kelchner, K. Iso, H. Yamada, M. Saito, K. Fujito, D.A. Cohen, J.S. Speck, S.P. DenBaars, and S. Nakamura, Jpn. J. Appl. Phys. **46**, L761 (2007).

[8] R.M. Farrell, P.S. Hsu, D.A. Haeger, K. Fujito, S.P. DenBaars, J.S. Speck, and S. Nakamura, Appl. Phys. Lett. **96**, 231113 (2010).

[9] A. Pourhashemi, R.M. Farrell, M.T. Hardy, P.S. Hsu, K.M. Kelchner, J.S. Speck, S.P. DenBaars, and S. Nakamura, Appl. Phys. Lett. **103**, 151112 (2013).

[10] A. Pourhashemi, R.M. Farrell, D.A. Cohen, J.S. Speck, S.P. DenBaars, and S. Nakamura, Appl. Phys. Lett. **106**, 111105 (2015).

[11] D.L. Becerra, L.Y. Kuritzky, J. Nedy, A.S. Abbas, A. Pourhashemi, R.M. Farrell, D.A. Cohen, S.P. Denbaars, J.S. Speck, S. Nakamura, D.L. Becerra, L.Y. Kuritzky, J. Nedy, A.S. Abbas, J.S. Speck, and S. Nakamura, Appl. Phys. Lett. **362**, 91106 (2016).

[12] B.P. Yonkee, E.C. Young, C. Lee, J.T. Leonard, S.P. DenBaars, J.S. Speck, and S. Nakamura, Opt. Express **24**, 7816 (2016).

[13] W.G. Scheibenzuber, U.T. Schwarz, R.G. Veprek, B. Witzigmann, and A. Hangleiter, Phys. Rev. B - Condens. Matter Mater. Phys. **80**, 115320 (2009).

[14] S.-H. Park and D. Ahn, in *Proc. SPIE 8625, Gall. Nitride Mater. Devices VIII*, edited by J.-I. Chyi, Y. Nanishi, H. Morkoç, J. Piprek, E. Yoon, and H. Fujioka (International Society for Optics and Photonics, 2013), p. 862511.

[15] L.Y. Kuritzky and J.S. Speck, MRS Commun. 1 (2015).

[16] J.C. Carrano, T. Li, C.J. Eiting, R.D. Dupuis, and J.C. Campbell, J. Electron. Mater. **28**, 325 (1999).

[17] R.M. Farrell, C.J. Neufeld, S.C. Cruz, J.R. Lang, M. Iza, S. Keller, S. Nakamura, S.P. DenBaars, U.K. Mishra, and J.S. Speck, Appl. Phys. Lett. **98**, 201107 (2011).

[18] J.R. Lang, N.G. Young, R.M. Farrell, Y. Wu, J.S. Speck, J.R. Lang, N.G. Young, R.M. Farrell, Y. Wu, and J.S. Speck, Appl. Phys. Lett. **101**, 1 (2012).

[19] C. Lee, C. Zhang, D.L. Becerra, S. Lee, C.A. Forman, S.H. Oh, R.M. Farrell, J.S. Speck, S. Nakamura, J.E. Bowers, and S.P. DenBaars, Appl. Phys. Lett. **109**, 101104 (2016).

[20] B.P. Yonkee, R.M. Farrell, J.T. Leonard, S.P. DenBaars, J.S. Speck, and S. Nakamura, Semicond. Sci. Technol. **30**, 75007 (2015).

[21] D.L. Becerra, D.A. Cohen, R.M. Farrell, S.P. DenBaars, and S. Nakamura, Appl. Phys. Express **9**, 92104 (2016).

[22] J.E. Bowers and C.A. Burrus, Jr, IEEE/OSA J. Light. Technol. **LT-5**, 1339 (1987).

[23] L.Y. Kuritzky, D.L. Becerra, A.S. Abbas, J. Nedy, S. Nakamura, S.P. DenBaars, and D.A. Cohen, Semicond. Sci. Technol. **31**, 75008 (2016).

[24] L.A. Coldren, S.W. Corzine, and M.L. Masanovic, *Diode Lasers and Photonic Integrated Circuits*, 2nd ed. (John Wiley & Sons, Inc., Hoboken, NJ, USA, 2012).

[25] H. Wang, M. Kumagai, T. Tawara, T. Nishida, T. Akasaka, N. Kobayashi, H. Wang, M. Kumagai, T. Tawara, and T. Nishida, Appl. Phys. Lett. **81**, 4703 (2002).

[26] M. Funato, Y. Seok, K. Yoshiaki, O. Akio, K. Yoichi, K. Takashi, and M.S. Nagahama, Appl. Phys. Express **6**, 122704 (2013).

[27] A. Banerjee, T. Frost, E. Stark, and P. Bhattacharya, Appl. Phys. Lett. **101**, 41108 (2012).

[28] T. Frost, A. Banerjee, and P. Bhattacharya, Appl. Phys. Lett. **103**, 211111 (2013).

[29] T. Frost, S. Jahangir, E. Stark, S. Deshpande, A. Hazari, C. Zhao, B.S. Ooi, and P. Bhattacharya, Nano Lett. **14**, 4535 (2014).

[30] T. Melo, Y.-L. Hu, C. Weisbuch, M.C. Schmidt, A. David, B. Ellis, C. Poblenz,

Y.-D. Lin, M.R. Krames, and J.W. Raring, Semicond. Sci. Technol. **27**, 24015 (2012).

[31] H. Zhao, R.A. Arif, Y.K. Ee, and N. Tansu, Opt. Quantum Electron. **40**, 301 (2008).

[32] J.E. Bowers, Solid. State. Electron. **30**, 1 (1987).

[33] T. Keating, X. Jin, S.L. Chuang, and K. Hess, IEEE J. Quantum Electron. **35**, 1526 (1999).

4

Demonstration of Violet Laser-based VLC

4.1 Introduction

Compared to white light generated using blue-emitting LDs pumping YAG:Ce phosphors, white light generated with a near ultraviolet (NUV) LDs pumping red-, green-, and blue-emitting (RGB) phosphors shows expected improvements in both color rendering index (CRI) and correlated color temperature (CCT).[1] Additionally, the spectral intensity of sunlight is lower in the NUV and violet spectral range than in the blue spectral range that is typically used for III-nitride emitters in solid-state lighting systems. As a result, NUV LDs enable VLC systems that can be robust in the presence of high intensities of sunlight, for example, in a room with many windows. Thus, NUV laser-based VLC is a

potentially attractive approach to achieve high performance white lighting and VLC functionalities.

4.2 System Design

The white light emitting free-space communication system consisted of a 410 nm LD exciting RGB phosphors mixed in silicone, as shown in Fig. 4.1. The NUV LD was grown on a semipolar $(20\bar{2}1)$ bulk GaN substrate and had a 4 μm ridge waveguide and a 1200 μm cavity with uncoated facets. Further details of the structure are reported elsewhere.[2]

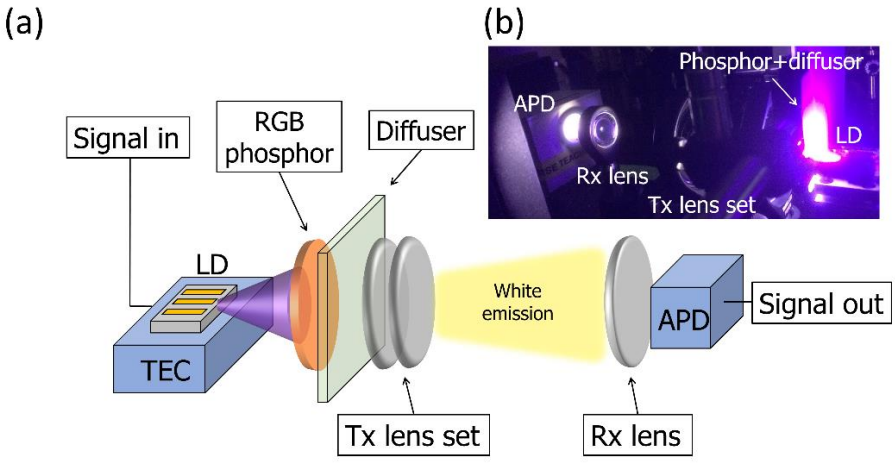

FIG. 4.1. (a) Schematic of the NUV laser-based white light communication system with RGB phosphors for color conversion, a diffuser to improve the uniformity of the phosphor emission, transmitter (Tx) and receiver (Rx) lenses to collimate the light, and a 1 GHz avalanche photodetector (APD) to collect the transmitted light. (b) Photograph of the experimental setup. Reprinted with permission from OSA Publishing[3]

The LD chip was mounted on a microwave probe station with a ground signal (GS) probe, a heat sink, and a thermoelectric cooler (TEC), as shown in Fig. 4.1(a). The phosphor mixture was placed 1–2 cm in front of the LD and was followed by polyethylene terephthalate (PET) diffuser to provide uniform white emission. The transmitter (Tx) and receiver (Rx) lenses were properly aligned to collimate the emitted beam as shown in the photograph in Fig. 4.1(b). At the receiver end, a 1 GHz Menlo System APD 210 silicon avalanche photodetector (APD) was placed approximately 15 cm from the Tx lens. An NUV bandpass filter does not necessarily need to be used in conjunction with the APD because the relatively slow phosphor response time does not interfere with the performance of the laser-based VLC system.[4] For DC characterization, the LD was tested using a Keithley 2520 diode laser test system with a half-moon integrating sphere and a calibrated Si photodetector. Excitation and emission spectra of the individual phosphors were measured using a fluorometer (Horiba) with a 15 cm integrating sphere (Quanta-ϕ) attachment for quantum yield measurements. The spectra of white emission from the laser-based VLC system were measured using an Ocean Optics HR 4000 spectrometer.

4.3 Red-, Green-, Blue-emitting Phosphors

The phosphor materials are prepared by mixing three different material of phosphors in one compound from Seshadri's group at UCSB. The optical excitation and emission properties of the RGB phosphors used are shown in Fig. 4.2.

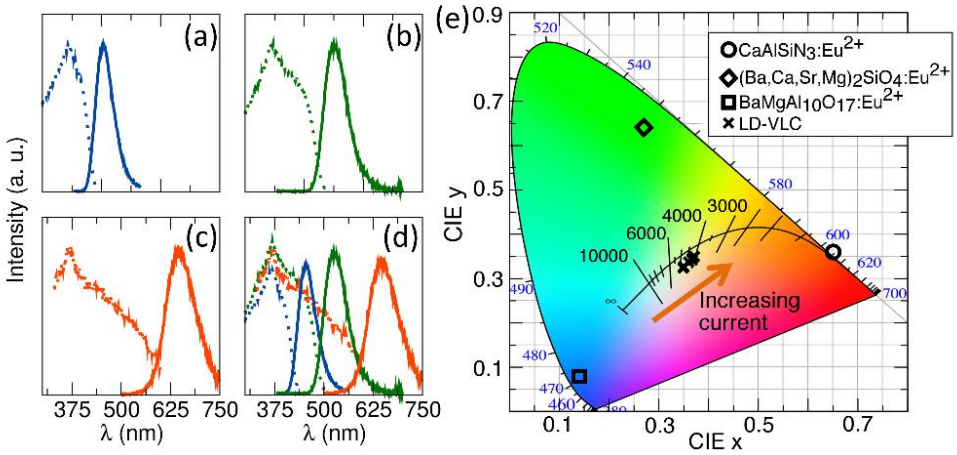

FIG. 4.2. Plots of excitation (dotted lines) and emission (solid lines) for (a) blue-, (b) green-, and (c) red-emitting phosphors used in this work, with (d) overlapping spectra of the three phosphors shown. (e) CIE diagram showing the chromaticity coordinates of the three phosphors and the LD-VLC RGB mixture. The chromaticity coordinates for the phosphors create a large triangle within the CIE diagram of potential colors that can be achieved from mixing the phosphors. The CIE coordinates of the LD-VLC RGB mixture for different laser currents lies just beneath the Planckian locus and shifts red (decreasing coordinated color temperature) to warmer white light as the laser current increases. Reprinted with permission from OSA Publishing[3]

The red-, green-, and blue-emitting phosphors are $CaAlSiN_3:Eu^{2+}$, $(Ba,Ca,Sr,Mg)_2SiO_4:Eu^{2+}$, and $BaMgAl_{10}O_{17}:Eu^{2+}$, respectively. The phosphors were mixed in silicone at a ratio of 1:1.5:3 to achieve white light[5]. The quantum

yields of the phosphor materials were measured to be (excited at 410 nm) 74 %, 78 %, and 78 %, respectively. The corresponding Commission Internationale de l'Eclairage (CIE) chromaticity coordinates for the phosphor emission excited using a 410 nm LD were (0.65, 0.36), (0.27, 0.64), and (0.14, 0.08), respectively (Fig. 4.2(e)). The CCT and CIE coordinates obtained by the LD (410 nm NUV LD exciting RGB phosphor mixture) ranged from 4700 K to 4050 K with increasing current from 100 mA to 600 mA, where the CCT finally saturated. A maximum CRI value of 79 was obtained between 500 mA and 600 mA, which is a significant improvement compared to the previously reported value of 58 for the white light generated using blue LD and yellow YAG:Ce phosphor.[4,6]

4.4 Device characteristics

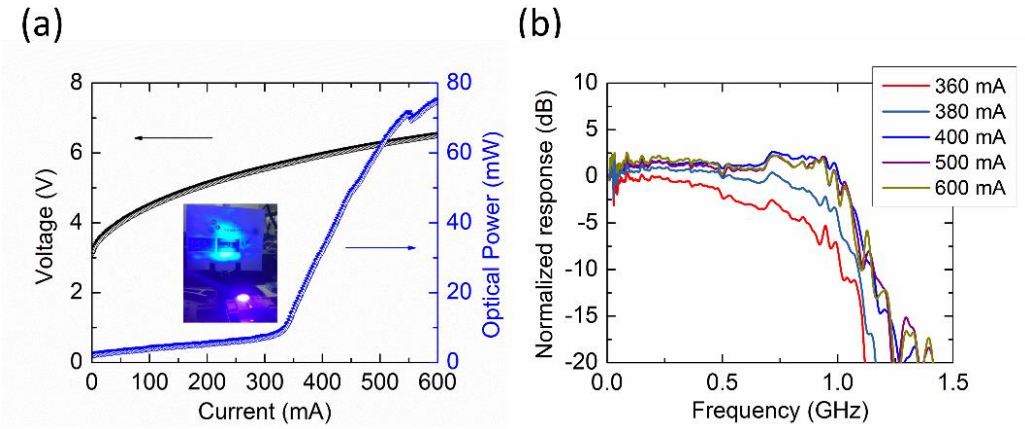

FIG. 4.3. (a) *L-I-V* characteristics of the LD under CW operation at 15 °C. (b) Small signal response of the LD with increasing driving current from 360 mA to 600 mA. Reprinted with permission from OSA Publishing[3]

The light-current-voltage (*L-I-V*) characteristics of the 4 μm × 1200 μm ridge waveguide LD are shown in Fig. 4.3(a). The threshold current (I_{th}), threshold current density (J_{th}), and threshold voltage (V_{th}) of the LD were 320 mA, 6.67 kA/cm^2, and 5.5 V, respectively, under continuous wave (CW) operation at 15 °C. The LD exhibited a slope efficiency of 0.36 W/A from a single facet. The modulation response for the LD operating between 360 mA and 600 mA is shown in Fig. 4.3(b). The frequency response shows that the –3 dB bandwidth is limited to approximately 1 GHz after 400 mA bias point. Although the LD is expected to have a higher bandwidth of more than 5 GHz,[2] the measured bandwidth of

approximately 1 GHz is limited by the bandwidth of the APD. The choice of the 1 GHz APD is an alternative method to detect the lowered signal level due to scattering in the phosphor conversion process. Higher modulation bandwidths are expected under the drive current of 400 mA to 600 mA for similar laser-based VLC systems with the eventual development of higher bandwidth Si APDs.

4.5 Spectral Characteristics

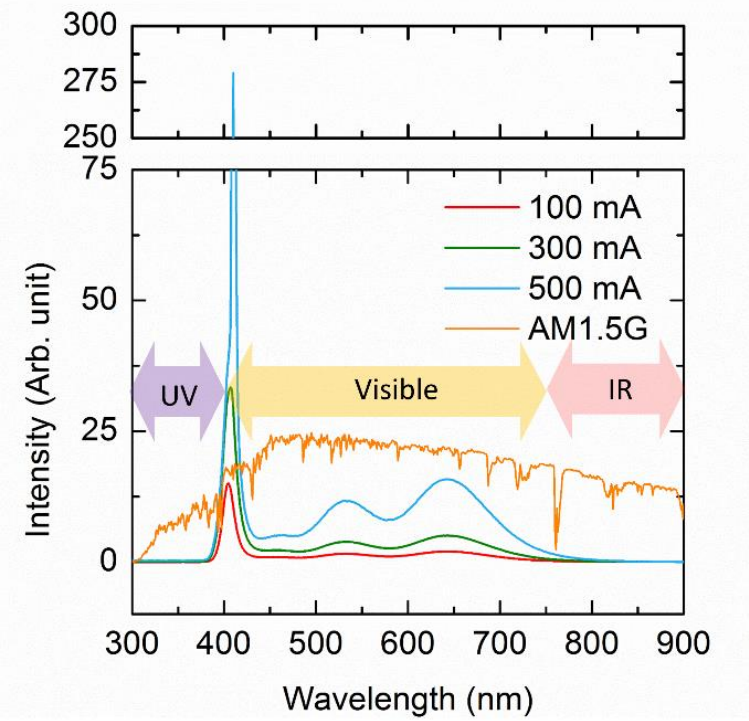

FIG. 4.4. Spectra of the laser-based white emission using the RGB phosphor mixture for increasing currents from 100 mA to 500 mA are shown. The ASTM G173-03 AM1.5G solar spectrum is also shown for comparison. Reprinted with permission from OSA Publishing[3]

The spectral characteristics of white light emission are shown in Fig. 4.4. The peak of the LD emission appears at 410 nm with only a 1 nm wavelength shift above the lasing threshold (> 300 mA) due to comparatively flat quantum wells (QWs) on the $(20\overline{21})$ semipolar orientation LD. The green- and red-phosphor emission peaks are at 520 nm and 650 nm, respectively. Blue phosphor emission was weak due to low absorption at 410 nm excitation. Increasing blue emission could be accomplished via higher blue phosphor loading, higher quantum yield blue emission, and/or using the LD with a shorter emission wavelength. The ASTM G173-03 AM1.5G solar spectrum is also shown in Fig. 4.4 for comparison. Sunlight has a reduced spectral intensity in the NUV region of the spectrum relative to the rest of the visible region of the spectrum. Thus, if an NUV optical bandpass filter were used at the receiver, NUV laser-based VLC system would be expected to have a lower signal-to-noise ratio (SNR) than a blue emitter-based VLC system, and would therefore be more appropriate for use in environments with high background intensities of sunlight (e.g. in rooms with many windows).

4.6. Demonstration of Data Transmission

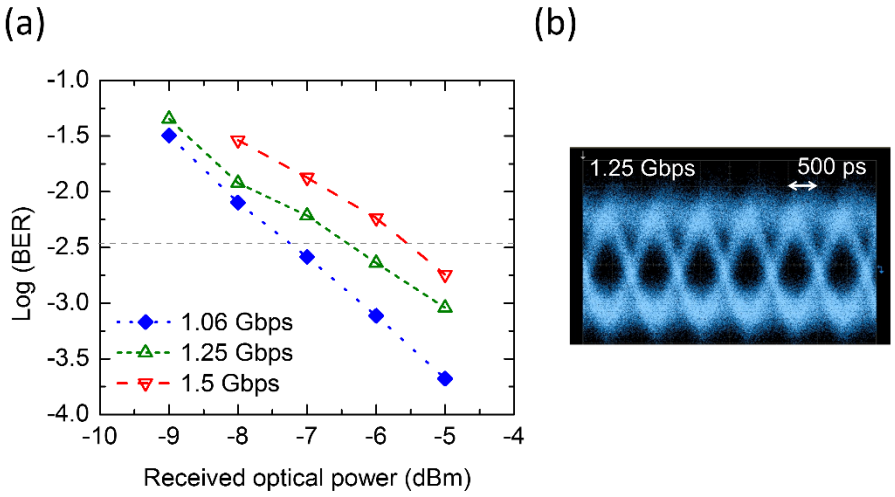

FIG. 4.2. (a) Dependence of BER on received optical power characteristics of the laser-based white light communication link at different data rates with the FEC criteria shown as a grey dashed line. (b) The eye diagram of the laser-based white emission. Reprinted with permission from OSA Publishing[3]

Data communication characteristics using a non-return-to-zero (NRZ) OOK modulation scheme were measured to evaluate the presented NUV laser-based white light communication system. A $2^{10} - 1$ pseudo-random binary sequences (PRBS) data stream from the bit error rate tester (Agilent N4903B J-BERT) was used to investigate bit error rates (BERs) and eye diagrams by using a digital communications analyzer (Agilent 86100). The BER of the laser-based phosphorescent VLC link at different attenuated received optical powers is shown

in Fig. 4.5(a). The modulation of the white emission passed the forward error correction (FEC) criteria of 3.8×10^{-3} at 1.5 Gbps with a BER of 1.8×10^{-3}. Figure 4.5(b) shows a clear open eye diagram of data transmission at 1.25 Gbps under the drive current of 570 mA. Since the APD limits the system bandwidth to 1 GHz, it is expected that the actual data rate is greater than 1.5 Gbps.

Many studies have reported systems for both lighting and data communication applications over the last several years. Table 1 summarizes the configuration and performance of various white light communication systems that use a combination of LDs and phosphors. As indicated by the table, the presently reported VLC system with RGB phosphors has a higher CRI and a lower CCT than previously reported systems that use yellow-emitting YAG:Ce phosphors. Dursun *et al.* demonstrated higher CRI and lower CCT, but the poor stability of Br-based perovskite materials and the toxicity of lead are critical limitations for commercial use. An NUV LD pumping RGB phosphors should also have a higher signal-to-noise ratio when bandpass filters are used, as discussed above. Hence, the VLC system in this work satisfies both lighting quality and communication data rate requirements. Moving forward, it is expected that the use of advanced modulation schemes, such as quadrature amplitude modulated orthogonal frequency division multiplexing (QAM OFDM), and higher speed photodetector (> 5 GHz) will significantly increase data rate in laser-based VLC systems.

Table 5.1. Summary of reported laser-based white light communication using phosphors

Ref.	Source	Color converter	CRI	CCT (K)	Modulation Scheme	Data rate (Gbps)
Lee *et al*.[4]	Blue LD	YAG:Ce	58	4740	OOK	2
Retamal *et al*.[7]	Blue LD	YAG:Ce	-	6409	16 QAM	4
Chi *et al*.[8]	Blue LD	YAG:Ce	-	5217	16 QAM	5.2
Dursun *et al*.[9]	Blue LD	Perovskite	89	3236	OOK	2
Chun *et al*.[10]	Blue LD	Organic	-	7092	64 QAM	6.52
This work	Violet LD	RGB	79	4050	OOK	1.25

References

[1] K.A. Denault, M. Cantore, S. Nakamura, S.P. DenBaars, and R. Seshadri, AIP Adv. **3**, 72107 (2013).

[2] C. Lee, C. Zhang, D.L. Becerra, S. Lee, C.A. Forman, S.H. Oh, R.M. Farrell, J.S. Speck, S. Nakamura, J.E. Bowers, and S.P. DenBaars, Appl. Phys. Lett. **109**, 101104 (2016).

[3] C. Lee, C. Shen, C. Cozzan, R.M. Farrell, J.S. Speck, S. Nakamura, B.S. Ooi, and S.P. DenBaars, Opt. Express **25**, 17480 (2017).

[4] C. Lee, C. Shen, H.M. Oubei, M. Cantore, B. Janjua, T.K. Ng, R.M. Farrell, M.M. El-Desouki, J.S. Speck, S. Nakamura, B.S. Ooi, and S.P. DenBaars, Opt. Express **23**, 29779 (2015).

[5] C. Cozzan, M.J. Brady, N. O 'Dea, E.E. Levin, S. Nakamura, S.P. DenBaars, and R. Seshadri, AIP Adv. **6**, 105005 (2016).

[6] M. Cantore, N. Pfaff, R.M. Farrell, J.S. Speck, S. Nakamura, and S.P. DenBaars, Opt. Express **24**, A215 (2016).

[7] J.R.D. Retamal, H.M. Oubei, B. Janjua, Y.-C. Chi, H.-Y. Wang, C.-T. Tsai, T.K. Ng, D.-H. Hsieh, H.-C. Kuo, M.-S. Alouini, J.-H. He, G.-R. Lin, and B.S. Ooi,

Opt. Express **23**, 33656 (2015).

[8] Y.-C. Chi, D.-H. Hsieh, C.-Y. Lin, H.-Y. Chen, C.-Y. Huang, J.-H. He, B. Ooi, S.P. DenBaars, S. Nakamura, H.-C. Kuo, and G.-R. Lin, Sci. Rep. **5**, 18690 (2015).

[9] I. Dursun, C. Shen, M.R. Parida, J. Pan, S.P. Sarmah, D. Priante, N. Alyami, J. Liu, M.I. Saidaminov, M.S. Alias, A.L. Abdelhady, T.K. Ng, O.F. Mohammed, B.S. Ooi, and O.M. Bakr, ACS Photonics **3**, 1150 (2016).

[10] H. Chun, S. Rajbhandari, D. Tsonev, G. Faulkner, H. Haas, and D. O'Brien, in *2015 IEEE Int. Conf. Commun. Work.* (IEEE, 2015), pp. 1392–1397.

5

Conclusions and Future Works

5.1 Summary and Conclusions

Many studies about the modulation and high-speed performance have been discussed in this dissertation. As LD-based VLC and high-speed III-nitride LD have never reported before except a few system studies, most of our studies were devoted to reporting the performances and its characteristics for the first time. Thus, Chapter 2 first demonstrated the high-speed performance of high power designed blue LD with the bandwidth of 2.6 GHz and OOK data rate of 4 Gbit/s. Then, its white lighting data transmission converted by YAG:Ce phosphor was demonstrated by overcoming bandwidth limiting effect from long relaxation lifetime of the phosphor. After proving the potential of LD for VLC, higher speed III-nitride LDs were developed on semipolar $(20\bar{2}\bar{1})$ substrate and shown record-

breaking modulation bandwidth over 5 GHz in Chapter 3. Corresponding OOK data transmission was performed over 5 Gbit/s. Also, internal parameters related to carrier injection, optical gain were studied by using the method of cavity length dependent measurement. By investigating the frequency response and its damping characteristics, K-factor of 0.35 ns, intrinsic maximum bandwidth of 27 GHz, differential gain of 2.84×10^{-16} cm^2, and its gain compression factor of 7.4×10^{-17} cm^3 were extracted. These are the first reported dynamic analysis and parameters in III-nitride QW LDs. Finally, Chapter 4 presented NUV laser-based phosphorescent white light communication was demonstrated using RGB phosphors. A semipolar LD with a modulation bandwidth of several GHz was used as a transmitter to achieve a data rate of greater than 1 Gbps. The system produced white light with a high CRI of 79 and a low CCT of 4050 K, which is a significant improvement over previously reported systems that used blue LDs and YAG:Ce phosphors. The system is expected to have a lower signal-to-noise ratio than a blue laser-based VLC system due to the reduced overlap with the solar spectrum. A 1.25 Gbps data rate with a clear open eye diagram was measured using NRZ OOK modulation. These results demonstrate that NUV laser-based VLC systems can satisfy both high quality lighting and high speed low noise communication requirements.

5.2 Future Works

5.2.1 Laser-based Visible Light Communication

The studies in this dissertation covered broad area including material growth, device fabrication, white lighting, and free space optical system, however, most of these experiments are based on the first demonstration or the first discussions. Even though our works are meaningful in terms of a novelty, further optimization and developments are still needed. Many aspects to improve high-speed performance also cover the factors for high-power performance. Listed points should be carefully studied in the future.

- VLC system
    - Data rate depending on the conversion ratio of phosphors
    - Data rate vs. emission angle after phosphor conversion
- Higher order modulation scheme (16-, 32-, 64-QAM OFDM)
- Space/Satellite communication applications
    - Radiation test
    - Diffraction of lasing at the facet vs. wavelength (NUV to IR)
- Noise vs. lateral modes
- CW lasing of 600 μm, 300 μm and 150 μm cavities

- Parasitic effect before package vs. after package
- Carrier transport effect in the frequency response
- Facet coating to reduce the threshold current density
- Epitaxial optimization for both high-efficiency and high-speed
    - Topside n-contact by reducing doping and using SiH_4 etch
    - QW/barrier thickness and numbers for both RC parasitics and loss
    - P^{++}GaN to reduce RC
    - EBL position (as far away as possible)
- III-nitride DFB lasers
- III-nitride VCSEL based VLC

5.2.2 High-speed Photodetector

Since most of VLC studies have done based on LEDs, the system bandwidth was mostly limited at low frequency below 1 GHz.[1–4] However, for LDs, many reports including our works had crucial constraint in the bandwidth limit of PDs from the market. Also, as researchers have recently faced the theoretical bandwidth limit of LEDs, obviously, LDs have gained more momentum for VLC. Also, elegant property of III-nitride for PD is low dielectric constant with ~ 9 even though the difference from Si (11.7) or GaAs (12.9) is less than an order of magnitude.[5,6]

This offers low junction capacitance, which is critical for high-speed operation especially in pin and schottky PDs. The absorption is 1 ~ 2 order higher than GaAs (~10^4 cm^{-1}) and Si/Ge (~10^3 cm^{-1}).[5,6] Thus, it is valuable to develop high-speed III-nitride based PDs.

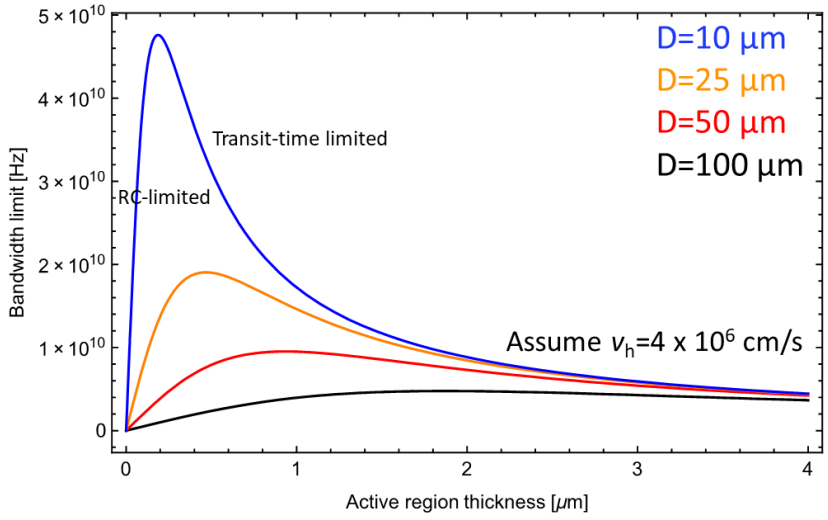

Figure 5.1 Calculated modulation bandwidth versus the active region thickness of III-nitride *p-i-n* PD. The assumption includes that the transit time is limited by hole velocity and RC is dominated by junction capacitance. D is the diameter of the active region. υ_h is hole velocity.

The calculated bandwidth reaches up to 40 GHz with the active region diameter of 10 µm and more practically, the diameter of 25 µm and 50 µm shown more than 10 GHz. Especially, using InGaN as an active region can provide high responsivity at blue-violet spectrum.[7] Epitaxial and device structures can be

optimized for different design of PDs such as *p*-*i*-*n*, avalanche PDs (APDs), Schottky PD, and metal-semiconductor-metal (MSM) PD.

References

[1] J.-W. Shi, K.-L. Chi, J.-M. Wun, J. Bowers, Y.-H. Shih, and J.-K. Sheu, IEEE Electron Device Lett. 1 (2016).

[2] R.X.G. Ferreira, E. Xie, J.J.D. McKendry, S. Rajbhandari, H. Chun, G. Faulkner, S. Watson, A.E. Kelly, E. Gu, R. V. Penty, I.H. White, D.C. O'Brien, and M.D. Dawson, IEEE Photonics Technol. Lett. **28**, 2023 (2016).

[3] C. Shen, C. Lee, T.K. Ng, S. Nakamura, J.S. Speck, S.P. DenBaars, A.Y. Alyamani, M.M. El-Desouki, and B.S. Ooi, Opt. Express **24**, 20281 (2016).

[4] D. V. Dinh, Z. Quan, B. Roycroft, P.J. Parbrook, and B. Corbett, Opt. Lett. **41**, 5752 (2016).

[5] J. Bowers and C. Burrus, J. Light. Technol. **5**, 1339 (1987).

[6] J.L. Polleux and C. Rumelhard, in *8th IEEE Int. Symp. High Perform. Electron Devices Microw. Optoelectron. Appl. EDMO 2000 [13-14 November, 2000, Univ. Glas.* (IEEE, Glasgow, UK, 2000), p. 280.

[7] R.M. Farrell, C.J. Neufeld, S.C. Cruz, J.R. Lang, M. Iza, S. Keller, S. Nakamura, S.P. DenBaars, U.K. Mishra, and J.S. Speck, Appl. Phys. Lett. **98**, 201107 (2011).